UNIVERSITY OF GENOA

DEPARTMENT OF EXPERIMENTAL MEDICINE

PhD COURSE IN EXPERIMENTAL MEDICINE

Curriculum: BIOCHEMISTRY

Role of the ABA/LANCL system in the insulin-independent stimulation of cell glucose uptake and energy metabolism in myoblasts and adipocytes through an AMPK-mediated mechanism

Candidate

Dott.ssa Sonia Spinelli

Tutor

Prof.ssa Laura Sturla

Coordinator of the PhD course

Prof. Ernesto Fedele

Academic Year 2021-2022

XXXIV Cycle

ABSTRACT

Abscisic acid (ABA) is a hormone with a very long evolutionary history, dating back to the earliest living organisms, of which modern (ABA-producing) cyanobacteria are likely the descendants, well before separation of the plant and animal kingdoms, with a conserved role as a signal regulating cell responses to environmental challenge. Nanomolar ABA is also present and active in mammals where it controls the metabolic response to glucose availability by stimulating glucose uptake in skeletal muscle and adipose tissue with an insulin-independent mechanism and increasing brown adipose tissue activity and browning through its receptor LANCL2. Previous data showed that, in LANCL2$^{-/-}$ mice, the genetic ablation of the receptor doesn't modify fasting glycemia values but results in the reduction of glucose tolerance compared with wild-type siblings. Animals are still responsive to exogenous ABA. The result that the effect of ABA was not completely abrogated by LANCL2 silencing, despite the very high percentage of reduction of protein and mRNA expression, suggests that other ABA receptors might be partly involved in the effect of ABA on muscle. LANCL1, a LANCL2 homolog, is indeed expressed in murine skeletal muscle at levels like those of LANCL2. Thus, I focused my attention on the metabolic function of the ABA/LANCL1 system. Recombinant human LANCL1 protein binds ABA with a K_d in a concentration range that lies between the low and high-affinity ABA binding sites of LANCL2. In rat L6 myoblasts, LANCL receptors similarly stimulate both basal and ABA-triggered fluorescently labeled deoxyglucose analog 2-NBDG uptake, activate mRNA levels and protein expression of the glucose transporters GLUT1 and GLUT4 and the signaling proteins AMPK/PGC-1α/Sirt1, stimulate mitochondrial respiration and the expression of the skeletal muscle (SM) uncoupling proteins sarcolipin and UCP3. Moreover, LANCL2$^{-/-}$ mice overexpress LANCL1 in the SM and respond to chronic ABA treatment (1 μg/kg body weight/day) with an improved glycemia response to glucose load and increased SM transcription of GLUTs, of the AMPK/PGC-1α/Sirt1 pathway and of sarcolipin, UCP3 and NAMPT. LANCL1 behaves as an ABA receptor with a somewhat lower affinity for ABA than LANCL2 but with overlapping effector functions: stimulating glucose uptake and the expression of muscle glucose transporters and mitochondrial uncoupling and respiration *via* the AMPK/PGC-1α/Sirt1 pathway. Furthermore, since adipose tissue seems to be a direct target of ABA, along with skeletal muscle, I investigated the browning effects of ABA in brown and white human adipocytes. ABA increases AMPK phosphorylation and AMPK and PGC-1α protein levels in pre-adipocytes overexpressing LANCL1 and LANCL2. The expression of genes related to browning, oxidative consumption, glucose transport, mitochondrial biogenesis, respiratory uncoupling and AMPK/PGC-1α/Sirt1 pathway is increased after adipocyte differentiation and further increases upon ABA treatment. Chronic ABA treatment stimulates mitochondrial DNA content in the brown adipose tissue of mice. These results

suggest that ABA may be used as an anti-obesity molecule. Concluding, receptor redundancy may have been advantageous in animal evolution, given the role of the ABA/LANCL1-2 system in the insulin-independent stimulation of cell glucose uptake and energy metabolism.

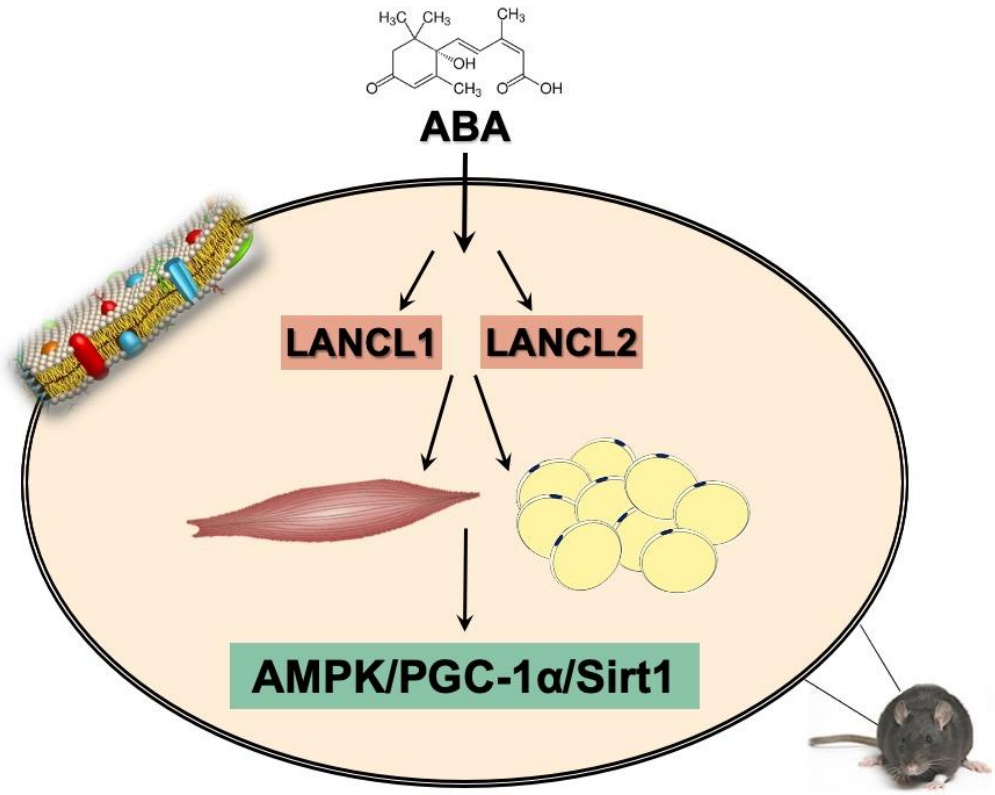

INDEX

1. INTRODUCTION

Abscisic acid, a plant and animal hormone. 2-cis, 4-trans-Abscisic acid (ABA) is a 15-carbon weak acid (pKa 4.8) terpenoid hormone (**Figure 1**) which plays important roles in the regulation of plant responses to environmental stress. The isoprenoid hormone is also present and active in lower Metazoa (Porifera and Hydroids), where it regulates the sponge response to an increase in water temperature and light-induced tissue regeneration in hydroids [1,2]. ABA is present as an endogenous hormone also in humans [3], where it controls innate immune cell function [4,5], the expansion of hemopoietic progenitors [6] and glucose homeostasis [3,7]. Conservation of ABA across the plant and animal kingdoms points to its very early evolution, in a common precursor to Metaphyta and Metazoa, as a messenger involved in the physiological adaptation of cells and organisms to changing environmental conditions. This general role of ABA in the living is in accordance with its most recently unveiled role in the regulation of blood glucose levels [7].

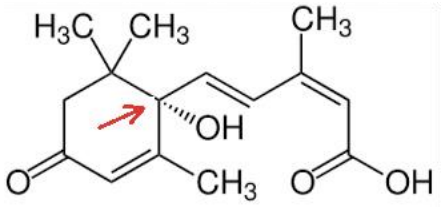

Figure 1. Structure of 2-cis, 4-trans-Abscisic acid. ABA has an asymmetric carbon atom (red arrow) generating two enantiomers S-(+)-ABA and R-(-)-ABA. (+)-ABA is the naturally occurring form in plants, although (-)-ABA is active in some vegetal functional assays.

The function of ABA as a stress signal and its signaling pathway are conserved in all plants, including mosses, and are believed to be the result of the very early adaptation of life to the terrestrial environment. Although the study of ABA in plants has been ongoing for several decades, also in view of its industrial application to improve stress tolerance in crops, it is only in the past decade that evidence has mounted regarding the presence and physiological significance of ABA also in animals. Le Page-Degivry et al. first described the presence of ABA in mammalian tissues, particularly brain [8], but their interesting observation remained isolated. The research group of Professor Zocchi of the University of Genoa became interested in ABA in the quest for the animal hormonal signal upstream of the second messenger cyclic ADP-ribose (cADPR), a universal Ca^{2+} mobilizer from intracellular stores that had been discovered to be involved in insulin release [9]. Intracellular Ca^{2+} movements are arguably the most ancient and conserved signaling mechanism throughout the animal and plant kingdoms. Indeed, cADPR had been reported to mediate the effect of ABA in guard cells [10]. Thus, a role for ABA as an animal, as well as a plant hormone was hypothesized, and

experiments were performed on the simplest and most ancient Metazoa (Sponges and Hydroids) to verify this hypothesis; the physiological functions of these animals are indeed limited to water filtration and respiration. However, being sessile, they are particularly exposed to environmental stress. It was discovered that temperature or light stimulated ABA production in sponges and hydroids, respectively, and that ABA stimulated specific functional responses to these environmental challenges. These functional responses were mediated by a signaling pathway sequentially involving cAMP, protein kinase A (PKA), cADPR and intracellular Ca^{2+} movements [1,2,11]. These discoveries warranted further investigations into the role of ABA in cell-specific functions of higher Metazoa.

ABA receptors and signaling. Among the several receptors identified in different plant tissues, a putative G-protein coupled receptor (GCR2) [12] indeed showed a significant amino acid sequence identity with a mammalian family of proteins, the lanthionine synthetase C-like protein (LANCL) family. GCR2 has since been disputed as a G protein-coupled receptor and its homology with the bacterial lanthionine synthetase protein superfamily, which catalyzes the addition of the thiol of cysteine to dehydrated serine in the biosynthesis of lanthionine-containing peptides (lanthipeptides) with antibiotic properties, has instead been advocated [13], a homology that also pertains to the mammalian LANCL proteins. Although the current consensus is that the PYR/PYL/RCAR family of intracellular receptors are the principal ABA receptors in land plants [14], the homology between mammalian LANCL proteins and plant GCR2 suggested to explore the possibility that they were implicated in ABA sensing. A role for the LANCL protein family in lanthionine biosynthesis has since been ruled out [15]. The LANCL family comprises three proteins: LANCL1 is the most highly expressed in mammals, particularly in the brain, and is a cytosolic protein; LANCL2 is membrane-anchored through its myristoylated N-terminal [16] and LANCL3 has the lowest expression levels of the LANCL proteins and appears to be cytosolic. The three proteins are encoded on chromosomes 2, 7 and X, respectively [17,18]. As the triple knockdown of LANCL1, LANCL2 and LANCL3 does not reduce the brain content of a downstream metabolite of lanthionine, lanthionine ketimine, it has been concluded that mammalian LANCL proteins are not involved in lanthionine synthesis [15], leaving their role in mammalian physiology open to investigation. The membrane-bound location of LANCL2 first attracted interest in this protein as a putative mammalian ABA receptor; indeed, several *in vitro* studies indicate that human recombinant LANCL2 binds ABA with a high affinity (K_d 2.6 nM) [19,20] and is required for ABA action in several different mammalian cell types [21]. LANCL2 has an unusual behavior as a hormone receptor as it is coupled to a G protein when membrane bound, but can also detach from the membrane when de-myristoylated and accumulate in

the cell nucleus [16]. Indeed, the nuclear translocation of LANCL2 occurs following ABA binding [22]. This behavior appears to combine features typical of the receptors for peptide (G protein coupling) and for steroid hormones (nuclear translocation), perhaps a heritage of the primordial origin of the hormone or the result of the solubility features of ABA. Binding of ABA to LANCL2 bound to the inner plasma membrane layer requires influx of the hormone through the plasma membrane, which occurs through transporters of the anion exchanger (AE) superfamily [23]. Protonated ABA can diffuse through the lipid bilayer [24]; however, a very low percentage of ABA is protonated at the near-neutral pH of plasma and interstitial liquid. For this reason, the presence of a transport system is essential for ABA trafficking between extra- and intracellular fluids. Conversely, the strongly acidic pH present in the stomach probably allows the diffusion of protonated ABA through the gastric lipid bilayer, accounting for the rapid absorption of the hormone after oral intake [7]. The signaling pathway downstream of LANCL2 has been studied in the target cells of the immune (monocytes, macrophages and T lymphocytes) [4,25] and of the metabolic actions of the hormone (adipocytes and muscle cells) [26,27]. In innate immune cells, such as granulocytes, ABA binding to its receptor leads to the activation of adenylate cyclase (AC) and the subsequent phosphorylation and activation of the ADP-ribosyl cyclase CD38 by PKA. The product of the enzyme action of CD38 on its substrate NAD^+, cADPR, then triggers an intracellular Ca^{2+} rise due to both intracellular Ca^{2+} release from ryanodine-sensitive endoplasmic Ca^{2+} channels and to extracellular Ca^{2+} influx due to ADPR-gated plasma membrane Ca^{2+} channels. Moreover, ABA binding to its receptor leads to the activation of phospholipase C (PLC), the overproduction of inositol-1,4,5-trisphosphate (IP_3) and the stimulation and activation of a protein kinase C (PKC)-dependent AC [4]. This sequence of events closely parallels the ABA signaling pathway first described in marine sponges [1]. The transcriptional effects of ABA observed on hemopoietic progenitors are also likely mediated by the observed increase of intracellular cAMP and the consequent activation of the cAMP-responsive transcription factor CREB [6]. A role for NF*k*B in the micromolar ABA-induced activation of the transcription of cyclooxigenase-2 has also been observed in quartz-stimulated rat alveolar macrophages [5], again pointing to intracellular Ca^{2+} movements as an important feature of the ABA signaling pathway in inflammatory cells. The effect of ABA on cells of the hemopoietic lineage (progenitors and innate immune cells) occurs at low micromolar concentrations, thus it is possible that a different signaling pathway is activated by the low nanomolar concentrations exerting its metabolic actions. The signaling pathway downstream of LANCL2 in macrophages and regulatory T cells was studied in silico by Leber et al., suggesting a role for this receptor in the induction of regulatory responses in macrophages and T cells during *H. pylori* infection [28]. In adipocytes, stimulation by ABA of glucose uptake *via* GLUT4 involves the activation of phosphoinositide 3-kinases (PI3K).

Interestingly, the N-terminal sequence of LANCL2 has been shown to bind to phosphatidylinositol phosphates (PIPs), particularly PI3P, on the plasma membrane, suggesting a spatial as well as functional correlation between LANCL2-dependent and PI3P-mediated signaling. In muscle cells, AMP-activated protein kinase (AMPK) appears to mediate the nanomolar ABA-induced increase of glucose transport, since the effect of ABA is abrogated by pre-treatment of cultured myocytes and of murine muscle biopsies with the AMPK inhibitor dorsomorphin [26]. Activation of AMPK in the ABA-signaling pathway is in sharp contrast with the signal transduction activated by insulin, which results in the inactivation of AMPK by Akt/PKB-mediated phosphorylation. Indeed, the effect of ABA on energy metabolism appears to be different from that of insulin, pointing to non-overlapping physiological functions of these hormones. Glucose intake induces an increase of plasma ABA (ABAp) and one could hypothesize that this hormone provides the first response to nutrient availability, stimulating muscle glucose uptake and thermogenic energy expenditure. Persistence of hyperglycemia, despite the action of ABA and in excess of muscle energy requirement, then results in insulin release and in the activation of the metabolic responses to nutrient abundance (glycogen and fatty acid synthesis, adipocyte differentiation and accumulation of triglycerides) (**Figure 2**). Interestingly, in 3T3-L1-derived murine adipocytes the siRNA-mediated downregulation of LANCL2 expression reduces both the ABA- and insulin-induced glucose uptake and downregulates Akt phosphorylation after insulin treatment [27], suggesting that levels of LANCL2 expression in adipocytes could affect insulin sensitivity.

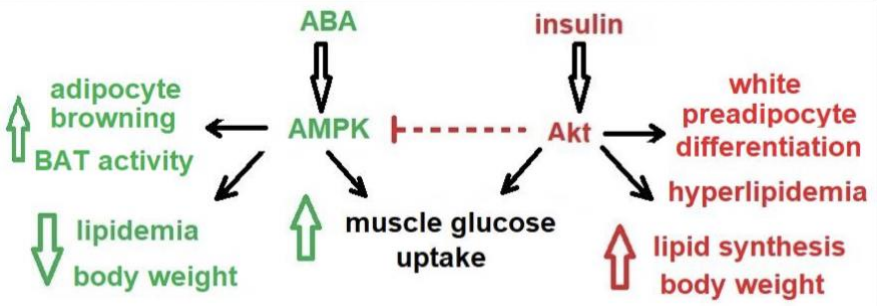

Figure 2. Non-overlapping roles of ABA and insulin in the regulation of energy metabolism.

ABA in glycemia control and adipocyte function. The response to hyperglycemia in mammals is mainly controlled by the interplay between two peptide hormones: insulin, released by pancreatic islet β-cells stimulated by high extracellular glucose levels, and the incretin glucagon-like peptide 1 (GLP-1), released by entero-endocrine cells stimulated by nutrients in the gut. GLP-1 in turn stimulates insulin release and suppresses the release of glucagon, the main glycemia-increasing hormone, from pancreatic islet α-cells. ABA stimulates the glucose-independent release of GLP-1 from enteroendocrine cells *in vitro* and the increase of plasma GLP-1 in fasted rats [29]. ABAp

increases after an oral glucose load in healthy humans, but not in subjects with type 2 diabetes (T2D) or with gestational diabetes (GDM). In the latter case, the resolution of the diabetic state that follows childbirth is accompanied by the restoration of a normal glycemic profile, suggesting a critical role for ABAp in the maintenance of a normal glucose tolerance and a new possible ABA-centered pathogenetic mechanism that may underlie the diabetic condition [30]. Low-dose oral ABA reduces glycemia and insulinemia in rats and in healthy humans undergoing a glucose load. The fact that ABA administration reduces both glycemia and insulinemia suggested that the mechanism underlying the glycemia-lowering action of low-dose ABA *in vivo* could depend on the stimulation of peripheral glucose uptake [7]. The identification of a second hormone beside insulin capable of stimulating muscle glucose uptake would bear significant consequences in clinical conditions where insulin deficiency or insulin resistance reduce glucose tolerance. Activation by ABA of the transcription and phosphorylation of AMPK opens new perspectives on the signaling pathways activated by the hormone. AMPK phosphorylates and inhibits the transcriptional activity of PPAR-γ, the main regulator of adipogenesis, thereby preventing the differentiation of preadipocytes [31] and triglyceride accumulation [32]. On the other side, AMPK is also an upstream positive regulator of p38 MAPK [33], which promotes PPAR-γ phosphorylation on Ser122, thus preventing PPAR-γ mediated inhibition of GLUT4 expression [34,35]. The partial suppression of the transcriptional activity of PPAR-γ in heterozygous PPAR-γ-deficient mice results in an improved insulin sensitivity and in a reduced tendency to obesity [36,37] and mice chimeric for wild-type and PPAR-γ null cells exhibit little or no contribution to adipose tissue formation by null cells [38]. The observations that low-dose ABA significantly reduces body weight in mice fed a high-glucose diet and in humans [39] and improves muscle glucose uptake are in agreement with the activation of AMPK in adipocytes and muscle cells. Downstream of LANCL2, ABA stimulates muscle glucose transports in an insulin-independent manner *via* activation of the AMPK/PGC-1α axis [26]. LANCL2 is also an activator of mTORC2 [40] and interacts with PPAR-γ, allowing PPAR-γ-mediated activation of adipogenic genes during insulin-stimulated triglyceride accumulation in white adipocytes [41]. Interestingly, LANCL2 is also involved in the activation of transcription of several browning genes in brown adipocytes *in vitro* and *in vivo* [27]. The observations that ABA is released from human adipose tissue (AT) stimulated with high glucose concentrations [3] suggest that AT could be both a producer and a target of ABA. Adipose tissue is one of the largest organs in the body and plays an important role in energy balance and glucose and lipid homeostasis. Two types of AT are present in mammals, white AT (WAT) and brown AT (BAT). WAT functions to store energy *via* synthesis of triglycerides (TGs), that accumulate in lipid vesicles, whereas BAT specializes in energy expenditure [42,43]. Excess WAT is related to several metabolic disorders as obesity, the metabolic syndrome, T2D and

cardiovascular disease [44]. Systemic insulin resistance is observed in mice lacking GLUT4 in adipocytes, indicating that glucose metabolism in these cells is critical to whole-body glucose homeostasis [45]. Insulin responsiveness is acquired during the maturation phase of adipocyte differentiation (adipogenesis) and involves the expression of proteins responsible for the specific functions of adipocytes, such as GLUT4, adiponectin and leptin, which are key regulators of adiposity and glucose homeostasis [46]. Gene expression profiling in AT has demonstrated that several genes related to adipocyte differentiation are decreased in T2D patients and in animal models of T2D, suggesting that altered or impaired adipocyte differentiation may underlie or promote the development of insulin resistance [47,48,49]. In contrast, BAT plays an important thermogenic function, helping to counteract the cold stress. In adult mammals, BAT has the capacity to modulate energy balance by degrading fatty acids (FA) and dissipating the energy produced as heat. Interestingly, brown fat-like cells (also known as beige cells) have been identified in WAT and studies have demonstrated that an increase of beige adipocytes in WAT enhances whole-body energy expenditure and should be expected to reduce the risk of diet-induced obesity and metabolic diseases [50,51]. The main transcriptional factors involved in the adipogenesis of brown and white adipocytes are PPAR-γ and several other transcription factors, notably the CCAAT/enhancer binding protein (C/EBPα) and sterol regulatory element-binding protein (SREBP) [52]. Among them, PPAR-γ is considered to be the main regulator of adipocyte differentiation [53,54,55]. Active PPAR-γ dimerizes with retinoid X receptor (RXR) [56] and binds specific DNA sequences to promote the transcription of several genes involved in insulin signaling, lipid and glucose metabolism and endocrine function in adipocytes. PPAR-γ activates the adipose tissue-specific form of adipocyte protein 2 (AP2), which in turn regulates the transcription of adipokines (leptin and adiponectin) and of other proteins (lipoprotein lipase and adipose differentiation related protein) which modulate lipid metabolism in response to insulin [52,55]. Association of PPAR-γ with PR domain-containing protein 16 (PRDM16) and the PPAR-γ coactivator 1α (PGC-1α) initiates selective induction of brown adipogenic and thermogenic gene expression [57]. PPAR-γ also induces PGC-1α, which exerts a positive feedback on PPAR-γ and promotes uncoupling protein 1 (UCP1) expression [58], a key marker of BAT, responsible for the regulated uncoupling of mitochondrial oxidative phosphorylation.

Role of LANCL1 as an ABA receptor in muscle and adipose tissue? Unlike inflammatory cells, where LANCL2 silencing abrogates the response to ABA [21], in adipocytes and muscle cells, silencing of LANCL2 reduces, but does not eliminate, the effect of ABA [3], suggesting a role for other receptors in the metabolic action of the hormone. A more direct indication that other receptors could contribute to mediate the metabolic actions of ABA comes from studies on LANCL2 knock-

out mice. Indeed, in C57Bl/6 mice, the genetic ablation of LANCL2 did not modify fasting glycemia values but resulted in the reduction of glucose tolerance compared with wild-type siblings, as indicated by a significantly increased AUC of glycemia after an oral glucose load; however, LANCL2$^{-/-}$ (KO) mice were still responsive to exogenous ABA, which significantly reduced the AUC of glycemia after glucose load, to values similar to those of wild-type (WT) animals (**Figure 3**) [59].

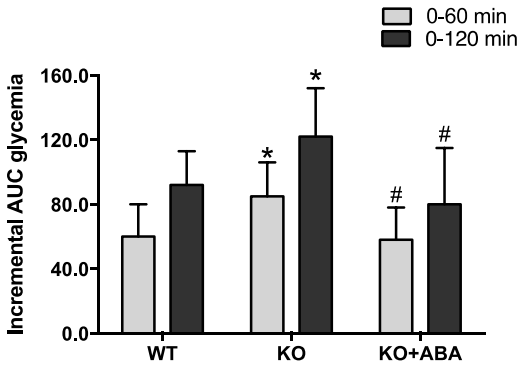

Figure 3. Male, seven week-old LANCL2$^{-/-}$ mice (KO) and their wild-type siblings (WT), 9 per group, were subjected to an oral glucose tolerance test (OGTT). Incremental AUC of glycemia calculated, in the indicated time frames, with the trapezoidal rule on the glycemia increase relative to time zero in WT and KO mice undergoing an OGTT with or without ABA at 1 μg/kg body weight (BW), in addition to glucose. LANCL2$^{-/-}$ mice have a reduced glucose tolerance but respond to ABA. *$p < 0.02$ relative to WT and $^{\#}p < 0.03$ relative to KO.

This result clearly indicates that the genetic ablation of LANCL2 negatively affects glucose tolerance. The fact that exogenous low-dose ABA (1 μg/kg body weight (BW)/day) improved glucose tolerance in LANCL2$^{-/-}$ mice suggests that another receptor can substitute for LANCL2 in the stimulation of muscle and adipose tissue glucose transport, although at higher ABA concentrations than those reached by the endogenous hormone. Indeed, intake of ABA at a dose of 1 μg/kg BW increases ABAp between 10 and 50 times compared to basal, endogenous levels in humans [7]. These high plasma concentrations, obtained by pharmacologic intervention, could activate a low-affinity receptor not normally participating in endogenous ABA signaling. An obvious candidate for this role is LANCL1, as it shares a significant sequence identity (54.2%), similar intracellular localization and tissue expression pattern with LANCL2. This study aimed at investigating whether LANCL1 could behave as an ABA receptor similarly to LANCL2. To test this hypothesis, I performed several experiments on glycemic and lipidemic control in a rat myoblast cell line and in human brown and white adipocytes, understanding the role of the ABA/LANCL1-2 system *via* the AMPK/PGC-1α/Sirt1 signaling pathway.

2. MATERIALS AND METHODS

2.1. Vector construction

2.1.1. Cloning of LANCL1 and LANCL2 in pGEX-6-P1 vector

Total RNA was extracted from HeLa cells using the RNeasy Micro Kit (Qiagen, Milan, Italy) according to the manufacturer's instructions and reverse transcribed into cDNA using the iScriptTM cDNA Synthesis Kit (Bio-Rad, Milan, Italy). The full-length human LANCL1 cDNA was amplified by PCR using the following primers: 5'-ATTGAATTCATGGCTCAAAGGGCCTTC-3' (forward-EcoRI restriction site underlined) and 5'-AATCTCGAGTCAGAGTTCAAATGCAGGGAA-3' (reverse-XhoI restriction site underlined) for the cloning in pGEX-6-P1 vector (GE Healthcare, Milan, Italy). The full-length human LANCL2 cDNA was amplified by PCR using the following primers: 5'-ATTGAATTCATGGGCGAGACCATGTCAAAG-3' (forward-EcoRI restriction site underlined) and 5'-AATCTCGAGTTAATCCCTCTTCGAAGAGTC-3' (reverse-XhoI restriction site underlined) for the cloning in pGEX-6-P1 vector (GE Healthcare, Milan, Italy). The PCR was performed in 25 µl containing 1X Reaction Buffer, 300 µl dNTP, 7.5 pmol of primers and 2.5 units of Pfx50^{TM} DNA Polymerase (Thermo Fisher Scientific, Milan, Italy). The PCR reaction profile was 1 cycle at 94°C for 2 min, 35 cycles at 94°C for 15 s, 60°C for 30 s and 68°C for 1 min with a final extension of 5 min at 68°C. The PCR products were purified from agarose gel with a QIAEX II Gel Extraction Kit (Qiagen, Milan, Italy), digested with related restriction enzymes (described above) and cloned into pGEX-6-P1 using a Rapid Ligation Kit (Roche, Milan, Italy). The LANCL1-pGEX-6-P1 and LANCL2-pGEX-6-P1 vectors were purified using Plasmid Mini Kit (Qiagen, Milan, Italy), sequenced by TibMolbiol (Genova, Italy) and used to transform *E. coli* BL21 (Agilent Technologies, Milan, Italy). The recombinant proteins produced by bacteria are LANCL1 and LANCL2 fused with glutathione S-transferase (GST); after purification, the GST part of the fusion proteins is cleaved by PreScission Protease to yield the final purified LANCL1 and LANCL2 proteins.

2.1.2. Cloning of LANCL1 and LANCL2 in pBABE vector

The full-length of human LANCL1 was amplified from 1 ng of the LANCL1-pGEX-6-P1 vector by PCR using the following primers: 5'-ATTGGATCCATGGCTCAAAGGGCCTTCCCG-3' (forward-BamHI restriction site underlined) and 5'-

AATGAATTCTCAGAGTTCAAATGCAGGGAACC-3' (reverse-EcoRI restriction site underlined) for the cloning in the pBABE vector (Addgene, MA, USA). The full-length of human LANCL2 was amplified from 1 ng of the LANCL2-pGEX-6-P1 vector by PCR using the following primers: 5'-ATTGAATTCATGGGCGAGACCATGTCAAAGAG-3' (forward-EcoRI restriction site underlined) and 5'-AATGTCGACTTAATCCCTCTTCGAAGAGTCAAG-3' (reverse-XhoI restriction site underlined) for the cloning in the pBABE vector (Addgene, MA, USA). The PCR amplification, digestion with restriction enzymes, purification of PCR products and cloning in the pBABE vector were performed as described for the LANCL1-pGEX-6-P1 and LANCL2-pGEX-6-P1 vectors in paragraph 2.1.1.

2.2. Expression and purification of recombinant human LANCL1 protein

E. coli BL21 cells containing vectors with the correct inserts were initially cultured in a Luria-Bertani medium (Difco, BD Italia, Rome, Italy) with 200 μg/ml ampicillin until the culture reached an A_{600} of 0.3. LANCL1-GST was expressed by adding isopropyl-b-D-thiogalactopyranoside (final concentration 0.1 mM) and incubating bacteria for 16 h at 20°C. Cells were harvested by centrifugation and lysed by sonication in 125 mM Tris-HCl pH 8.0 and 150 mM NaCl. After addition of Triton X-100 to a final concentration of 1% and incubation for 30 min at 4°C, lysates were centrifuged at 10000xg for 15 min. The LANCL1-GST fusion protein was purified by affinity chromatography using Glutathione (GSH)-Sepharose-4B (GE Healthcare, Milan, Italy) following the manufacturer's instructions. The release of native LANCL1 was achieved with the PreScission Protease (GE Healthcare, Milan, Italy) by incubating the GSH-Sepharose-bound fusion protein for 16 h at 4°C in Tris-HCl pH 7.5 and 150 mM NaCl. The PreScission Protease was preemptively activated in the presence of 1 mM dithiothreitol (DTT) for 30 min at 4°C; the final concentration of DTT in the cleaving incubation was less than 0.5 μM. The protein was concentrated through an Amicon Ultra 30 kDa (Millipore, Milan, Italy). Protein concentrations were determined by the Bradford assay (Bio-Rad, Milan, Italy) and protein purity was monitored by SDS-PAGE and by gel filtration; gels were stained with ProSieve Blue Protein Staining solution (Lonza, Milan, Italy). Size exclusion chromatography was performed using an HPLC system equipped with a TSKgel G3000SWXL column (Merck, Milan, Italy), with a mobile phase consisting of 50 mM Tris-HCl pH 7.5 containing 300 mM NaCl and at a flow rate of 0.7 ml/min. Unrelated negative control-GST fusion recombinant proteins were purified as described above for native LANCL1.

2.3. [^{3}H]ABA binding

The (±)-[^{3}H]-2-cis, 4-trans Abscisic acid ([^{3}H]ABA) saturation binding experiments were obtained with human LANCL1. Incubations were performed with 10 μg protein in 150 mM NaCl, 20 mM Phosphate Buffer pH 7.5 and 1 mM EDTA (binding buffer) in a final volume of 100 μL in triplicate for 60 min at 25°C with 0.05 μM (±)-[^{3}H]ABA (20 Ci/mmol, Biotrend Radiochemicals, Köln, Germany) and in the presence of increasing concentrations of unlabeled (±)-ABA (50 nM-5 μM) (Merck, Milan, Italy). At the end of incubation, samples were filtered on 0.2 μm-nitrocellulose membranes (Bio-Rad, Milan, Italy); the filters were washed with 3.5 ml of an ice-cold binding buffer and then dried; the radioactivity was measured in 4.0 ml Ultima-Gold (Perkin Elmer, Italy) with a Packard ß-counter. The specific (±)-[^{3}H]ABA binding was calculated as the difference between the total binding and nonspecific binding, obtained with excess unlabeled (±)-ABA (5.0 μM). The maximal binding capacity (B_{max}) and the dissociation constant (K_d) were calculated using the program Saturation Binding in the GraphPad Prism 7.0 Software (San Diego, CA, USA). In this program, the data are analyzed by nonlinear regression fit.

2.4. Surface plasmon resonance (SPR)

The direct binding of unlabeled ABA to recombinant human LANCL1 was measured by surface plasmon resonance (SPR) on a Biacore T200 instrument (GE Healthcare, Milan, Italy) at 25°C using a CM7 sensor chip (GE Healthcare, Milan, Italy). First, we evaluated the pre-concentration ability of the chip in a range of pH values compatible with protein stability (10 mM Na acetate, pH 5.5, 5.8, 6.0 and 6.5) at a standard concentration (30 mg/ml). The covalent coupling of human LANCL1 was then performed using 10 mM Na acetate pH 5.8 through standard amine coupling. A surface without the immobilized protein was used as a reference channel. All experiments were performed with a running buffer consisting of PBS with the addition of 0.05% Tween 20 (PBS-P) using a flow rate of 30 μl/min. Evaluation of (±)ABA binding to human LANCL1 was performed by injecting ABA dissolved in PBS-P at 1, 2.5, 5, 10 and 20 μM at a flow rate of 30 ml/min, with a contact time of 30 s and a dissociation time of 120 s. Bound ABA was removed by a subsequent regeneration step through the injection of 1 M NaCl for 30 s at 30 μl/min. The obtained sensorgrams were used for equilibrium state affinity analysis using the Biacore Evaluation Software version 3.1 (GE Healthcare, Milan, Italy).

2.5. Fluorescence quenching study on the interaction of recombinant LANCL1 with ABA

For quenching titrations, small aliquots of ABA were added to human LANCL1 (8.65 μM) from a stock solution (100 μM) to obtain a molar ratio ranging from 1:2 to 1:450; the fluorescence spectra were recorded after each addition. Fluorescence intensities were corrected for volume changes before further analysis of the quenching data. All emission spectra were recorded on a luminescence spectrometer (Perkin Elmer LS50B, Italy) at l_{ex}=280 nm (slit width=5 nm). Absorption measurements were made using a Shimadzu UV-2700 spectrophotometer. To eliminate the inner-filter effects, the fluorescence intensities were corrected by the equation described in [60]. The dynamic quenching constants were determined using the Sterne Volmer equation: $F_0/F=1+K_{SV}[Q]$, where F_0 and F correspond to the fluorescence intensities of LANCL1 without ABA and with ABA, respectively; [Q] is the concentration of ABA and K_{SV} is the Sterne Volmer quenching constant [61]. The static quenching constant, K_a, and the number of binding sites, n, between LANCL1 and ABA were calculated using the following equation: $\log[(F_0-F)/F]=\log K_a+n\log[Q]$.

2.6. Binding of 8-Anilinonaphthalene 1-Sulfonic Acid (ANS) to recombinant human LANCL1

To evaluate the effect of pH on human LANCL1 unfolding, we monitored the ANS emission after the addition of small quantities of HCl 1M or of NaOH 1M to the protein solution. Two aliquots of LANCL1 in 10 mM Na acetate and Na phosphate buffer were analyzed in parallel. The pH was measured by a micro pH electrode. To assess the exposure of hydrophobic protein domains, 2.5 μL of 500 μM ANS in PBS was added to 47.5 μL of LANCL1 solution to obtain a final concentration of 25 μM ANS. The concentration of LANCL1 in Na acetate and Na phosphate was 6.4 μM and 5.4 μM, respectively. The resulting fluorescence was measured using a Luminescence Spectrometer Perkin Elmer LS50B. ANS was excited at λ_{ex}=360 nm (slit width=5 nm), the emission spectrum was recorded from 420 nm to 560 nm (slit width=5 nm) and emitted fluorescence at λ_{em}=460 nm was followed. The fluorescence experiments were repeated at least twice for each sample.

2.7. Circular dichroism spectroscopy (CD)

For the CD experiments, all samples were placed into 0.5 cm-path length quartz cuvettes; the spectra from 200 to 250 nm were obtained using a Jasco J-500A Spectropolarimeter (Japan) equipped with a Jasco IF-500-2 data processor. The spectropolarimeter was calibrated with an aqueous solution of (1S)-(+)-10-camphor sulfonic acid at 290.5 nm. The spectrum at each pH value was obtained by

averaging three scans from 200 to 250 nm at a rate of 20 nm/min with a step resolution of 0.2 nm, a time constant of 4 s and a bandwidth of 2.0 nm. All spectra were corrected by subtracting the background of the Na phosphate or Na acetate buffer solutions.

2.8. Cell culture

HEK-293T cell line was purchased from ATCC (ATCC CRL-3216) and HEK-Platinum-A (Plat-A) cell line was provided by Cell Biolabs (RV-102) (**Figure 4**). Both were cultured in DMEM containing 10% fetal bovine serum (FBS), 100 IU/ml penicillin and 100 μg/ml streptomycin.

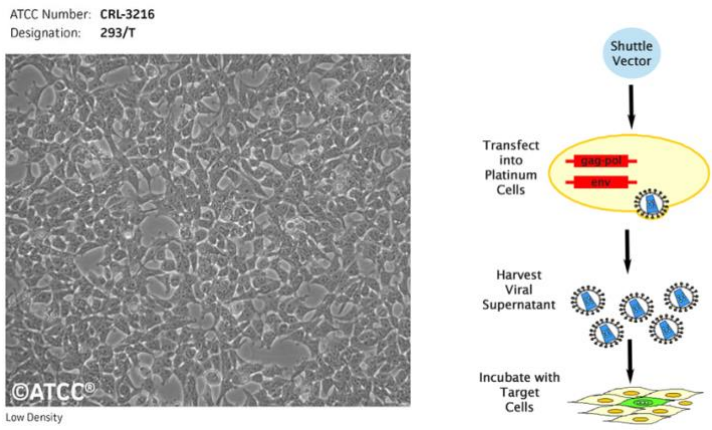

Figure 4. HEK-293T cell line (left panel) and retrovirus production in packaging cells (right panel).

Rat L6 myoblasts (ATCC CRL-1458) (**Figure 5**) were maintained in a humidified 5% CO_2 atmosphere at 37°C with Dulbecco's modified Eagle's medium (DMEM) supplemented with 10% FBS, 100 IU/ml penicillin and 100 μg/ml streptomycin.

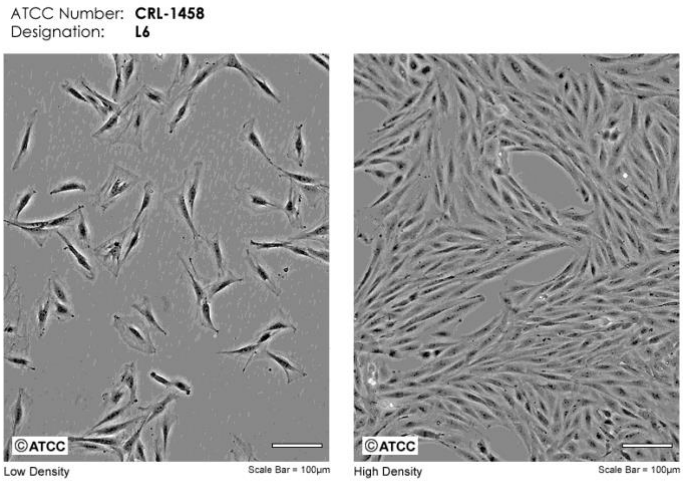

Figure 5. Rat L6 myoblasts.

TERT-immortalized polyclonal brown and white pre-adipocyte cell models (TERT-hBA and TERT-hWA, respectively) (**Figure 6**) were kindly provided by Professor Jacob B. Hansen from Department of Biology of the University of Copenhagen (Denmark) and cultured in Advanced DMEM/F12 supplemented with 10% FBS, L-glutamine (2 mM), penicillin (62.5 μg/ml), streptomycin (100 μg/ml) and basic fibroblast growth factor (bFGF) (2.5 ng/ml). The cells were kept at 37°C in a humidified atmosphere with 5% CO_2.

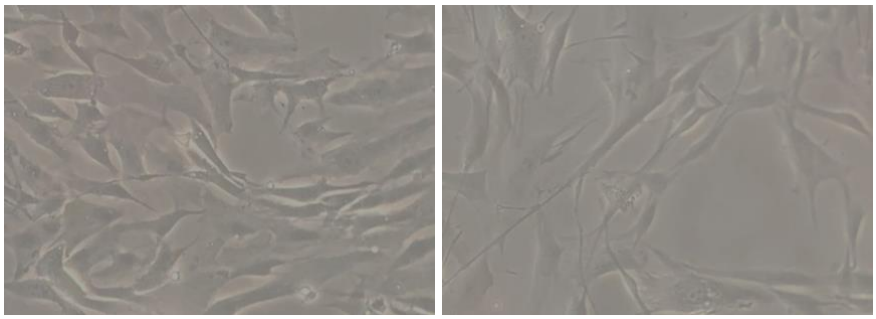

Figure 6. TERT-hBA (left panel) and TERT-hWA (right panel) cells.

2.9. Lentiviral and retroviral cell transduction

The lentiviral plasmids pLV[shRNA]-Puro-U6 encoding for a control scramble shRNA (shRNA-SCR), for the shRNA targeting rat LANCL1 (shRNA-L1) and for the shRNA targeting rat LANCL2 (shRNA-L2) (plasmid ID: VB010000-0005mme, VB181016-1107sen, VB181016-1124zjp), were purchased from Vector Builder (Chicago, IL, USA). Overexpression of human LANCL1 (ovLANCL1) and human LANCL2 (ovLANCL2) was obtained in rat L6 myoblasts using pBABE vectors constructed as described before, with the empty vector pBABE (Addgene) as negative control (PLV). To obtain L6 cells stably silenced or overexpressed for LANCL1 and LANCL2, the following protocols were used. For silencing of LANCL1 and LANCL2, Lentiviral Vector Particles (LVPs) were generated in HEK-293T cells. Briefly, HEK-293T cells were plated (3×10^5 cells on 6-cm plates) in Dulbecco's modified Eagle medium, 10% FBS and 1% penicillin-streptomycin. After 24 hours, cells were cotransfected with a Δ891 and a VSV-G encoding vector along a shRNA transfer lentiviral plasmid (in parallel, shRNA-SCR, shRNA-L1 or shRNA-L2) using TransIT® Transfection Reagent (Mirus, Madison, USA). After another 24 hours, the HEK-293T medium was changed with Dulbecco's modified Eagle medium, 10% FBS and 1% penicillin-streptomycin to promote viral production. The supernatant containing lentiviral particles was collected 48 and 72 hours after transfection, filtered with a 0.45-μm-diameter filter and used to infect L6 cells (1×10^6 cells on 10-cm plates) in the presence of protamine sulfate (final concentration 5 μg/mL). After the second cycle of infection, cells were selected with puromycin (5 μg/mL). The knockdown efficiency was validated

by evaluating LANCL1 and LANCL2 mRNA and protein levels by Real Time PCR and Western blot analysis, respectively. For overexpression of LANCL1 and LANCL2, we used the same method described before, except for the plasmids (previously indicated) and the cells used for retrovirus packaging (HEK-Plat-A cells). Overexpression efficiency was assessed using Western blot analysis. This last procedure was also performed for overexpression of LANCL1 and LANCL2 on human TERT-hBA and TERT-hWA pre-adipocytes.

2.10. qPCR analysis

After sacrifice, quadriceps muscles and samples of interscapular brown adipose tissue (approximately 30 mg) were taken from mice chronically treated with or without ABA for 4 weeks (1 μg/kg BW/day administered in the drinking water). L6 cells and brown and white pre-adipocytes were instead incubated with or without 100 nM ABA for 4 hours. Total RNA was extracted from muscle and brown adipose tissue of mice using QIAzol Lysis Reagent and Tissue Lyser instrument (Qiagen, Milan, Italy) and from rat myoblasts and human pre-adipocytes using RNeasy Micro Kit (Qiagen, Milan, Italy) according to the manufacturer's instructions. The cDNA was synthesized by using iScript cDNA Synthesis Kit (Bio-Rad, Milan, Italy) starting from 1 μg of total RNA and was used as a template for qPCR analysis: reactions were performed in an iQ5 Real-Time PCR detection system (Bio-Rad, Milan, Italy). The mouse-, rat- and human-specific primers were designed using Beacon Designer 2.0 software (Bio-Rad, Milan, Italy) and their sequences are listed in **Table 1** (primer sequences used to amplify mouse target genes), **Table 2** (primer sequences used to amplify rat target genes) and **Table 3** (primer sequences used to amplify human target genes). Each sample was assayed in triplicate in a 25 μl amplification reaction, containing 4 ng of cDNA, primers mixture (0.4 μM each of sense and antisense primers) and 12.5 μl of 2X iQ SYBR Green Supermix Sample (Bio-Rad, Milan, Italy). The amplification program included 40 cycles of two steps, each comprising heating to 95°C and to 62°C, respectively. Fluorescence products were detected at the last step of each cycle. To verify the purity of the products, a melting curve was produced after each run. Values for human, mouse and rat genes were normalized on hypoxanthine-guanine phosphoribosyltransferase-1 (Hprt1) and ß-Actin mRNA expression. Statistical analysis of the qPCR was performed using the iQ5 Optical System Software version 1.0 (Bio-Rad Laboratories) based on the $2^{-\triangle\triangle Ct}$ method [62]. The dissociation curve for each amplification was analyzed to confirm the absence of nonspecific PCR products.

Table 1

Mouse genes	Accession N°	Forward Primer 5'-3'	Reverse Primer 5'-3'
Actb	NM_007393	GCGAGAAGATGACCCAGATC	GGATAGCACAGCCTGGATAG
Hprt1	NM_013556	CCCTGGTTAAGCATACAGCCCC	AGTCTGGCCTGTATCCAACACTTCG
Lancl1	NM_001190985	GAGGGCCTTTCCGAATCCTT	GGAGTCAGCCTCCCAGTAGA
Lancl2	NM_133737	GCCTCCCTTTCCACCCTAACG	GTCCGCTGTCTTCAGTCCTTCC
MT-DNA	AP014941	CCGTCACCCTCCTCAAATTA	GGGCTAGGATTAGTTCAGAGTG
Nampt	NM_021524	AATGTCTCCTTCGGTTCTGGTG	CCCGCTGGTGTCCTATGTAAAG
Ppargc1a	NM_008904	CCCTGCCATTGTTAAGACC	TGCTGCTGTTCCTGTTTTC
Prkaa1	NM_001013367	AGAAGCAGAAGCACGACGG	TTGCCCACCTTCACTTTCCC
Sirt1	NM_019812	GCAGGTTGCAGGAATCCAAAGGA	GGGCACCGAGGAACTACCTGA
Sirt6	NM_181586	GGCTACGTGGATGAGTGAT	GGCTCAGCCTTGAGTGCTAC
Slc2a1	NM_011400	GCCCATCCCATCCACCACACTC	CCATAAGCACAGCAGCCACAAAGG
Slc2a4	NM_009204	CCAGCCTACGCCACCATAG	TTCCAGCAGCAGCAGAGC
Sln	NM_025540	CAGGAGCTGTTTATCAACTTCACA	TTGGTAGGACCTCACGAGGAG
Ucp1	NM_009463	GGAGGTGTGGCAGTGTTCAT	AAGCATTGTAGGTCCCCGTG
Ucp3	NM_009464	CCCTCTGCACTGTATGCTGAA	CATCACGTTCCAAGCTCCCA

Table 2

Rat genes	Accession N°	Forward Primer 5'-3'	Reverse Primer 5'-3'
Actb	NM_031144	GGGAAATCGTGCGTGACATT	GCGGCAGTGGCCATCTC
Hprt1	NM_012583	TTGGTCAAGCAGTACAGCCC	TGGCCTGTATCCAACACTTCG
Lancl1	NM_053723	TCTTGCTCCTCATCCTGCTCATC	CACTGTACTCGCCGAAGGTCTC
Lancl2	NM_001014187	GGTGCCACGGTGCTCCAG	CCTCGCTGCCAAATCACATCAC
MT-DNA	KJ530565	CCGTCACCCTCCTCAAATTA	ATTCCAAGCACACTTTCCAGT
Nampt	NM_177928	TCGGTTCTGGTGGAGGTTTGCTAC	TCCCTGCTGGCGTCCTATGTAAAG
Ppargc1a	NM_031347	GCACACATCGCAATTCTCCC	CTCTGCGGTATTCGTCCCTC
Prkaa1	NM_019142	AGAAGCAGAAGCACGACGG	GAAGGTGCCGACGCCC-
Sirt1	NM_001372090	CAGTGTCATGGTTCCTTTGC	CACCGAGGAACTACCTGAT
Slc2a1	NM_138827	GACCCTGCACCTCATTGGT	CTCAGATAGGACATCCAGGGC
Slc2a4	NM_012751	CCAGCCTACCGCCACCATAG	TTCCAGCAGCAGCAGAGC
Sln	NM_001013247	CAGGAGCTGTTTATCAACTTCACA	TTGGTAGGACCTCACGAGGAG
Tbc1d1	XM_032917081	AGTCAGGACCCGAGCTACTT	CTGCCGGATGGAGCTAATGA
Ucp1	NM_012682	CTTCCCTCAGGATTGGCCTC	GTCATCAAGCCAGCCGAGA
Ucp3	NM_013167	CCCCCTACACTGTATGCTGA	TTCCAGGATCCCAGACGCA

Table 3

Human genes	Accession N°	Forward Primer 5'-3'	Reverse Primer 5'-3'
Ucp1	NM_021833	GTGTGCCCAACTGTGCAATG	GTTCCAGGATCCAAGTCGCA
Ucp3	NM_022803	ATACAGCGGGACTATGGACG	ACCTCAGCACAGTTGACGAT
Slc2a4	NM_001042	AATGCTGCTGCCTCCTATG	ATCAGAATGCCGATAACAATGG
PPARG	NM_138712 NM_015869	CGAAGACATTCCATTCACAAG	CTCCACAGACACGACATTC
CPT1B	NM_004377	AAACAGTGCCAGGCGGTC	CGTCTGCCAACGCCTTG
CIDEA	NM_001279	AGGCAGGTTCACGTGTGGATA	GAAACACAGTGTTTGGCTCAAGA
MT-DNA	AY665667	CCCACCCAAGAACAGGGTTT	TAGGAGGTTGGCCATGGGT
MPC1	NM_001376568	CCTCGGAACTGGCTTCTGTT	CTCGTGTTTGATAAGCCGCC
PDHA1	NM_001173456	ATGGATATCCTGTGCGTCCG	GTGTCCGTGGTAACGGTAAGT
ADRB3	NM_000025	CCTCCAACATGCCCTACGTG	CGTAGACGAAGAGCATCACGA
c-erbA-1	X55005	ATGACACGGAAGTGGCTCTG	AGGTACGCCTCCTGACTCTT
THRB	NM_000461	AGCCACTGGAAGCAAAAACG	CTTTCCACCTTCTGGGGCAT
INSR	AH002851	CTGGGTTTCAAGCGGAGCTA	AAGGATTGGACCGAGGCAAG
Prkaa1	NM_006251	TACATTCTGGGTGACACGCT	AGGCTCCGAATCTTCTGTCG
Sirt1	AF083106	AGGCCACGGATAGGTCCATA	GTGGAGGTATTGTTTCCGGC
Ppargc1a	NM_001330751	CTGTGTCACCACCCAAATCCTTAT	TGTTCGAGAAAAGGACCTTGA
Lancl1	NM_006055	TCTCACAACGCTTGACCAATAAG	GCCCAGCCAGTGTAACCG
Lancl2	AF353942	AGGCGTACAAGGTCTTTAAGGAG	GCTCGGTAGAGGTACTTCTTATCC
Hprt1	NM_000194	GGTCAGGCAGTATAATCCAAAG	TTCATTATAGTCAAGGGCATATCC
Actb	XM_005249818	AATGAGCTGCGTGTGGCTCC	CAATGGTGATGACCTGCCG

2.11. Western blot and subcellular fractionation

L6 rat myoblasts (1 x 10^6/well) and brown and white human pre-adipocytes (1 x 10^6/well) were seeded in 6-well plates. After 24 hours, the supernatant was removed, cells were washed once in Krebs-Ringer HEPES buffer (KRH) and then incubated in KRH with 5 mM glucose for 60 min at 37°C with or without 100 nM ABA. After removal of the supernatant, the cells were scraped in a volume of 300 μL lysis buffer (20 mM Tris-HCl pH 7.4, 150 mM NaCl, 1 mM EDTA, 1% NP40) containing a protease inhibitor cocktail. After brief sonication, the protein concentration was determined on an aliquot of each lysate. Western blot experiments were also performed on quadriceps muscles isolated from wild type or LANCL2$^{-/-}$ mice, either treated or not treated with 100 nM ABA. After the explant, muscles were lysed with Tissue Lyser (Qiagen, Milan, Italy) and centrifuged for 10 min at 12000xg; the supernatants were analyzed by Western blot. Lysates (70 μg proteins from tissues and 30 μg proteins from cells) were loaded on 10% polyacrylamide gel and separated by SDS-

PAGE and proteins were transferred to nitrocellulose membranes (Bio-Rad, Milan, Italy) according to standard procedures. The membranes were blocked for 1 h with 20 mM Tris-HCl pH 7.4, 150 mM NaCl and 1% Tween 20 (TBST) containing 5% non-fat dry milk and incubated for 1 h at room temperature with primary antibodies (**Table 4**). Following incubation with the appropriate secondary antibodies (**Table 4**) and ECL detection (GE Healthcare, Milan, Italy), band intensity was quantified with the ChemiDoc imaging system (Bio-Rad, Milan, Italy).

Table 4

Primary Antibody	**Host**	**Concentrations**	**Manufacturer**
Anti-LANCL1	Rabbit	1:250	Novus Biologicals
Anti-LANCL2	Mouse	1:1000	[63]
Anti-PGC-1α	Mouse	1:1000	Sigma-Aldrich
Anti-AMPK tot	Rabbit	1:1000	Cell Signaling Technology, Danvers, MA
Anti-pAMPK (Ser473)	Rabbit	1:1000	Cell Signaling Technology, Danvers, MA
Anti-GLUT4	Mouse	1:200	Cell Signaling Technology, Danvers, MA
Anti-GLUT1	Mouse	1:1000	Abcam, Cambridge, UK
Anti-Caveolin	Rabbit	1:1000	Santa Cruz Biotechnology Inc., California
Anti-UCP1	Rabbit	1:1000	Novus Biologicals
Anti-Vinculin	Rabbit	1:1000	Cell Signaling Technology, Danvers, MA
Anti-β-Actin	Mouse	1:1000	Santa Cruz Biotechnology Inc., California
Secondary Antibody	**Concentrations**		**Manufacturer**
Anti-Mouse	1:2000		Santa Cruz Biotechnology Inc., California
Anti-Rabbit	1:1000		Santa Cruz Biotechnology Inc., California

Separation of plasma membranes from whole cell lysates of L6 cells with stable overexpression of LANCL1 or LANCL2 or control cells (infected with negative control retrovirus PLV) was performed as follows. L6 cells (1.6 x 10^6 cells) were seeded on a 10-cm-diameter Petri dish (4 dishes/condition) and were starved in serum-free medium (3 h) and incubated, or not, with 100 nM ABA for 20 min at

37°C. After 3 washings with ice-cold HES buffer (20 mM HEPES, 1 mM EDTA and 255 mM sucrose, pH 7.4), cells were collected by scraping in HES buffer (2 ml/dish) containing a protease inhibitor cocktail (Sigma, Milan, Italy) and homogenized by passing 10 times through a 22-gauge needle. All subsequent steps were performed at 4°C. The homogenate was centrifuged (Optima L90K; Beckman-Coulter) at 16000xg in a SW28 rotor for 30 min. The pellet was resuspended in 10 ml HES buffer and centrifuged again at 16000xg for 30 min. The resulting pellet was resuspended in 5 ml HES buffer and layered on top of a 5-ml sucrose cushion (38.5% sucrose, 20 mM HEPES and 1 mM EDTA, pH 7.0) and centrifuged at 100000xg for 60 min. The interface containing the plasma membrane (PM) fraction was carefully removed, resuspended in 10 ml HES buffer and centrifuged at 40000xg for 20 min, yielding the PM fraction in the pellet. This fraction was resuspended in H_2O and total protein content in each sample was measured by the Bradford method. PM fractions (20 μg proteins) were resuspended in the sample buffer (62 mM Tris-HCl pH 6.8, 2% sodium dodecyl sulfate, 10% w/v glycerol and 1% w/v ß-mercaptoethanol), heated for 5 min at 99°C and loaded on 10% SDS-polyacrylamide gels. Proteins were transferred to a nitrocellulose membrane according to standard protocols; staining was performed using the primary antibodies against GLUT1/GLUT4 and Caveolin and the secondary antibodies anti-mouse and anti-rabbit, respectively (**Table 4**). Band intensity was evaluated with the ChemiDoc system (Bio-Rad, Milan, Italy).

2.12. Evaluation of cell oxygen consumption

Rat L6 myoblasts overexpressing human LANCL1 or human LANCL2 or negative control cells (PLV) were seeded at 1.5 x 10^6/well in a 6-well plate in complete DMEM. After 24 hours, cells were incubated in DMEM without serum for 18 hours, in the presence or absence of 100 nM ABA at 37°C. At the end of incubation, cells were recovered by trypsin treatment, resuspended at 1.5 x 10^6/ml in HBSS buffer and incubated at 37°C under continuous stirring in a 300 μL closed chamber equipped with an oxygen micro-amperometric electrode (Unisense A/S, Denmark). The rate of oxygen consumption was measured continuously for 10 minutes.

2.13. Glucose transport assays

L6 cells overexpressing human LANCL1 or human LANCL2 or silenced for the expression of both rat LANCL1 and rat LANCL2 with respective negative controls (PLV and shRNA-SCR) were cultured overnight at 1 x 10^4/well in a 96-well plate in 5 mM DMEM without serum. Cells were washed once with DMEM and then incubated for 5 min at 37°C in DMEM containing 100 nM ABA

or 2 mM metformin. At the end of incubation, cells were washed with KRH at 37°C. The fluorescently labeled deoxyglucose analog 2-NBDG (50 μM) was added to each well and, after 10 minutes, the supernatant was removed, wells were washed once with ice-cold KRH, 50 μL KRH was added to each well and the mean fluorescence (l_{ex}=465 nm, l_{em}=540 nm) from 10 acquisitions/well was calculated. Each experimental condition was assayed in at least 8 wells. Unspecific 2-NBDG uptake, determined in the presence of the glucose transport inhibitors cytochalasin B (20 mM) and phloretin (200 mM) [26], was subtracted from each experimental value.

2.14. Adipocyte differentiation

TERT-hBA and TERT-hWA cells were seeded at 1 x 10^6 per well in 6-well plates. At two-day post confluence (designated day 0), adipogenesis was induced with a differentiation cocktail containing Advanced DMEM/F12 supplemented with 2% FBS, L-glutamine (2 mM), penicillin (62.5 μg/ml), streptomycin (100 μg/ml), insulin (5 μg/ml), dexamethasone (1 μM), 3-isobutyl-1-methylxanthine (IBMX) (0.5 mM), rosiglitazone (1 μM), human cortisol (1 μM) and T_3 (1 nM). At day 3, the medium was refreshed with the same medium used at day 0. At day 6 and 9 of differentiation, IBMX, dexamethasone, insulin, rosiglitazone and cortisol were omitted from the medium. At day 12, the adipocytes were considered mature. TERT-hWA used for rosiglitazone-induced browning were differentiated until day 12 as described above, except that T_3 was omitted from day 6 [64]. At day 6, approximately 60% of cells showed an adipocyte morphology, with accumulation of lipid droplets, while at day 10 this percentage increased to about 80-90%. At day 12, mature TERT-hWA were treated with 1 μM rosiglitazone and harvested at day 15. Moreover, from day 0 to day 12, TERT-hBA and TERT-hWA cells were treated with or without 100 nM ABA and, from day 12 to day 15, TERT-hWA cells were treated with or without 100 nM ABA, 1 μM rosiglitazone or both. Adipocyte differentiation was also performed on human TERT-hBA and TERT-hWA pre-adipocytes overexpressing LANCL1 and LANCL2 compared to control cells, infected with the control retrovirus (PLV). The cells were incubated with or without 100 nM ABA until day 12 for brown cell line and until day 15 for white cell line. Adipogenic differentiation was monitored at days 12 and 15 by qPCR analysis and at day 12 by lipid staining with Oil Red O staining. The general differentiation protocol for cells is depicted in **Figure 7**.

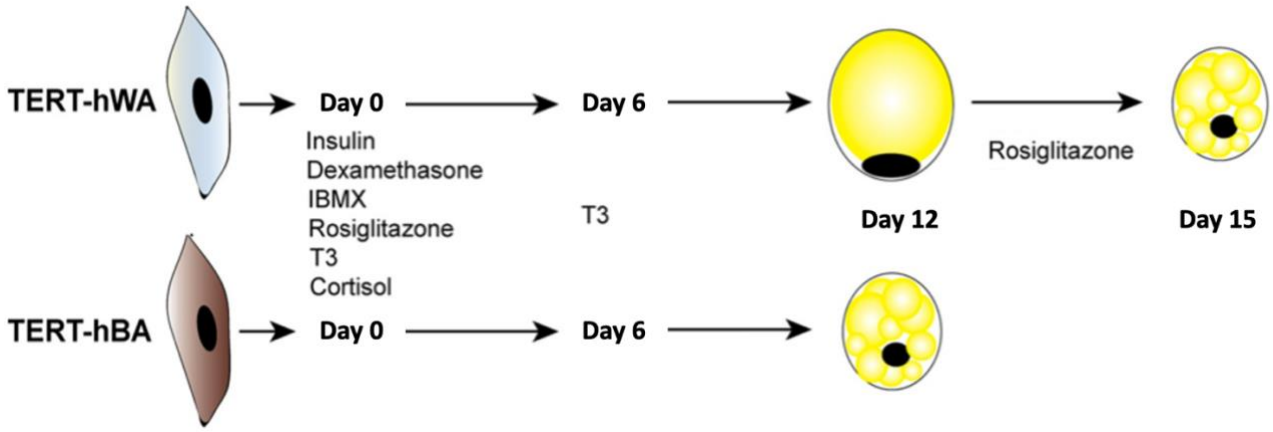

Figure 7. Differentiation protocol for TERT-hBA and TERT-hWA [64].

2.15. Oil Red O staining

To measure cellular neutral lipid droplet accumulation, mature TERT-hBA and TERT-hWA adipocytes were washed three times with iced phosphate-buffered saline (PBS) and fixed with 4% paraformaldehyde for 30 minutes. After fixation, cells were washed three times and stained with Oil Red O solution (working solution 0.5 g Oil Red O power dissolved in 60% ethanol) for 15 minutes at room temperature. Cells were washed again three times with PBS to remove unbound staining. Mature adipocytes were examined under a light microscope and the red oil droplets stained in the cells indicate lipid accumulation. Two different microscopic fields (20X and 40X magnifications) per culture were photographed. The red oil droplets stained in the cells were extracted in 100% isopropanol. The absorbance was evaluated at 510 nm to the spectrophotometer.

2.16. *In vivo* experiments

LANCL2$^{-/-}$ C57Bl/6 mice and their wild-type siblings, obtained from heterozygous breeding [59], were housed at the animal facility of the IRCCS San Martino Hospital (Genova, Italy). All mice used in this study were derived from a heterozygous LANCL2$^{+/-}$ x LANCL2$^{+/-}$ breeding scheme. Genotyping of the offspring allowed the selection of LANCL2$^{+/+}$ (henceforth referred to as control or wild-type or WT) and LANCL2$^{-/-}$ (KO) mice. Protocols of animal use were approved by the Italian Ministry of Health, in line with the EU Directive 2010/63/EU for animal experiments. Almost all of the experiments were conducted on male mice, although no specific differences were observed between the two genders. Seven week-old mice (9/group) fed a standard chow were administered (±) 2-cis, 4-trans Abscisic acid (ABA) (Merck, Milan, Italy) at a dose of 1 μg/kg BW in the drinking

water for 4 weeks. The duration of treatment and the dose of ABA were derived from a previously published protocol [26]. The daily volume of water consumed by the animals and the average weight of the mice were preliminarily determined to calculate the ABA concentration in the drinking water necessary to yield the indicated dose. The animals were weighed weekly and the concentration of ABA in the water was adjusted to the mean BW in each cage. One week before the end of the 4-week diet enriched with ABA or not (control), mice were fasted for 17 h before the OGTT, then 1 g/kg BW glucose was administered by gavage in 150 μL water. Blood was drawn from the tail vein before gavage (time 0) and 15, 30, 60 and 120 min after gavage: glycemia was immediately measured with a glucometer (Ascensia, Milan, Italy). Each measure was performed in duplicate. One week after the OGTT, the animals were sacrificed and samples of plasma (for the determination of the ABA concentration; ELISA, Agdia) and quadriceps muscles (for qPCR and/or Western blot analysis) were taken and immediately frozen in liquid nitrogen. Male, six week-old CD1 LANCL2$^{+/+}$ (WT) and LANCL2$^{-/-}$ (KO) mice (5/group) were fed a standard diet and were treated, or not (controls), with ABA, administered through the drinking water. The concentration of ABA in the water was calculated taking into consideration the average daily volume introduced by each mouse (≅4 ml), so as to reach a daily dose of approximately 1 μg/kg BW of ABA. After 30 days, the animals were sacrificed and samples of interscapular brown adipose tissue were excised and immediately processed for RNA extraction for qPCR analysis.

3. RESULTS

3.1. Recombinant hLANCL1 protein binds ABA

Recombinant human LANCL1 (hLANCL1) was expressed as an N-terminal fusion protein with the enzyme glutathione S-transferase (GST). hLANCL1 was released from the GST fusion protein immobilized on GSH-Sepharose-4B by incubation with PreScission Protease. Separately, pre-activated with DTT, in order not to expose the protein to the high DTT concentration required for activation of the PreScission Protease and similarly to the protocol used to produce hLANCL2 [3], hLANCL1 purity was checked by SDS-PAGE, revealing a single band of approximately 45 kDa, as expected (**Figure 8,** left panel). hLANCL1 was eluted from a gel filtration column as a single symmetrical peak, confirming the purity of the protein (**Figure 8**, right panel).

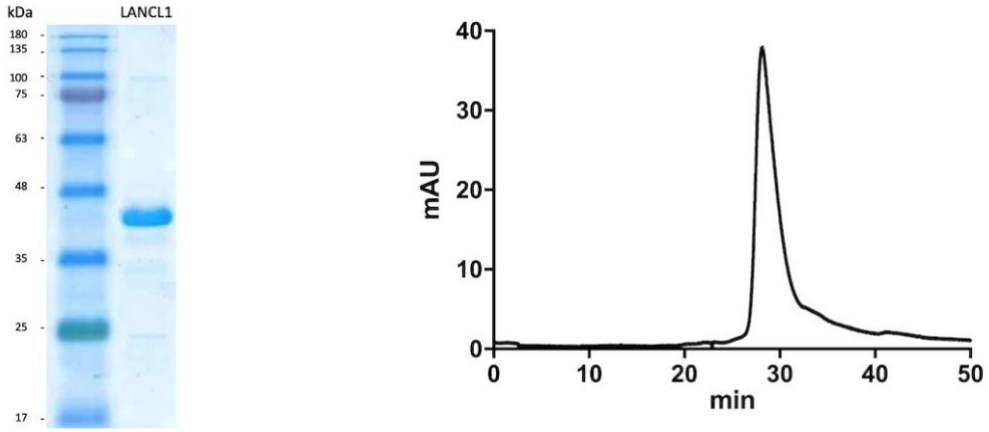

Figure 8. Determination of recombinant human LANCL1 protein purity; left panel, representative SDS-PAGE of 5 µg purified hLANCL1 used in the binding experiments; the gel was stained with ProSieve Blue Protein Staining solution; hLANCL1 migrated as a single band with an apparent molecular mass of 45 kDa; right panel, size exclusion chromatography of purified hLANCL1 on a TSK-gel 3000SWXL column revealed a single symmetrical peak.

Preliminary tests were performed to assess the pH stability of the protein in anticipation of the subsequent binding experiments. To assess the stability of the recombinant protein, the fluorescent probe 8-Anilinonaphthalene-1-Sulfonic Acid (ANS) was used. When ANS is in an aqueous solution, its excitation at 360 nm produces a low emission at about l_{em}=545 nm. When the dye binds to exposed hydrophobic regions of the protein, the fluorescence intensity increases and the maximum peak emission shifts to lower wavelengths l_{em}=460-480 nm. The use of this fluorophore provides information about the solvent exposure and accessibility of the hydrophobic protein domains. We performed ANS interaction experiments by incubating human LANCL1 at different pH values and

in two different buffers, Na acetate (AcB) (**Figure 9**, left panel) and Na phosphate (PB) (**Figure 9**, right panel).

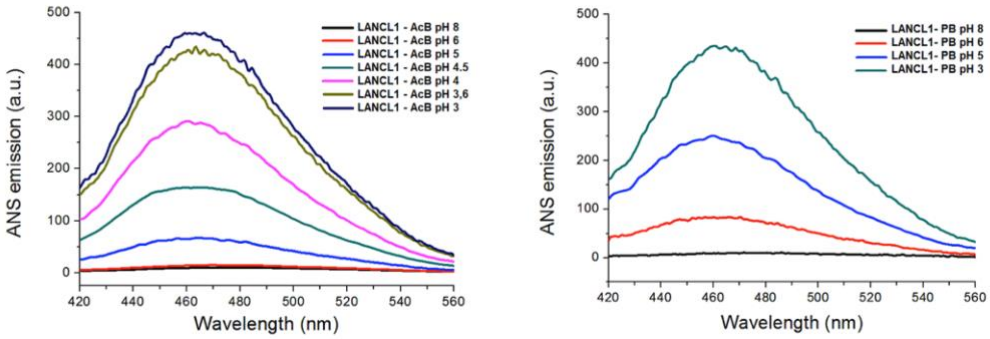

Figure 9. Representative fluorescence emission spectra of ANS incubated with LANCL1 at different pH values and in Na acetate (left panel) or in Na phosphate (right panel). The concentration of LANCL1 protein in AcB and PB was 6.4 μM and 5.4 μM respectively.

These experiments showed that the ANS emission increased at pH values lower than 6, implying that the hydrophobic domains of hLANCL1 were increasingly exposed to the solvent due to protein unfolding. Moreover, the structure of the protein was more stable in the AcB buffer than in the PB buffer, in which a loss of stability had already occurred below pH 7 (**Figure 10**).

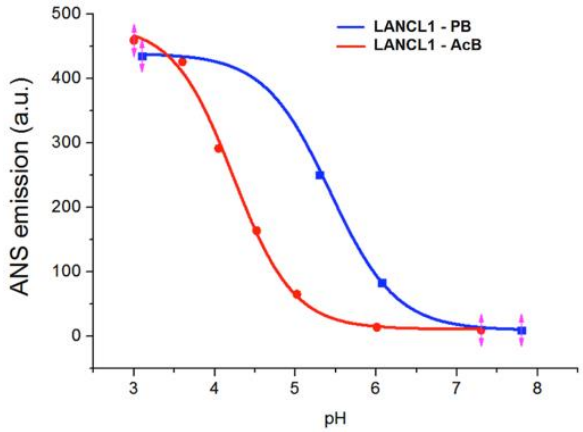

Figure 10. Binding of 8-Anilinonaphthalene 1-Sulfonic Acid (ANS) to recombinant hLANCL1; representative fluorescence emission spectrum of ANS incubated with hLANCL1 at different pH values. The effect of pH on LANCL1 unfolding was evaluated by monitoring the ANS emission in Na acetate (red line) or in Na phosphate (blue line) buffer.

This behaviour was also evident in the Circular Dichroism (CD) experiments, in which an initial loss of the secondary structure was observed when the protein was incubated in the Na acetate buffer below pH 6. Furthermore, parallel change in the CD spectrum was observed when the protein was incubated in the Na phosphate buffer at pH values between 6 and 8, confirming reduced stability of the protein in this buffer (**Figure 11**, right panel). At neutral pH, human LANCL1 protein showed a

prevailing alpha helix secondary structure (minimum peaks at 209 and 222 nm), while at acidic pH values, the protein lost this organization and precipitated (**Figure 11**).

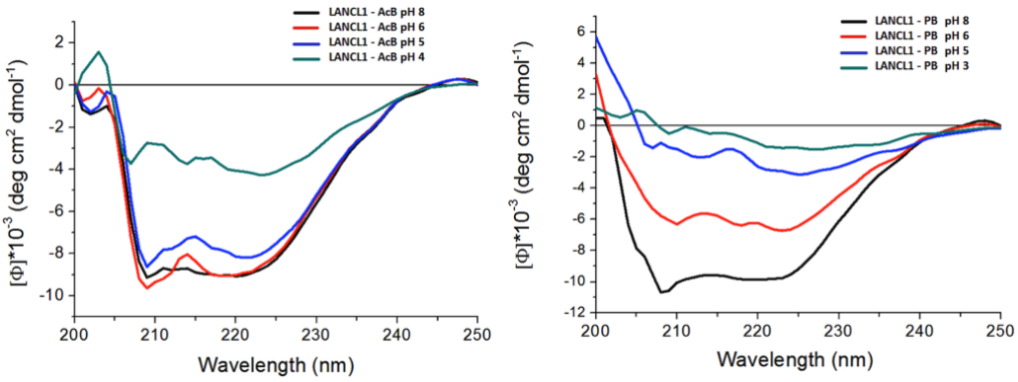

Figure 11. Circular Dichroism (CD) spectroscopy; representative CD spectra of recombinant hLANCL1 incubated in AcB (left panel) and PB (right panel) at different pH values.

Therefore, subsequent equilibrium binding experiments with (±)-[^{3}H] ABA were performed at pH 7.5 in Na acetate buffer. Saturable binding of (±)-[^{3}H] ABA to hLANCL1 was explored at ligand concentrations ranging from 50 nM to 5 μM (**Figure 12**). Heat-denatured hLANCL1, used as the negative control, did not show any specific ABA binding. The results revealed a binding curve with a single K_d in the low micromolar range (1.0 ± 0.4 μM), a value lying in between the K_d values of the high- and the low-affinity binding sites previously discovered in hLANCL2 [20], and a B_{max} of 254 pmol/mg protein. Equilibrium binding experiments were performed both in the presence and absence of 1.0 mM GSH and no significant difference in the affinity constant was observed.

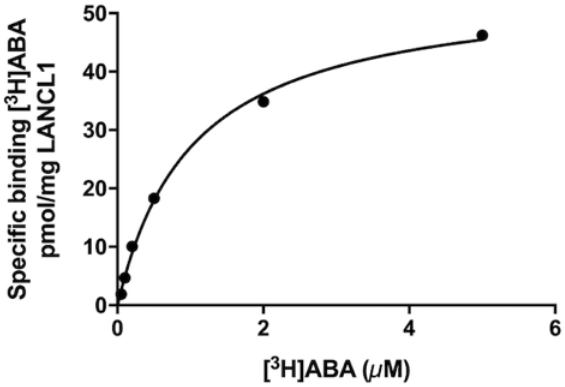

Figure 12. [^{3}H]ABA equilibrium binding; human purified LANCL1 protein was incubated with 50 nM (±)-[^{3}H]ABA in the presence of increasing concentrations of unlabeled ABA. The specific binding was analyzed by nonlinear regression, using the GraphPad Prism software. Results are the mean ± SD of 6 experiments.

Surface Plasmon Resonance (SPR) experiments of human LANCL1 with or without (±)-ABA were performed at pH 5.8 to compromise between an acidic pH, yielding the highest binding of the protein

to the chip, and a value compatible with a conserved protein structure (**Figure 13**, left panel). Based on the results obtained by CD on the folding state of hLANCL1 in the Na acetate buffer at various pH values (**Figure 11**), the covalent coupling ability of the protein to the SPR CM7 chip was evaluated in a range of pH values compatible with protein stability (10 mM Na acetate buffer pH 5.5, 5.8, 6.0 and 6.5 at a constant protein concentration of 30 μg/ml) to determine the best conditions for achieving the highest pre-concentration possible. The results suggested performing the covalent amine coupling of hLANCL1 to the carboxymethyl groups of the sensor chip in 10 mM Na acetate pH 5.8 (**Figure 13**, left panel). The total amount of human LANCL1 immobilized was 36980 resonance units (RUs). The binding of ABA to hLANCL1 was performed by injecting ABA dissolved at a micromolar concentration range. SPR analysis revealed the presence of an ABA binding site with an affinity constant of 11.5 ± 3.1 μM (**Figure 13,** right panel).

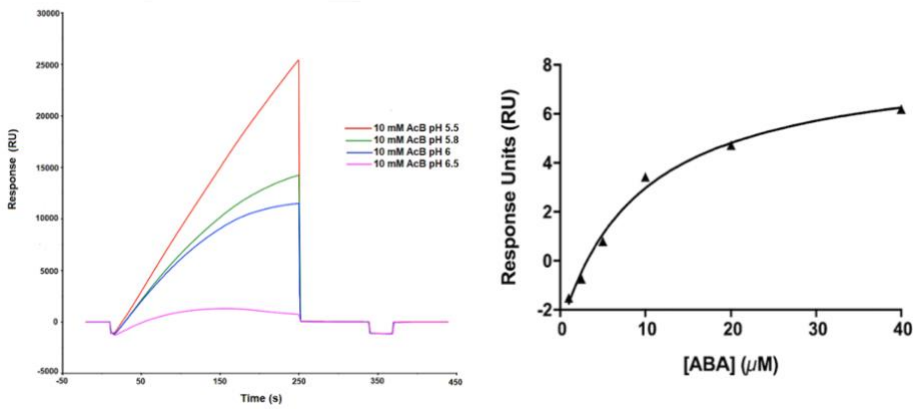

Figure 13. SPR analysis; left panel, the pre-concentration ability of hLANCL1 on the chip used for SPR analysis was evaluated in a range of pH values compatible with protein stability (10 mM Na acetate, pH 5.5, 5.8, 6.0 and 6.5), at a protein concentration of 30 μg/ml. Traces from a representative experiment are shown; right panel, hLANCL1 was immobilized by amine coupling on a CM7 chip in 10 mM Na acetate pH 5.8. The steady-state K_d value (11.5 μM) was estimated using the Biacore T200 evaluation software. The values shown are the mean ± SD from 3 experiments.

To further confirm ABA binding to hLANCL1, a fluorescence analysis based on the emission spectra of tryptophan residues at 335 nm was used. When the tryptophan residues of the hLANCL1 protein were selectively excited by irradiating at 280 nm, the emission spectrum showed a maximum at 335 nm, indicating that the tryptophan residues are buried inside the hydrophobic core of the protein [65]. When ABA was added to LANCL1 in the solution to obtain a molar ratio between LANCL1 and ABA ranging from 1:2 to 1:450, the intensity of the spectra decreased (**Figure 14**, left panel), indicating that ABA was able to quench the tryptophan emission of human LANCL1 protein. Two common mechanisms for fluorescence quenching are dynamic and static quenching. To determine which was taking place, the linearity of the Sterne Volmer plot was interpreted, as previously

described [61]. The Sterne Volmer plot of F_0/F, where F_0 and F corresponded to the fluorescence intensities of hLANCL1 without and with ABA, respectively, relative to the ABA concentration, results in an exponential curve, which is typical of proteins that have tryptophan residues in different environments (**Figure 14**, central panel). For static quenching, the binding constant (K_a) for the formation of an adduct between the hLANCL1 and ABA was determined using a double logarithmic plot. The binding site values (n) were also determined from the slope using the following equation: $\log[(F_0\text{-}F)/F]=\log K_a+n\log[Q]$. The calculated K_a value for LANCL1 and ABA was 2.3 x 10^4, for a K_d of 4.3 μM (**Figure 14**, right panel).

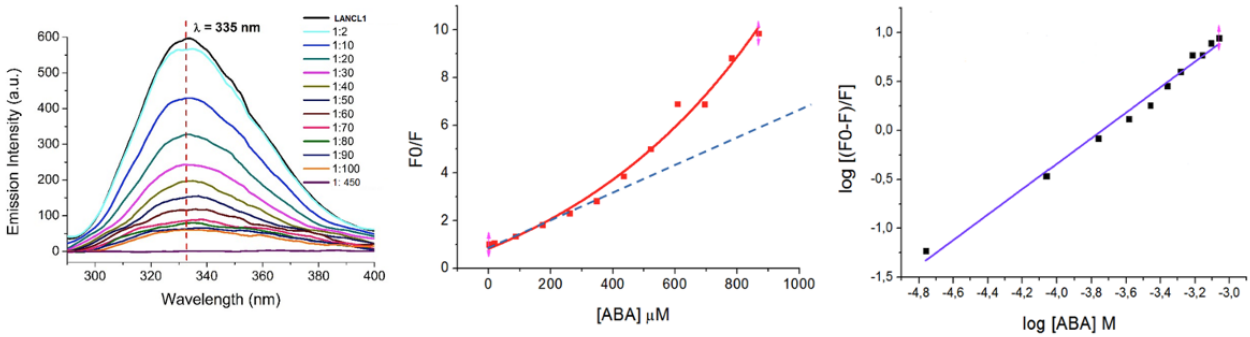

Figure 14. Fluorescence quenching emission analysis of the interaction between ABA and recombinant human LANCL1 protein; left panel, the emission spectrum of hLANCL1 (8.65 μM) in 10 mM Na acetate pH 7.0, excited at 280 nm, was analyzed in the presence of increasing ABA concentrations, to obtain a molar ratio ranging from 1:2 to 1:450; central panel, dynamic quenching: LANCL1 (8.65 μM) was incubated with increasing concentrations of ABA to obtain a molar ratio LANCL1/ABA ranging from 1:2 to 1:450. All emission spectra were recorded on a luminescence spectrometer at excitation wavelengths of 280 nm (slit width=5 nm). The dynamic quenching constants were determined using the equation: $F_0/F=1+K_{SV}[Q]$, where F_0 and F are the fluorescence intensities of hLANCL1 without and with ABA, respectively, [Q] is the concentration of ABA and K_{SV} is the Stern Volmer quenching constant; right panel, static quenching: the static quenching constant, or binding constant, K_a, and the number of ABA-binding sites, n, were calculated using the equation: $\log[(F_0\text{-}F)/F]=\log K_a+n\log[Q]$.

Taken together, results obtained with three different techniques allow us to conclude that hLANCL1 binds to ABA with a constant affinity in the low micromolar range (1.0 μM by equilibrium binding, 4.3 μM by fluorescence quenching analysis and 11.5 μM by SPR). The higher K_d calculated with the SPR may be due to the acidic pH required to optimize the protein binding to the chip (pH 5.8), a pH which lies close to values denaturing the native protein structure, as observed by ANS analysis and CD experiments (**Figure 10** and **Figure 11**), possibly unmasking low-affinity sites also present in LANCL2 with a similar K_d value (approximately 18 μM) [20].

3.2. LANCL proteins are involved in glucose transport *via* GLUT4

As LANCL2 has been reported to stimulate glucose transport in muscle cells via an insulin-independent increase of GLUT4 expression [26], we investigated a possible role of LANCL1 protein in the same function. To this end, we undertook the overexpression of each individual protein, LANCL1 and LANCL2, and the stable silencing of both proteins in rat L6 myoblasts. Overexpression of LANCL1 (ovLANCL1) and LANCL2 (ovLANCL2) proteins was obtained by retroviral infection and was confirmed by immunoblot (**Figure 15**, left panel). As can be seen, the overexpression of one receptor increases slightly the expression of the other receptor, suggesting a transcriptional control between the two proteins. In all subsequent experiments, ovLANCL1 and ovLANCL2 cells showed an approximately 4- and 6-fold higher expression of LANCL1 and LANCL2, respectively, as compared with negative control cells (PLV). Silencing both proteins was achieved by the lentiviral infection of L6 with rat LANCL1- and rat LANCL2-specific shRNAs. After puromycin selection of the infected cells, knockdown of both LANCL1 and LANCL2 was confirmed by both qPCR (**Figure 15**, central panel) and immunoblot (**Figure 15**, right panel). Cells silenced for the expression of LANCL1 and LANCL2 showed an 80% reduction of the expression of LANCL1 and LANCL2 as compared to control cells infected with a scramble shRNA.

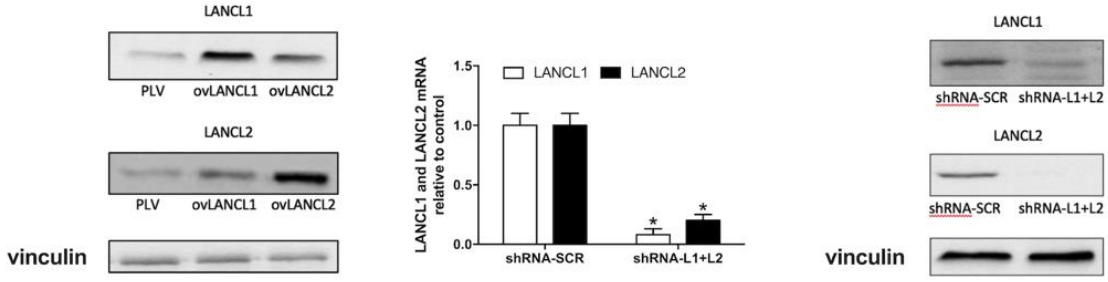

Figure 15. LANCL1 and LANCL2 were stably overexpressed or silenced in rat L6 myoblasts by viral infection; left panel, representative Western blot of LANCL1/2 proteins in cells overexpressing LANCL1 (ovLANCL1) or LANCL2 (ovLANCL2); central panel, LANCL1/2 mRNA levels relative to control in LANCL1/2-silenced cells; right panel, representative Western blot of LANCL1/2 proteins in cells silenced for both proteins (shRNA-L1+L2). All results are the mean ± SD from 3 different determinations. *$p < 0.0002$ by unpaired two-tailed t-test compared with control cells, infected with the scramble shRNAs (shRNA-SCR).

Glucose transport assays was performed using fluorescently labeled deoxyglucose analog 2-NBDG. In L6 negative control cells (PLV), ABA stimulated NBDG uptake approximately 2-fold compared to untreated controls. Overexpression of either LANCL1 or LANCL2 increased the ABA-induced stimulation of NBDG uptake (**Figure 16**, left panel) and increased the effect of metformin, a stimulator of cell glucose uptake *via* GLUT4 [66]. Conversely, silencing both LANCL1 and LANCL2

had the opposite consequence, abrogating the effect of ABA on NBDG uptake and significantly reducing the metformin (**Figure 16**, right panel), indicating that ABA and metformin share the same effector on AMPK.

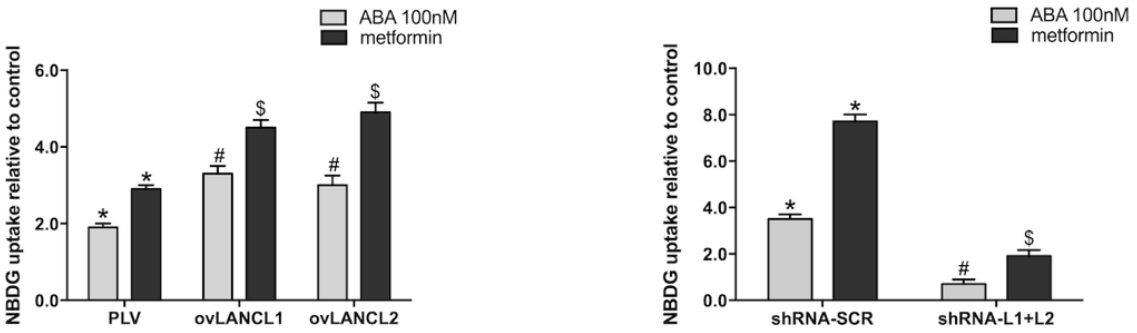

Figure 16. Glucose transport assays; L6 cells overexpressing LANCL1 (ovLANCL1) or LANCL2 (ovLANCL2) or silenced for the expression of both proteins (shRNA-L1+L2) were serum-starved for 12 h, then treated with 100 nM ABA or with 2 mM metformin for 5 min prior to incubation with the fluorescent glucose analog NBDG. Left panel, NBDG uptake in overexpressing cells, relative to control, untreated cells, infected with the empty vector (PLV); *$p < 0.0004$ relative to untreated PLV; $^{\#}p < 0.001$ relative to ABA-treated PLV; $^{\$}p < 0.0002$ relative to metformin-treated PLV; right panel, NBDG uptake in silenced cells, relative to control, untreated cells, infected with the scramble (shRNA-SCR) shRNA; *$p < 0.00004$ relative to untreated shRNA-SCR-infected cells; $^{\#}p < 0.00007$ relative to ABA-treated shRNA-SCR-infected cells; $^{\$}p < 0.00001$ relative to metformin-treated shRNA-SCR-infected cells. All results are the mean ± SD from at least 3 separate experiments.

Indeed, the stimulation of glucose transport by ABA *via* LANCL2 occurs by the activation of AMPK and increased transcription of PGC-1α [26]; thus, we compared the effect of the overexpression of either LANCL1 or LANCL2 on the transcription of AMPK and PGC-1α in L6 myoblasts. In LANCL2-overexpressing cells as compared to cells infected with the empty vector, an increased mRNA level of AMPK, PGC-1α and Sirtuin 1 (Sirt1), all key players in muscle function and metabolism [67], was observed, together with an increased GLUT4 mRNA level (**Figure 17**). Interestingly, GLUT1-specific mRNA was also more abundant in LANCL2-overexpressing cells. Treatment with 100 nM ABA for 4 hours further increased the transcription of all mRNAs (**Figure 17**). A similar pattern of results was observed on LANCL1-overexpressing cells, indicating that AMPK, PGC-1α, Sirt1, GLUT1 and GLUT4 are also targets of LANCL1 (**Figure 17**).

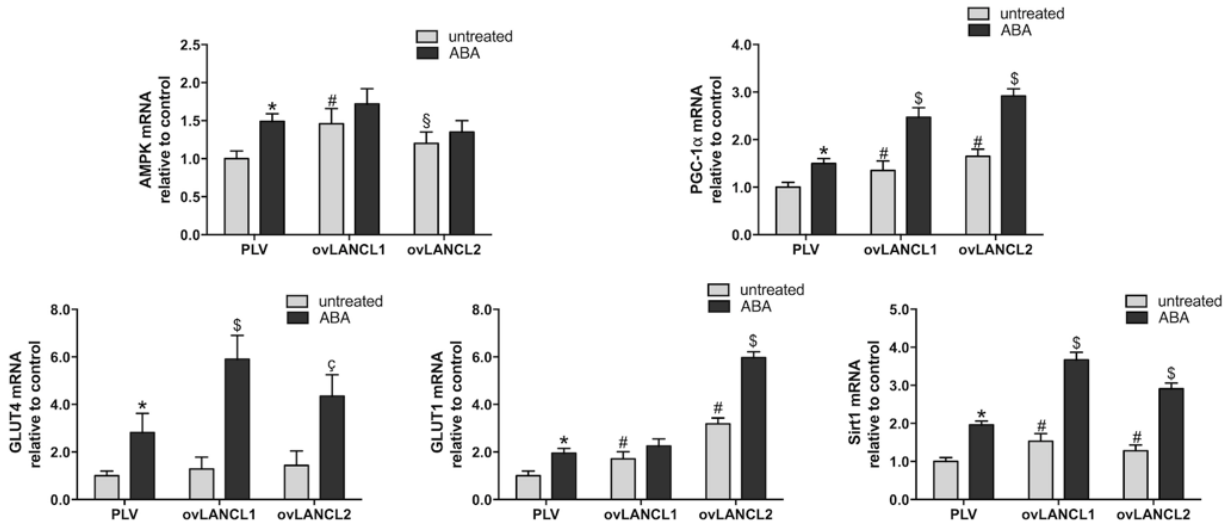

Figure 17. qPCR analysis; L6 cells overexpressing LANCL1 (ovLANCL1) or LANCL2 (ovLANCL2) were serum-starved for 12 h and treated with 100 nM ABA for 4 h. mRNA levels of the indicated proteins are expressed relative to untreated control cells, infected with the empty vector (PLV). Results are the mean ± SD from 3 separate experiments; *$p < 0.02$ relative to untreated control cells, $^{\#}p < 0.05$ and $^{\S}p < 0.05$ relative to untreated control; $^{\$}p < 0.01$ and $^{ç}p < 0.02$ relative to ABA-treated control. P values are calculated by unpaired, two-tailed t-test.

3.3. LANCL1 and LANCL2 regulate the transcription of GLUTs by the AMPK/PGC-1α/Sirt1 pathway and ABA-sensitive AMPK, pAMPK and PGC-1α protein levels in L6 myoblasts

The fact that LANCL1- or LANCL2-overexpression *per se* increased mRNA levels of AMPK, GLUT4, GLUT1, PGC-1α and Sirt1 suggested to investigate the effect of LANCL1/2 silencing the transcription of the genes encoding the same regulatory proteins. Indeed, the combined silencing of LANCL1 and LANCL2 significantly reduced the basal level of mRNAs for all the regulatory proteins and GLUT4 compared to control cells infected with scramble-shRNAs (**Figure 18**). Upon incubation with 100 nM ABA for 4 h, the levels of all mRNAs explored increased in LANCL1/2-silenced cells, except for the GLUT4 mRNA, though they remained below those measured in untreated, scramble-silenced cells (**Figure 18**). The partial abrogation of the response to ABA may be attributed to the incomplete knockdown of LANCL1/2 expression accomplished by shRNA infection (approximately 80%). Taken together, the observations of increases in the overexpression of either LANCL1 or LANCL2 and that silencing LANCL1/2 reduces mRNA levels of AMPK, PGC-1α, Sirt1 and GLUT4, indicate a transcriptional control by LANCL1/2 on these genes.

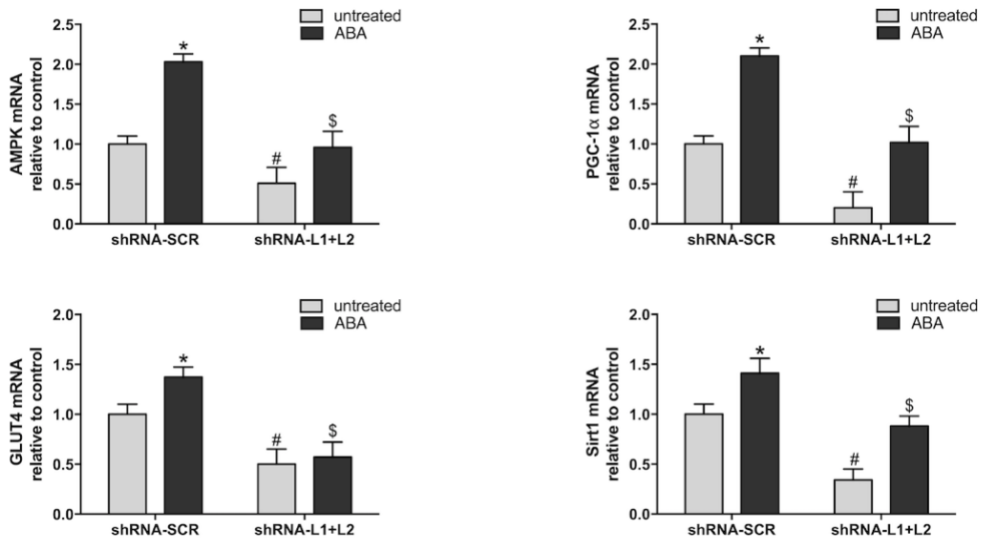

Figure 18. qPCR analysis; L6 cells silenced for the expression of both LANCL1 and LANCL2 (shRNA-L1+L2) were serum-starved for 12 h and treated with 100 nM ABA for 4 h. mRNA levels of the indicated proteins are expressed relative to untreated control cells, infected with the scramble shRNAs. Results are the mean ± SD from 3 separate experiments; *$p < 0.02$ relative to untreated control cells, $^{\#}p < 0.05$ and $^{\S}p < 0.05$ relative to untreated control; $^{\$}p < 0.01$ and $^{\varsigma}p < 0.02$ relative to ABA-treated control. P values are calculated by unpaired, two-tailed t-test.

To confirm the results obtained by qPCR analysis on mRNA expression, we also analyzed the protein levels by Western blot experiments. The total level of AMPK protein increased slightly in L6 cells overexpressing LANCL2, but not LANCL1; upon treatment with ABA, both AMPK (**Figure 19**, upper left panel) and pAMPK (**Figure 19**, upper right panel) significantly increased in cells overexpressing either LANCL1 or LANCL2, indicating that both LANCL1 and LANCL2 stimulate AMPK protein expression and phosphorylation upon ABA binding. A higher amount of the total and phosphorylated AMPK increases the enzymatic activity of the kinase, both potential and actual, on its different substrates. Thus, although the pAMPK/AMPK ratio was similar in control and in LANCL1/2-overexpressing cells incubated with ABA, the significantly higher total amounts of pAMPK and AMPK in the overexpressing cells implies a higher kinase activity. PGC-1α, GLUT1 and GLUT4 protein expression increased in both LANCL1- and LANCL2-overexpressing L6 cells approximately 2-fold compared to control cells and treatment with ABA further increased PGC-1α, GLUT1 and GLUT4 protein levels (**Figure 19**, lower panel). Thus, upon ABA treatment, L6 cells overexpressing either LANCL1 or LANCL2 respond similarly with an increase of total and phosphorylated AMPK, PGC-1α, GLUT1 and GLUT4, confirming the results obtained by qPCR.

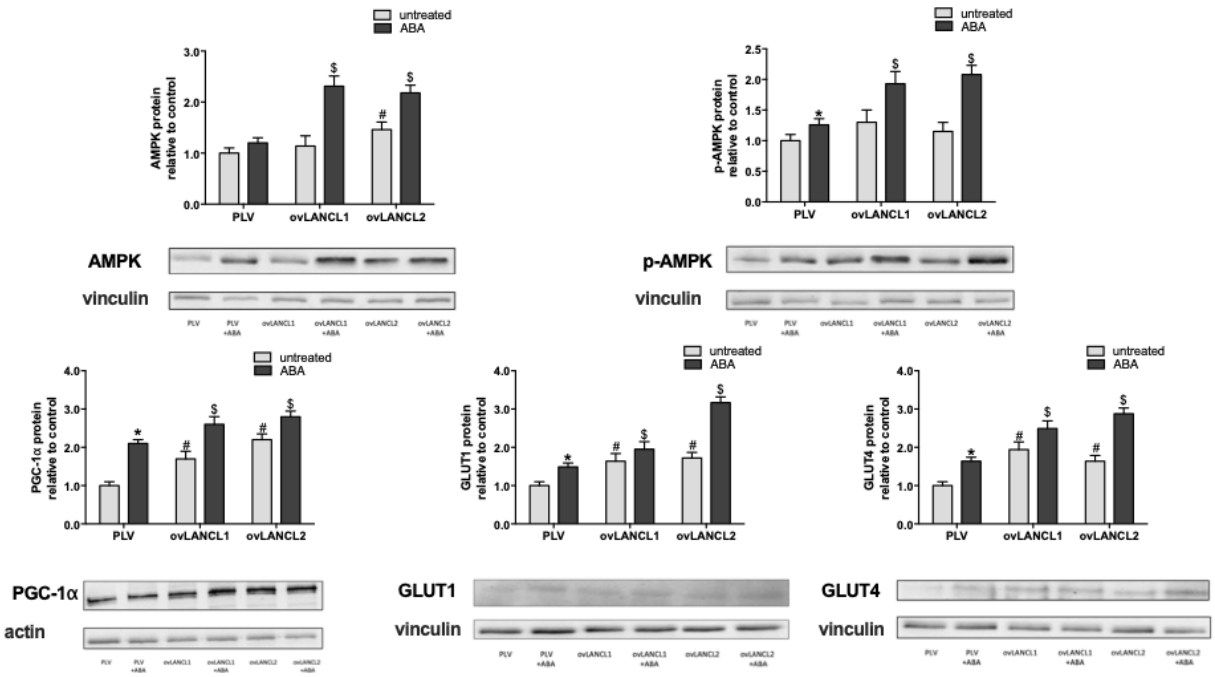

Figure 19. Western blot experiments; L6 cells overexpressing LANCL1 (ovLANCL1) or LANCL2 (ovLANCL2), serum-starved for 12 h and then incubated without or with 100 nM ABA for 1 h, were also analyzed by Western blot for expression of the indicated proteins. Upper left panel, total AMPK in cells overexpressing LANCL1 (ovLANCL1) or LANCL2 (ovLANCL2), relative to control cells, infected with the empty vector and untreated (PLV). Upper right panel, phosphorylated (Ser473) AMPK (pAMPK) relative to PLV. Lower left panel, PGC-1α relative to PLV. Lower central panel, GLUT1 relative to PLV. Lower right panel, GLUT4 relative to PLV. *$p < 0.03$ relative to untreated control, $^{\#}p < 0.006$ relative to untreated control; $^{\$}p < 0.02$ relative to ABA-treated PLV-infected cells. P values are calculated by unpaired, two-tailed t-test.

Silencing both LANCL1 and LANCL2 resulted in a significant reduction of total and phosphorylated AMPK, which increased slightly upon ABA treatment of the cells but remained lower than in control cells infected with scramble-shRNAs (**Figure 20**, upper right and left panels). PGC-1α, GLUT1 and GLUT4 protein levels were lower in double-silenced cells as compared to that in control cells and remained below the levels of control cells upon treatment with ABA (**Figure 20**, lower panel).

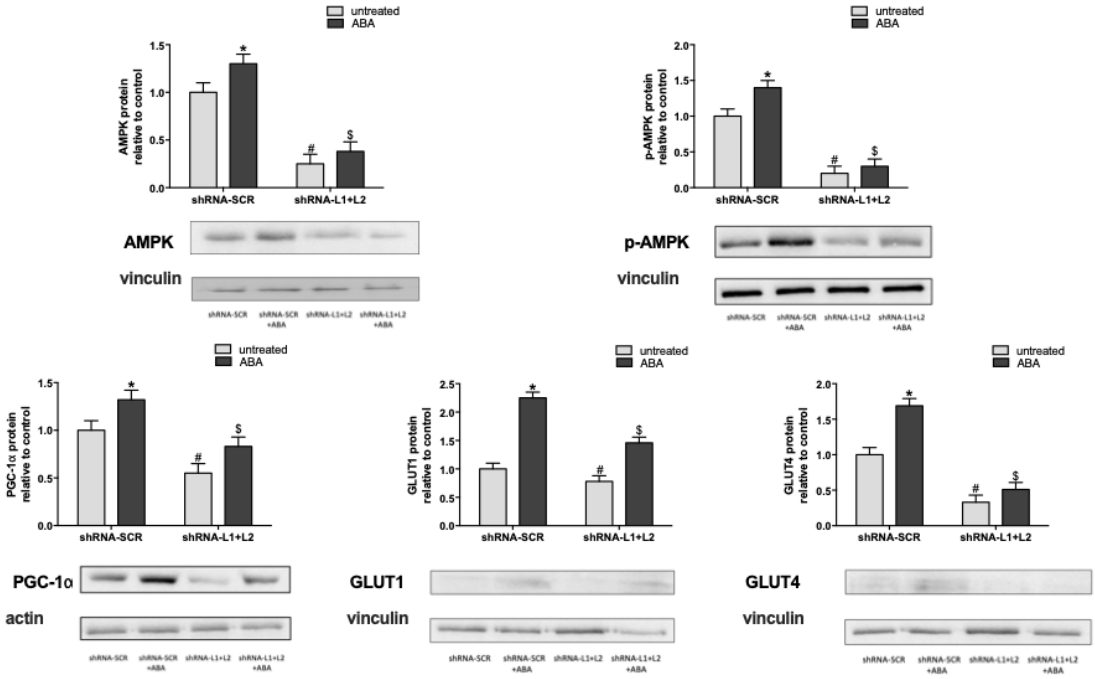

Figure 20. Western blot experiments; L6 cells silenced for the expression of both LANCL1 and LANCL2 (shRNA-L1+L2), serum-starved for 12 h and then incubated without or with 100 nM ABA for 1 h, were also analyzed by Western blot for expression of the indicated proteins. Upper left panel, total AMPK in cells silenced for LANCL1 and LANCL2 expression (shRNA-L1+L2) relative to control cells, infected with the scramble shRNAs and untreated (shRNA-SCR). Upper right panel, phosphorylated (Ser473) AMPK (pAMPK) relative to shRNA-SCR. Lower left panel, PGC-1α relative to shRNA-SCR. Lower central panel, GLUT1 relative to shRNA-SCR. Lower right panel, GLUT4 relative to shRNA-SCR. *$p < 0.02$ relative to untreated control, $^{\#}p < 0.01$ relative to untreated control; $^{\$}p < 0.008$ relative to ABA-treated shRNA-SCR-infected cells. P values are calculated by unpaired, two-tailed t-test.

Finally, GLUT1 and GLUT4 proteins increased significantly in the plasma membrane-enriched fractions from both LANCL1- and LANCL2-overexpressing L6 cells compared to control PLV-infected cells (approximately 4-fold for GLUT1 and 2-fold for GLUT4) (**Figure 21**). Treatment with ABA further significantly increased the plasma membrane translocation of both glucose transporters in LANCL1/2-overexpressing cells (approximately 8-fold for GLUT1 and 4-fold for GLUT4, relative to control cells). Together, the results obtained on LANCL1/2-overexpressing or -silenced L6 cells suggest that both LANCL proteins transduce an ABA-triggered response, activating AMPK transcription and phosphorylation, increased expression of the transcription factor PGC-1α and higher levels of GLUT1 and GLUT4 transcription, protein expression and translocation to the plasma membrane.

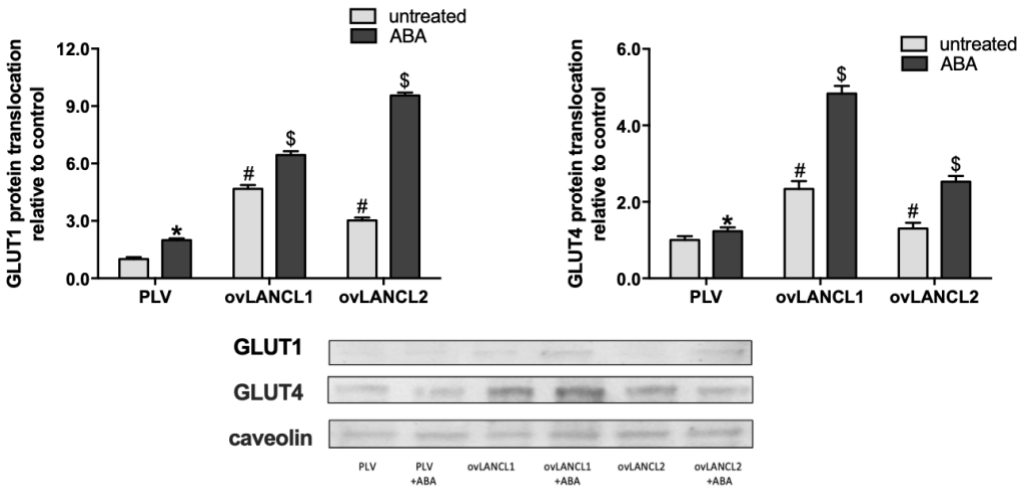

Figure 21. Western blot experiments; L6 cells overexpressing LANCL1 (ovLANCL1) or LANCL2 (ovLANCL2), serum-starved for 12 h and then incubated without or with 100 nM ABA for 1 h, were also analyzed by Western blot for expression of the indicated proteins. Plasma membrane-enriched lysates from LANCL1/2-overexpressing L6 cells treated or not with ABA. Left panel, GLUT1 relative to PLV. Right panel, GLUT4 relative to PLV. *$p < 0.04$ relative to untreated control, $^{\#}p < 0.008$ relative to untreated control; $^{\$}p < 0.03$ relative to ABA-treated PLV-infected cells. Each panel shows the mean ± SD of at least 3 separate experiments. P values are calculated by unpaired two-tailed t-test.

3.4. LANCL receptors stimulate mitochondrial respiration and control expression levels of uncoupling proteins sarcolipin and UCP3 in rat myoblasts

ABA treatment has been previously shown to increase the expression of browning genes *in vitro*, in murine preadipocytes, and *in vivo*, in the brown adipose tissue from ABA-treated mice [27]. Overexpression of LANCL1, but not of LANCL2, increased the expression of the SM-specific uncoupling protein sarcolipin; upon treatment with ABA, both LANCL1- and LANCL2-overexpressing cells showed a significantly increased sarcolipin expression, higher than that observed in control cells treated with ABA (**Figure 22**, upper left panel). Silencing both LANCL1 and LANCL2 significantly reduced sarcolipin expression and abrogated the effect of ABA (**Figure 22**, lower left panel), indicating that both LANCL proteins control the expression of sarcolipin. Total mitochondrial DNA, a measure of a mitochondrial number, did not increase in LANCL1- or LANCL2-overexpressing cells (**Figure 22**, upper central panel); however, the combined silencing of both proteins significantly reduced mitochondrial DNA content in L6 cells compared to control cells (**Figure 22**, lower central panel). These results indicate that the basal L6 cell expression of LANCL1/2 is both required and sufficient for the maintenance of mitochondrial DNA levels. Expression of UCP3, the most abundantly expressed member of the UCP family in the SM [68], was also investigated. UCP3 mRNA increased approximately 10-fold in LANCL1-overexpressing L6 compared to control cells; a significant (approximately 5-fold) increase of UCP3 mRNA was also

observed in LANCL2-overexpressing cells (**Figure 22**, upper right panel). Silencing both LANCL proteins drastically reduced UCP3 mRNA levels compared to control cells and significantly reduced the response to the stimulatory effect of ABA on UCP3 transcription (**Figure 22**, lower right panel).

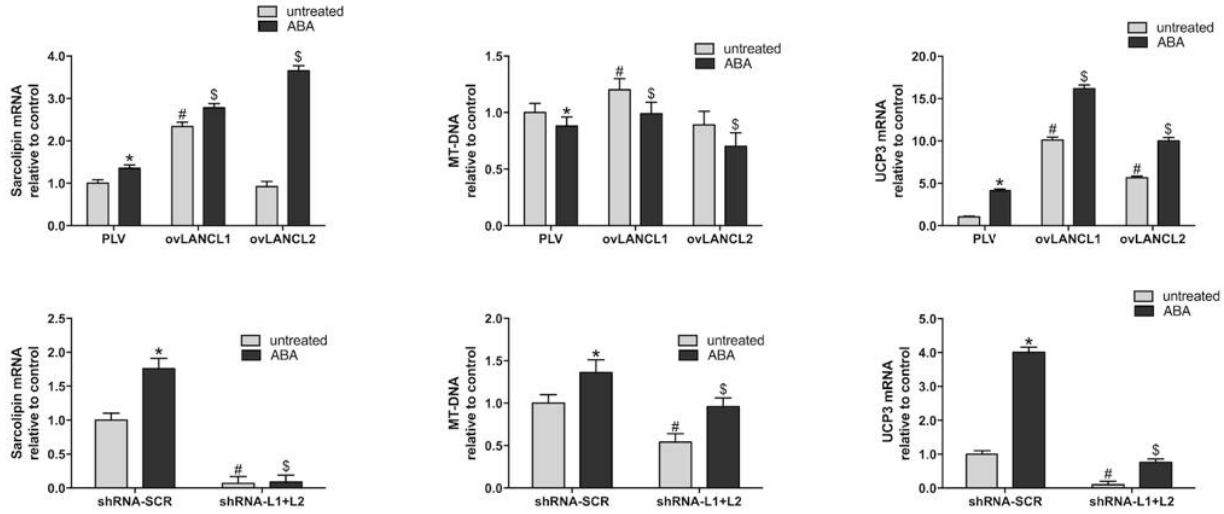

Figure 22. qPCR analysis; L6 myoblasts overexpressing LANCL1 (ovLANCL1) or LANCL2 (ovLANCL2) or silenced for the expression of both proteins (shRNA-L1+L2) were serum-starved for 12 h and then incubated without or with 100 nM ABA for 4 h. Upper left panel, sarcolipin mRNA; upper central panel, mitochondrial DNA (MT-DNA); upper right panel, UCP3 mRNA in LANCL1/2 overexpressing cells relative to control cells, infected with the empty vector and untreated (PLV); *$p < 0.008$ relative to untreated PLV-infected cells, $^{\#}p < 0.05$ relative to untreated control, $^{\$}p < 0.03$ relative to ABA-treated PLV-infected cells. Lower left panel, sarcolipin mRNA; lower central panel, mitochondrial DNA (MT-DNA); lower right panel, UCP3 mRNA in cells silenced for LANCL1 and LANCL2 relative to control cells, infected with the scramble shRNAs and untreated (shRNA-SCR). *$p < 0.02$ relative to untreated control, $^{\#}p < 0.005$ relative to untreated control; $^{\$}p < 0.02$ relative to ABA-treated shRNA-SCR-infected cells. Each panel shows the mean ± SD of at least 3 separate experiments. P values are calculated by unpaired two-tailed t-test.

Conversely, the expression of UCP1, both at the mRNA (**Figure 23**, left panel) and protein level (**Figure 23**, right panel), was only slightly increased in LANCL1/2-overexpressing cells.

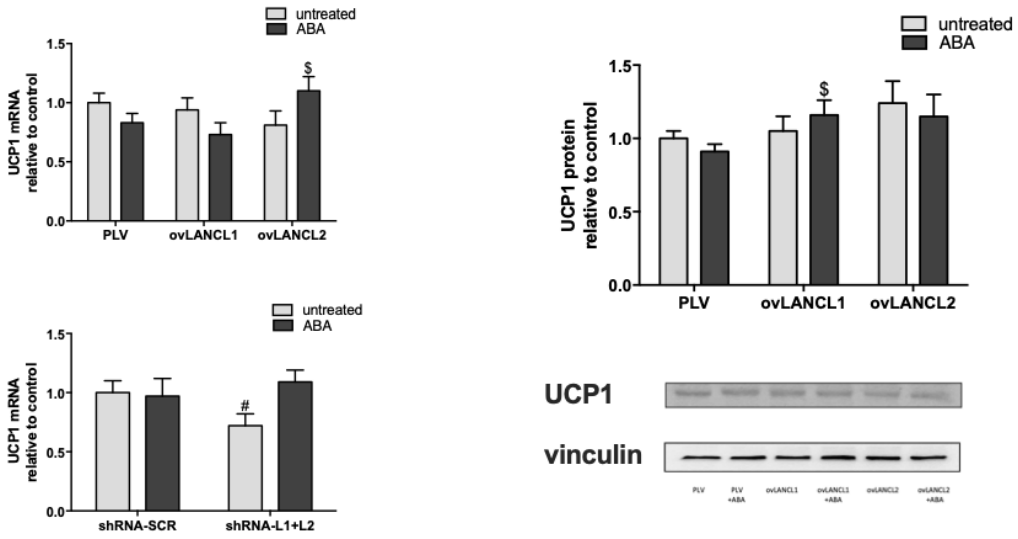

Figure 23. qPCR analysis and Western blot experiments; serum-starved L6 myoblasts overexpressing LANCL1 (ovLANCL1) or LANCL2 (ovLANCL2) or silenced for both proteins (shRNA-L1+L2) were incubated without or with 100 nM ABA for 1 h and 4 h for protein level and mRNA, respectively. Upper left panel, UCP1 mRNA in LANCL1/2 overexpressing cells relative to control cells infected with the empty vector and untreated (PLV); $^{\$}p < 0.03$ relative to ABA-treated PLV-infected cells. Lower left panel, UCP1 mRNA in cells silenced for LANCL1 and LANCL2 relative to control cells infected with the scramble shRNAs and untreated (shRNA-SCR). $^{\#}p < 0.03$ relative to untreated control. Upper and lower right panel, UCP1 in ovLANCL1 or ovLANCL2 relative to control cells infected with the empty vector and untreated (PLV). $^{\$}p < 0.02$ relative to ABA-treated PLV-infected cells. Each panel shows the mean ± SD of 3 separate experiments. P values are calculated by unpaired two-tailed t test.

Finally, cell respiration was evaluated: in L6 cells overexpressing either LANCL1 or LANCL2, O_2 consumption increased significantly compared to control cells and the preincubation of cells with 100 nM ABA for 12 h further stimulated respiration, which is significantly more in the overexpressing cells compared to cells infected with the empty vector (**Figure 24**).

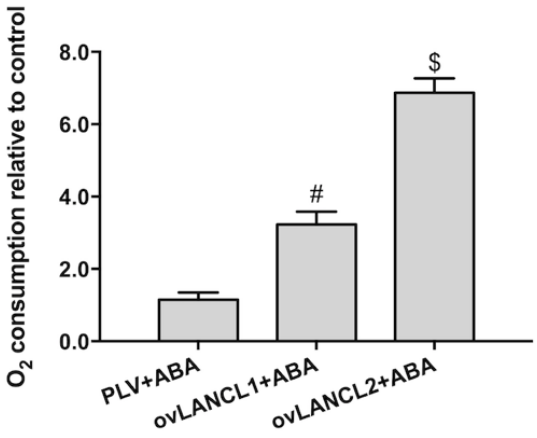

Figure 24. O_2 consumption by L6 myoblasts ovLANCL1 or ovLANCL2 increased approximately 4- and 6-fold relative to cells infected with the empty vector (PLV). Cells were incubated for 18 h at 37°C in DMEM in the presence or absence

of 100 nM ABA. Oxygen consumption was measured in a cell suspension with a micro-amperometric electrode. The panel shows the rate of oxygen consumption of ABA-treated cells relative to control cells not treated with ABA. $^{\#}p < 0.0009$ relative to ABA-treated PLV-infected cells; $^{\$}p < 0.00002$ relative to ABA-treated PLV-infected cells. Data are means ± SD of 3 different experiments.

Expression levels of both LANCL1 and LANCL2, which increased over several weeks of the culture of the cells, correlated with UCP3 mRNA levels and with cell respiration. The correlation between the LANCL1 expression and UCP3 mRNA levels (Pearson R=0.906; p=0.013) or O_2 consumption (Pearson R=0.886; p=0.019) was best described by an exponential curve, whereas the correlation between LANCL2 expression and UCP3 mRNA (Pearson R=0.839; p=0.009) or O_2 consumption (Pearson R=0.849; p=0.008) was best described by a line. When the expression levels of both LANCL proteins were plotted against UCP3 mRNA levels (Pearson R=0.837; p=0.0004) or cell O_2 consumption (Pearson R=0.802; p=0.0006), a linear correlation was observed (**Figure 25**). The expression of the LANCL1 receptor is more associated with mitochondrial uncoupling and respiration than that of the LANCL2 protein. This behavior could be due to the multiplicity of signaling pathways downstream of LANCL1 and LANCL2, which could activate different functional responses in the same cell.

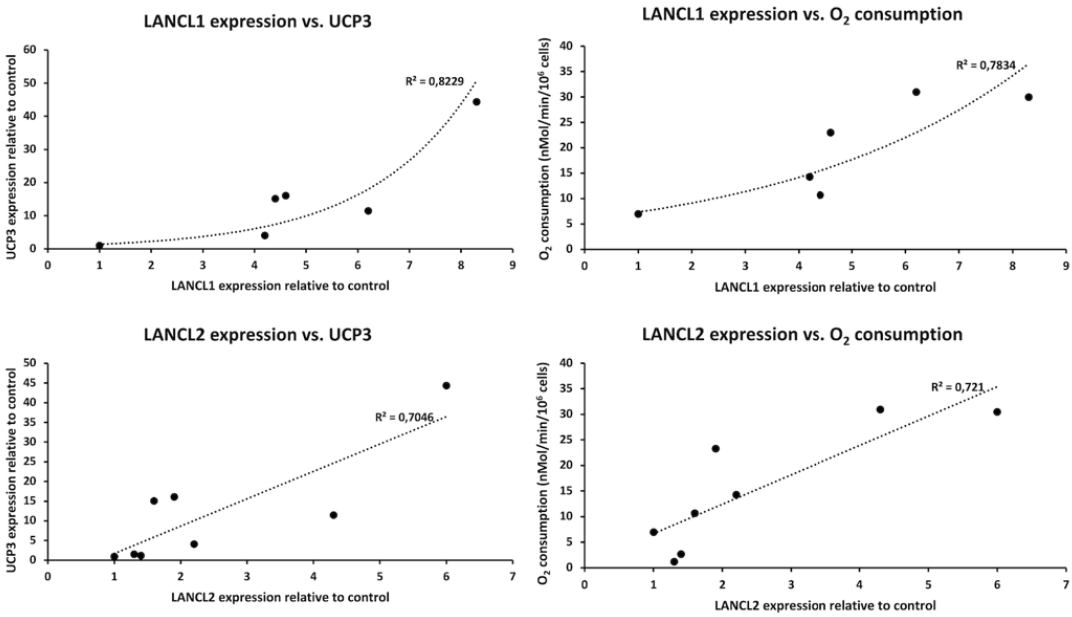

Figure 25. Correlation between the expression level of LANCL1 (upper panels) or of LANCL2 (lower panels) in ovLANCL1 or ovLANCL2 cells and UCP3 mRNA (left panels) or cell O_2 consumption (right panels). LANCL1/2 and UCP3 mRNA levels are relative to the respective mRNA in cells infected with the empty vector (control). O_2 consumption is expressed in nMoles/min/10^6 cells. Each point is the mean of at least two separate determinations, performed on cells at different time points after infection and antibiotic selection. The value of R^2 of the best-fitting curve is shown.

Together, these results suggest that both LANCL1 and LANCL2 control the expression of UCP3 and cell respiration rate, with LANCL1 transcription levels correlating with a logarithmic increase in UCP3 expression and cell respiration. Indeed, silencing both LANCL1 and LANCL2 greatly reduced the expression of PGC-1α (**Figure 18**, upper right panel), a main regulator of mitochondrial function [69]. Interestingly, silencing both LANCL1 and LANCL2 also greatly reduced (by approximately 75%) the expression of Sirt1 (**Figure 18**, lower right panel), another key regulator of skeletal muscle metabolism and function [67].

3.5. Abscisic acid improves glucose tolerance in LANCL2$^{-/-}$ mice *via* the AMPK/PGC-1α /Sirt1 axis

A normal fasting glycemia but a significantly reduced glucose tolerance had been previously observed in male LANCL2$^{-/-}$ mice [59] and was confirmed by comparing the glycemia profile of wild-type (WT) and LANCL2$^{-/-}$ (KO) mice after an oral glucose load (**Figure 26**, left panel). Within a 0-30 min time frame, glycemia increased significantly faster in KO mice than WT mice (3.7 ± 1.3 vs. 2.3 ± 0.9 mg/dL/min, p=0.001). Both WT and KO mice responded to chronic ABA treatment (1 μg/kg BW/day for 4 weeks) with a significant reduction of the area-under-the-curve (AUC) of glycemia (**Figure 26**, right panel), indicating that the absence of LANCL2 did not abrogate sensitivity to the glycemia-lowering action of ABA.

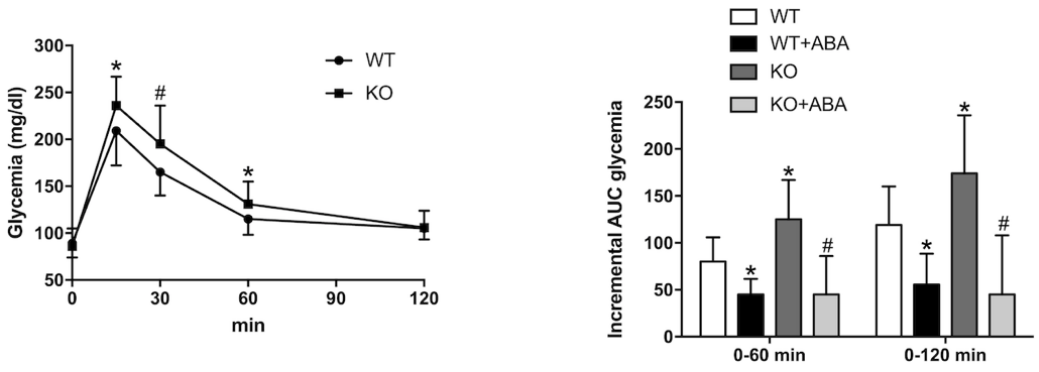

Figure 26. Male, seven week-old LANCL2$^{-/-}$ mice (KO) and their wild-type siblings (WT), 9 per group, were subjected to an oral glucose tolerance test (OGTT). Left panel, glycemia profile as monitored by tail vein puncture at the indicated time points after gavage. *$p < 0.04$ and $^{\#}p < 0.01$ relative to WT. Right panel, incremental AUC of glycemia calculated, in the indicated time frames, with the trapezoidal rule on the glycemia increase relative to time zero in WT and KO mice undergoing an OGTT with or without ABA at 1 μg/kg BW, in addition to glucose. *$p < 0.05$ relative to WT; $^{\#}p < 0.003$ relative to KO.

Therefore, the expression levels of LANCL1 in the SM from LANCL2$^{-/-}$ and WT mice were compared. SM expression of LANCL1 was significantly higher in quadriceps muscles from

LANCL2$^{-/-}$ mice compared to WT controls and chronic treatment of the animals with oral ABA further increased LANCL1 expression, at both the protein (**Figure 27**, left panel) and mRNA (**Figure 27**, right panel) levels.

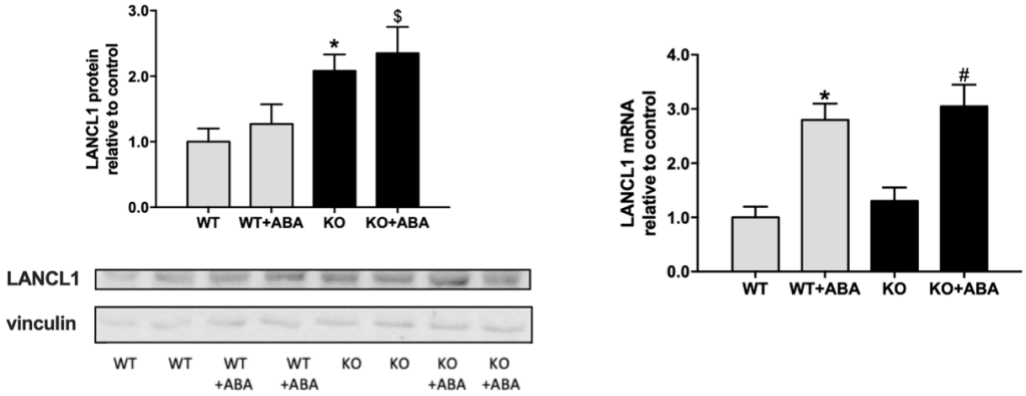

Figure 27. LANCL2$^{-/-}$ and WT mice were treated without or with ABA (1 μg/kg BW/day administered in the drinking water) for 4 weeks. At the end of treatment, mice were euthanized and samples of skeletal muscle were taken for Western blot analysis and qPCR of the indicated proteins. Results shown are relative to the WT expression level and are the mean ± SD from 4 to 6 mice per group. P values are calculated by unpaired t-test. LANCL1 protein (left panel) and mRNA (right panel). *$p < 0.05$ relative to WT; $^{\#}p < 0.02$ relative to KO; $^{\$}p < 0.05$ relative to ABA-treated WT.

LANCL1 and LANCL2 controlled levels of AMPK/PGC-1α/Sirt1 and GLUT1/4 in L6 cells (**Figures 17-21**); thus, we compared the expression of these proteins in SM biopsies from WT and LANCL2$^{-/-}$ mice treated with ABA or not. Chronic ABA treatment significantly increased muscle expression of AMPK, PGC-1α and GLUT4 in the SM from WT mice. SM from LANCL2$^{-/-}$ mice showed higher protein levels of PGC-1α and GLUT4 than WT controls, which did not further increase upon ABA treatment (excluding AMPK) and were similar to those of WT mice treated with ABA (**Figure 28**, left panel). The ratio between pAMPK and AMPK protein levels in ABA-treated and -untreated mice, both WT and KO, was similar and approximately 1, in line with what was observed in L6 cells overexpressing LANCL1 or LANCL2. mRNA levels of AMPK, PGC-1α, GLUT4 and GLUT1 were all significantly higher in the SM from WT and LANCL2$^{-/-}$ mice treated with ABA compared to the respective untreated controls (**Figure 28**, right panel) and the extent of increase was similar in WT and LANCL2$^{-/-}$ mice, indicating that the genetic ablation of LANCL2 does not affect the stimulatory effect of oral ABA on the transcription of the genes encoding those proteins. Finally, chronic ABA treatment significantly increased mRNA levels of Sirt1 and NAMPT in the SM from both WT and LANCL2$^{-/-}$ mice (**Figure 28**).

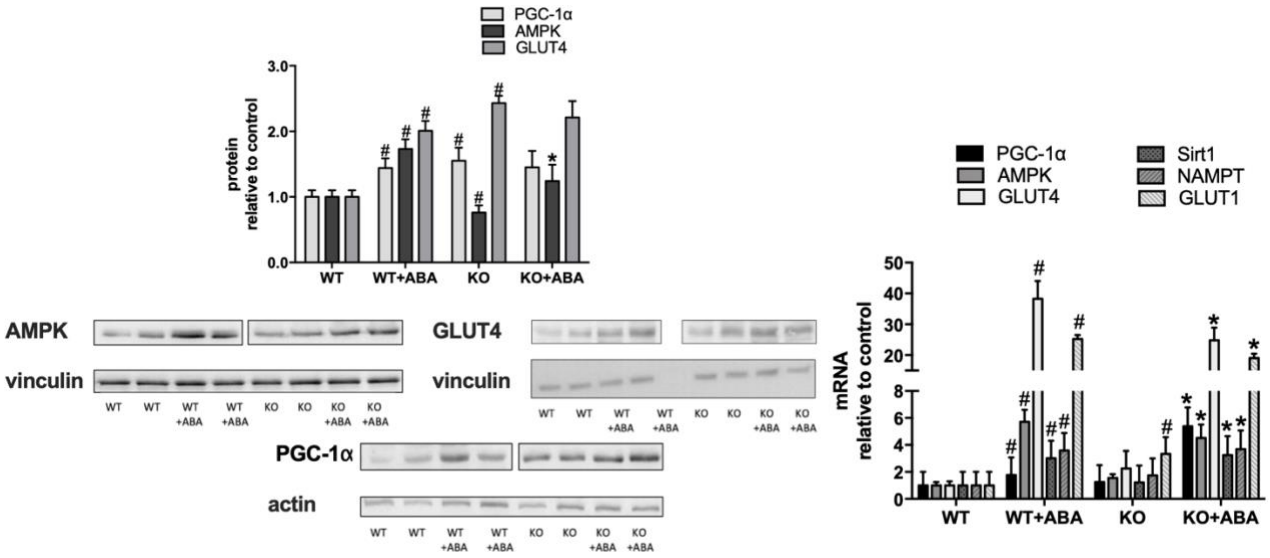

Figure 28. LANCL2$^{-/-}$ and WT mice were treated without or with ABA (1 µg/kg BW/day administered in the drinking water) for 4 weeks. At the end of treatment, mice were euthanized and samples of skeletal muscle were taken for Western blot analysis and qPCR of the indicated proteins. Results shown are relative to the WT expression level and are the mean ± SD from 4 to 6 mice per group. P values are calculated by unpaired t-test. Protein expression (left panel) or mRNA transcription (right panel) of GLUT4, GLUT1, the AMPK/PGC-1α/Sirt1 signaling axis and NAMPT are expressed relative to levels in untreated WT muscle. $^{\#}p < 0.05$ relative to WT; $^{*}p < 0.04$ relative to KO.

NAMPT overexpression in SM has been reported to promote cell survival (by maintaining mitochondrial NAD^+ levels [70]) and to increase mitochondrial gene expression and ameliorate exercise endurance in mice [71]. Indeed, we observed an increased physical endurance in mice chronically treated with low-dose ABA [26]. Interestingly, increased mRNA levels of both Sirt1 and NAMPT were observed as early as 30-60 min after the addition of 100 nM ABA to muscle biopsies from WT mice *ex vivo* (**Figure 29**), indicating that the transcriptional stimulation by ABA on these target proteins is fast and direct.

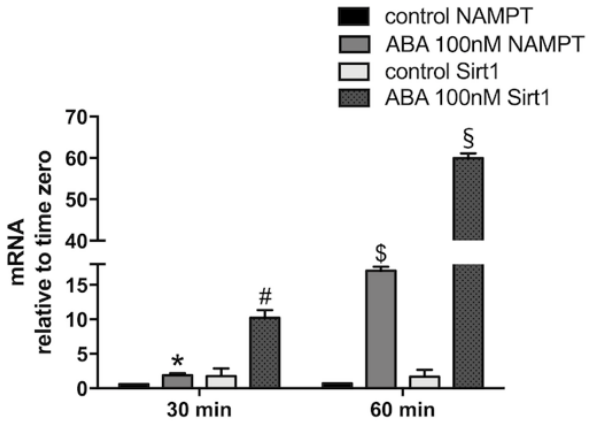

Figure 29. Freshly excised samples of femoral quadriceps from WT mice (30 mg) were incubated *ex vivo* without (control) or with 100 nM ABA for 30 or 60 min. The mRNA levels of NAMPT and Sirt1 were determined by qPCR; *p

< 0.01 relative to control at 30 min; #p < 0.0007 relative to control at 30 min; $p < 0.000003 relative to control at 60 min; §p < 0.0000003 relative to control at 60 min. The mean ± SD from 3 experiments is shown.

Sarcolipin and mitochondrial DNA content were affected by LANCL1/2 expression levels and by ABA in L6 myoblasts (**Figure 22** and **Figure 25**); in the SM from ABA-treated WT and KO mice, sarcolipin increased significantly (approximately 5-fold) and similarly to the respective ABA-untreated controls (**Figure 30**, left panel). The mitochondrial DNA content in the SM from ABA-treated WT mice also increased compared to untreated controls (approximately 2-fold), whereas LANCL2$^{-/-}$ mice had higher levels of mitochondrial DNA compared to WT animals, possibly the result of higher LANCL1 expression levels (**Figure 27**), which further slightly and not significantly increased upon treatment with ABA (**Figure 30**, central panel). These results confirm the role of ABA in increasing the SM expression of sarcolipin and mitochondrial DNA content *in vivo* and indicate that LANCL2 is not essential in mediating this effect. UCP3 was highly expressed in the SM from ABA-treated WT mice compared to untreated controls (approximately 9-fold). SM from LANCL2$^{-/-}$ mice showed a 2-fold higher expression of UCP3 compared to SM from WT mice and also responded to ABA with a further significant increase of UCP3 expression, similar to that observed in ABA-treated WT mice (**Figure 30**, right panel).

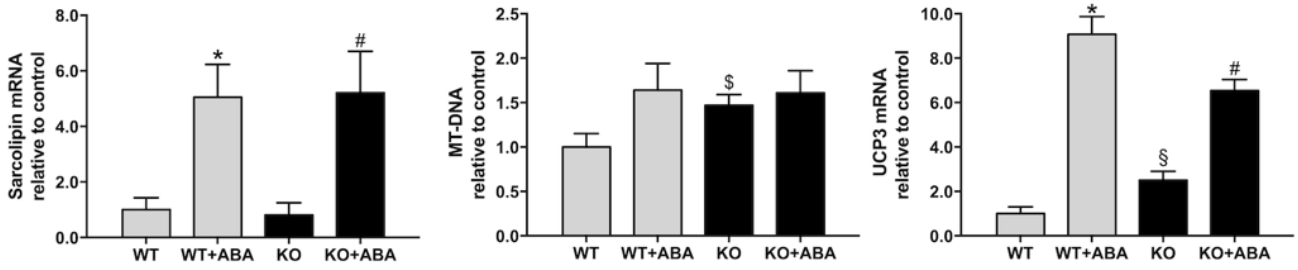

Figure 30. LANCL2$^{-/-}$ and WT mice were treated without or with ABA (1 μg/kg BW/day administered in the drinking water) for 4 weeks. At the end of treatment, mice were euthanized and samples of skeletal muscle were taken for qPCR analysis of the indicated proteins. Results shown are relative to the WT expression level and are the mean ± SD from 4 to 6 mice per group. P values are calculated by unpaired t-test. Sarcolipin (left panel) and UCP3 (right panel) mRNAs and the mitochondrial DNA content (MT-DNA) (central panel) are expressed relative to the respective content in WT mice (control). *p < 0.009, $p < 0.05 and §p < 0.01 relative to WT; #p < 0.004 relative to KO.

3.6. ABA increases AMPK phosphorylation and AMPK and PGC-1α protein levels in pre-adipocytes overexpressing LANCL1 and LANCL2

LANCL1 and LANCL2 have been identified as the ABA receptors in mammalian cells [19,21,72]. To investigate whether LANCL1/2 expression modulates glucose uptake in adipocytes, we undertook

the overexpression of either of the proteins in brown and white human pre-adipocytes (TERT-hBA and TERT-hWA, respectively) [64]. Overexpression of LANCL1 and LANCL2 proteins was obtained by retroviral infection and was confirmed by Western blot analysis. As in L6 rat myoblasts, the overexpression of one receptor increases slightly the expression of the other receptor. All experiments were performed with an overexpression of approximately 6-fold for LANCL1 and 15-fold for LANCL2 in white pre-adipocytes (**Figure 31**, left panel) and of approximately 6-fold for LANCL1 and 13-fold for LANCL2 in brown pre-adipocytes (**Figure 31**, right panel) relative to control cells infected with an empty PLV vector.

Figure 31. LANCL1 and/or LANCL2 were stably overexpressed in human TERT-hWA and TERT-hBA pre-adipocytes by viral infection; left panel, representative Western blot of LANCL1/2 proteins in TERT-hWA cells overexpressing LANCL1 (ovLANCL1), LANCL2 (ovLANCL2) or both LANCL1 and LANCL2 (ovLANCL1+2); right panel, representative Western blot of LANCL1/2 proteins in TERT-hBA cells overexpressing LANCL1 (ovLANCL1), LANCL2 (ovLANCL2) or both LANCL1 and LANCL2 (ovLANCL1+2).

At the protein level, in TERT-hWA cells, the total AMPK increased slightly in pre-adipocytes overexpressing LANCL2, but not LANCL1, while the phosphorylated AMPK increased in pre-adipocytes overexpressing LANCL1 and/or LANCL2; upon treatment with 100 nM ABA, both AMPK and pAMPK significantly increased in cells overexpressing LANCL1 and/or LANCL2 (**Figure 32**, left panel). In TERT-hBA cells, total and phosphorylated AMPK increased in pre-adipocytes overexpressing LANCL1 and/or LANCL2 only upon incubation with 100 nM ABA, indicating that both LANCL1 and LANCL2 stimulate AMPK protein expression and phosphorylation upon ABA binding (**Figure 32**, right panel).

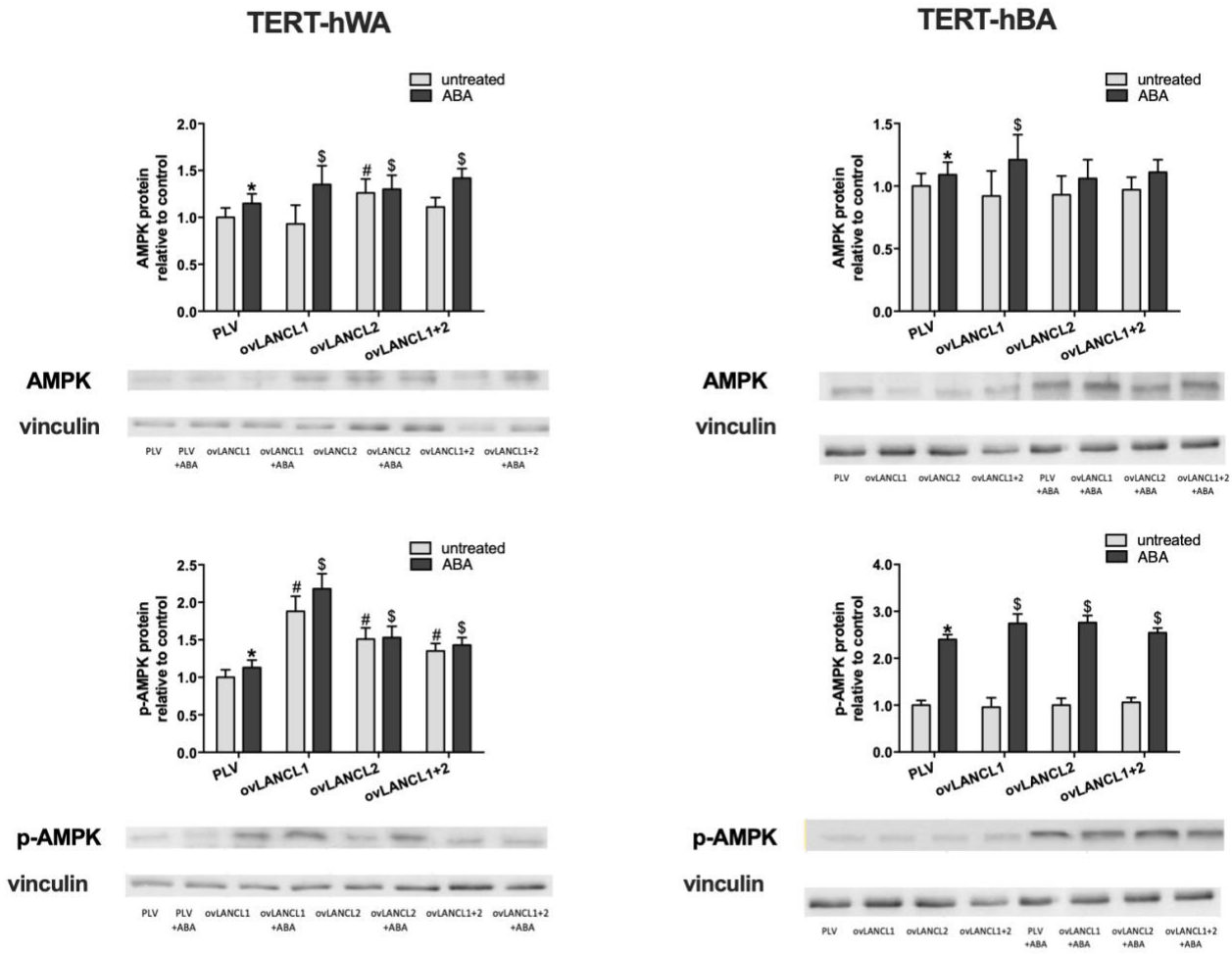

Figure 32. Western blot experiments; human TERT-hWA and TERT-hBA pre-adipocytes overexpressing LANCL1 and/or LANCL2, serum-starved for 12 h and then incubated without or with 100 nM ABA for 1 h, were also analyzed by Western blot for expression of the indicated proteins. Upper left panel, total AMPK in TERT-hWA cells overexpressing LANCL1 (ovLANCL1), LANCL2 (ovLANCL2) or both LANCL1 and LANCL2 (ovLANCL1+2), relative to control cells infected with the empty vector and untreated (PLV). Lower left panel, phosphorylated (Ser473) AMPK (pAMPK) relative to PLV in TERT-hWA cells. Upper right panel, total AMPK in TERT-hBA cells overexpressing LANCL1 (ovLANCL1), LANCL2 (ovLANCL2) or both LANCL1 and LANCL2 (ovLANCL1+2), relative to control cells infected with the empty vector and untreated (PLV). Lower right panel, phosphorylated (Ser473) AMPK (pAMPK) relative to PLV in TERT-hBA cells. *$p < 0.02$ relative to untreated control, $^{\#}p < 0.005$ relative to untreated control; $^{\$}p < 0.01$ relative to ABA-treated PLV-infected cells. P values are calculated by unpaired, two-tailed t-test.

In TERT-hWA cells, PGC-1α protein expression increased in both LANCL1 and/or LANCL2-overexpressing pre-adipocytes approximately 2-fold compared to control cells and treatment with ABA further increased PGC-1α protein levels (**Figure 33**, left panel). In TERT-hBA cells, PGC-1α protein expression increased only upon incubation with 100 nM ABA (**Figure 33**, right panel). Together, these results suggest that both LANCL proteins transduce an ABA-triggered response, activating AMPK phosphorylation and increasing AMPK and PGC-1α protein expression.

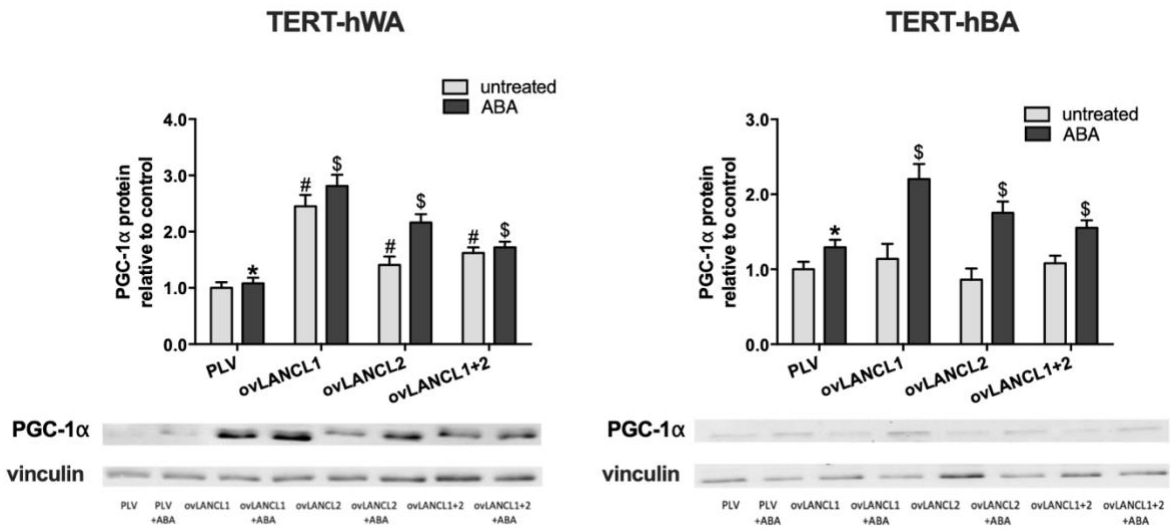

Figure 33. Western blot experiments; human TERT-hWA and TERT-hBA pre-adipocytes overexpressing LANCL1 and/or LANCL2, serum-starved for 12 h and then incubated without or with 100 nM ABA for 1 h, were also analyzed by Western blot for expression of PGC-1α protein. Left panel, PGC-1α in TERT-hWA cells overexpressing LANCL1 (ovLANCL1), LANCL2 (ovLANCL2) or both LANCL1 and LANCL2 (ovLANCL1+2), relative to control cells infected with the empty vector and untreated (PLV). Right panel, PGC-1α in TERT-hBA cells overexpressing LANCL1 (ovLANCL1), LANCL2 (ovLANCL2) or both LANCL1 and LANCL2 (ovLANCL1+2), relative to control cells infected with the empty vector and untreated (PLV). *$p < 0.03$ relative to untreated control, $^{\#}p < 0.004$ relative to untreated control; $^{\$}p < 0.005$ relative to ABA-treated PLV-infected cells. P values are calculated by unpaired, two-tailed t-test.

3.7. Transcriptional effects of ABA on brown and white human adipocytes

Previous studies evaluated the effect of ABA on gene transcription during adipocyte differentiation in 3T3-L1 cells, exploring the expression of the typical adipocyte markers at days 1, 3 and 8 of the differentiation process. Adiponectin and leptin mRNAs were both significantly increased in ABA-treated 3T3-L1 derived adipocytes compared with untreated controls (2.9- and 2.5-fold, respectively) as early as 24 hours after induction of differentiation and this up-regulation persisted, although to a lower extent, also at day 3. Transcription of PPAR-γ, also increased, slightly but significantly, in ABA-treated cells, both at day 1 and at day 3 of differentiation (with a 15% and 26% increase relative to controls, respectively). Conversely, the fatty acid synthase (FAS) mRNA levels were slightly increased by the presence of ABA only at day 3 of differentiation. Finally, the transporters of free fatty acids (FFA) AP2 and of glucose (GLUT4) were up-regulated by ABA treatment as compared with control cells, showing a significant increase both at day 1 and 3, yet with different kinetics. The browning effect of ABA was also monitored at days 2, 5 and 8 by analyzing the expression of the browning-specific markers UCP1, PGC-1α, CIDE-A, TMEM26 and PRDM16. mRNA levels from all genes explored were up-regulated in ABA-treated compared with control cells at all time points

(days 2, 5 and 8 post-induction of differentiation), except for PRDM16, which increased over control values at days 5 and 8, but not at day 2. mRNA levels of UCP1 and PRDM16 progressively increased during exposure of the cells to ABA, reaching 3-fold higher values relative to controls at day 8. When 100 nM ABA was added at the end of the differentiation process (day 10) for 24 hours, a significant increase of mRNA levels of UCP1, PGC-1α, CIDE-A and FGF21 was observed relative to ABA-untreated cells (3.2 ± 0.5, 2 ± 0.1, 2.9 ± 0.2, 7.5 ± 0.9, respectively) [27]. In light of these considerations, both TERT-hWA and TERT-hBA cells were induced to differentiate (**Figure 34**), by culture in the respective differentiation cocktails as described in Materials and Methods, in the presence or absence of 100 nM ABA: expression of markers was explored at days 0 and 12 of the differentiation process in TERT-hBA cells and at days 0, 12 and 15 in TERT-hWA cells.

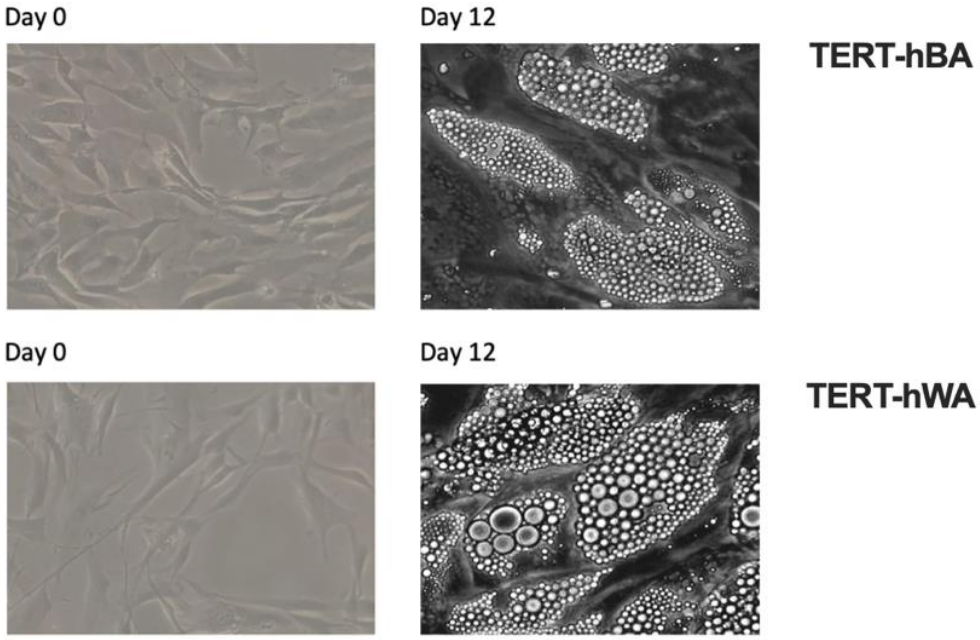

Figure 34. Representative micrographs of TERT-hBA (upper panels) and TERT-hWA (lower panels) pre-adipocytes and adipocytes at days 0 and 12.

We investigated whether ABA could induce the activation of adipocyte genes regulating the "browning" process *via* the AMPK/PGC-1α/Sirt1 axis. To this purpose, mRNA levels of the browning-specific markers UCP1, PGC-1α, CIDE-A and PPAR-γ [53,54,55,73] were compared in ABA-treated and in control cells. The levels of all mRNAs explored were up-regulated in basal unstimulated cells; treatment with 100 nM ABA further increased the transcription of the genes encoding those proteins at all time points (days 12 and 15 post-induction of differentiation) (**Figure 35**, upper left panel). Expression levels of CPT1ß, MPC1 and PDHα1 (**Figure 35**, upper right panel), involved in oxidative metabolism, and GLUT4 (**Figure 35**, lower left panel) significantly increased

in ABA-treated adipocytes compared to control cells after differentiation. Mitochondrial DNA content also increased during differentiation and following exposure with ABA (**Figure 35**, lower right panel). Taken together, these results demonstrate that differentiation is associated with high expression of mRNAs levels and mature TERT-hWA adipocytes can convert into brown-like adipocytes upon exposure to rosiglitazone and ABA. It appears that these two players may have a synergistic effect on gene expression.

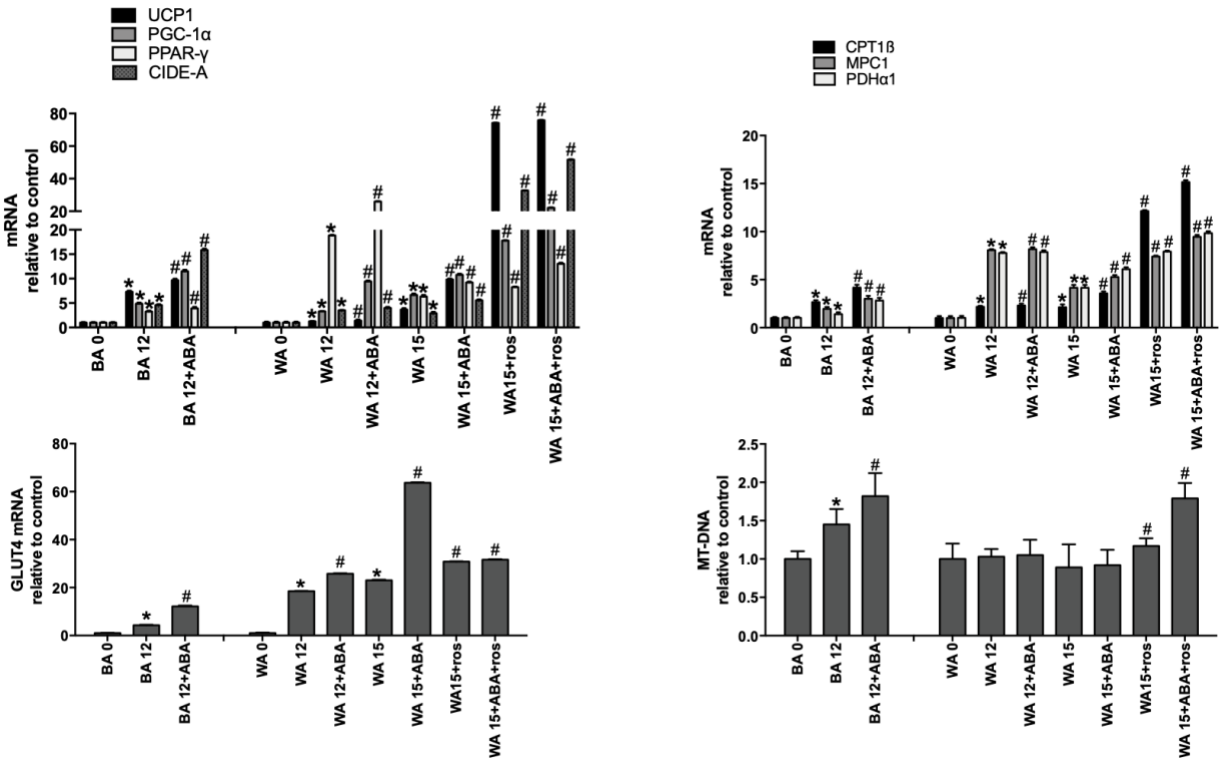

Figure 35. qPCR analysis; human TERT-hWA and TERT-hBA pre-adipocytes differentiated to adipocytes in the absence (control) or presence of 100 nM ABA: at the indicated time points (day 0, day 12 or day 15), the mRNA levels of the indicated genes were evaluated by qPCR. Upper left panel, UCP1, PGC-1α, PPAR-γ and CIDE-A mRNAs; upper right panel, CPT1ß, MPC1 and PDHα1 mRNAs; lower left panel, GLUT4 mRNA; lower right panel, the mitochondrial DNA content (MT-DNA). Results shown are the mean ± SD from at least 4 experiments; *$p < 0.04$ relative to undifferentiated untreated control, $^{\#}p < 0.004$ relative to differentiated control. P values are calculated by unpaired, two-tailed t-test.

3.8. Effect of ABA on lipid droplets and on gene expression in mature human adipocytes overexpressing LANCL1 and LANCL2

To understand the implication of LANCL1 and LANCL2 receptors in adipose tissue function and metabolism, the overexpression of both LANCL proteins in TERT-hBA and TERT-hWA pre-adipocytes was considered. Adipocytes were treated or not with 100 nM ABA, during brown and

white differentiation, and at day 12 were stained with Oil Red O staining. The differentiation of white (**Figure 36**, left panel) and brown (**Figure 36**, right panel) adipocytes overexpressing LANCL1 and/or LANCL2 revealed that a high percentage of pre-adipocytes became lipid-laden (approximately 90%). Accumulation of lipid droplets is slightly increased after exposure with ABA and basally in adipocytes overexpressing ABA receptors.

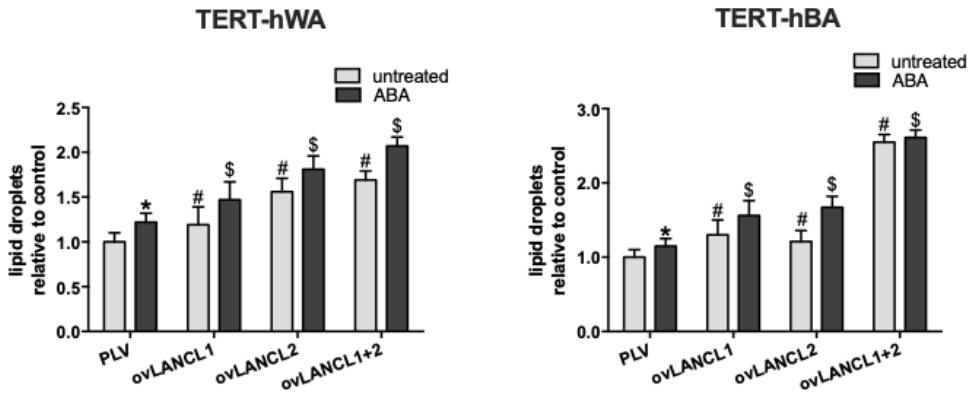

Figure 36. TERT-hWA (left panel) and TERT-hBA (right panel) pre-adipocytes overexpressing LANCL1 (ovLANCL1), LANCL2 (ovLANCL2) or both LANCL1 and LANCL2 (ovLANCL1+2) were cultured for 12 days with a differentiating cocktail, without or with 100 nM ABA. Lipids accumulated were stained with Oil Red O staining. Results are the mean ± SD from 3 separate experiments; *$p < 0.05$ relative to untreated control, $^{\#}p < 0.005$ relative to untreated control; $^{\$}p < 0.005$ relative to ABA-treated PLV-infected cells. P values are calculated by unpaired, two-tailed t-test.

As revealed by qPCR analysis, differentiation after LANCL1+2-overexpression *per se* increased mRNA levels of genes related to uncoupling proteins (UCP1 and UCP3), to oxidative metabolism (MPC1, PDHα1 and CPT1ß), to AMPK/PGC-1α/Sirt1 axis, to receptors for browning hormones (ADRß3, THRα1, THRß and INSR) [64,74,75,76] and to mitochondrial DNA content (MT-DNA). ABA further increases the levels of all mRNAs explored, indicating an additive function to rosiglitazone-induced browning. Thus, we investigate mRNAs levels in TERT-hWA (**Figure 37**) and TERT-hBA (**Figure 38**) adipocytes overexpressing LANCL1 and LANCL2 compared to control cells infected with PLV.

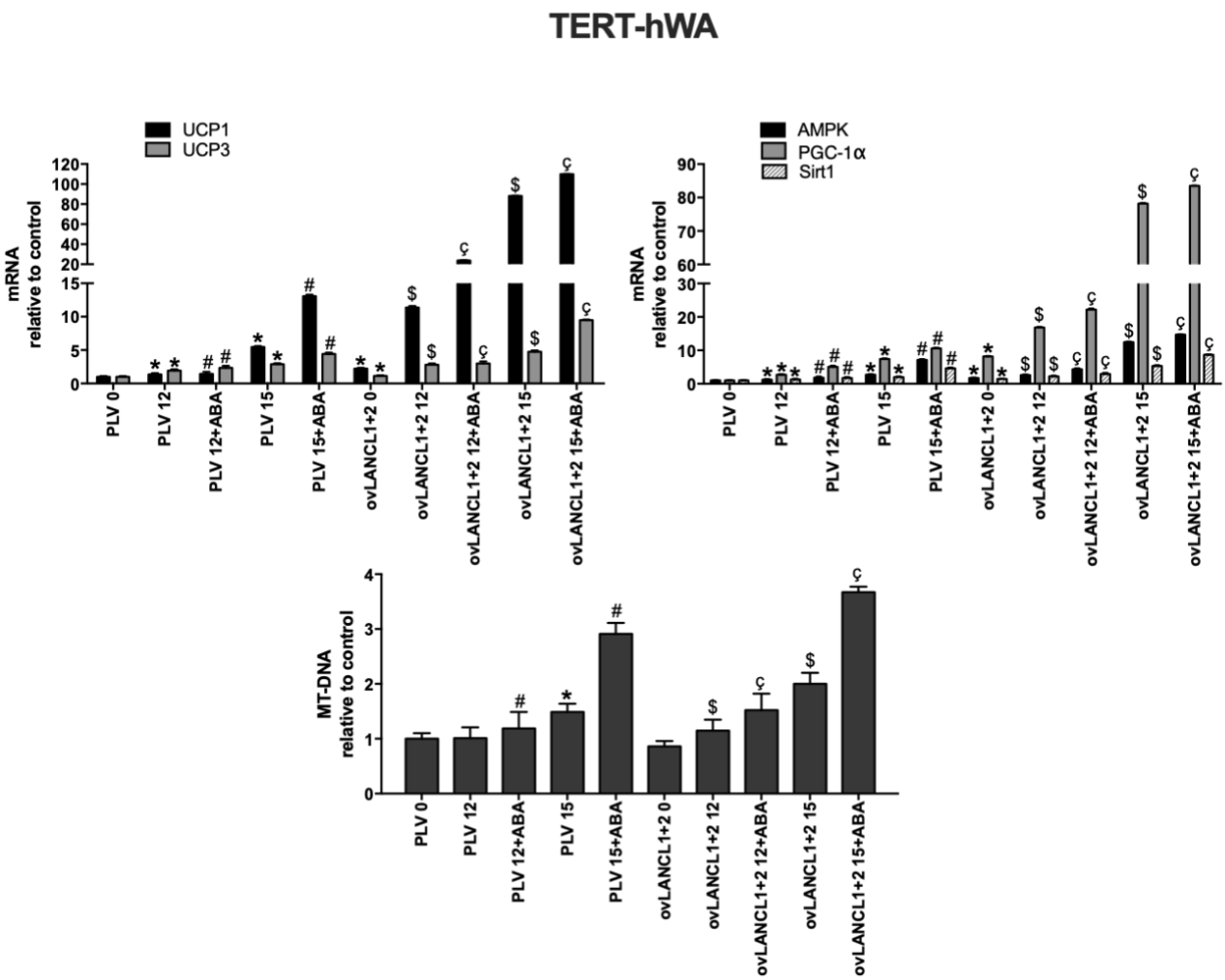

Figure 37. qPCR analysis; human TERT-hWA pre-adipocytes overexpressing LANCL1 and LANCL2 (ovLANCL1+2) differentiated to adipocytes in the absence (control) or presence of 100 nM ABA: at the indicated time points (day 0, day 12 or day 15), the mRNA levels of the indicated genes were evaluated by qPCR; upper left panel, UCP1 and UCP3 mRNAs; upper right panel, AMPK, PGC-1α and Sirt1 mRNAs; lower panel, the mitochondrial DNA content (MT-DNA) in TERT-hWA adipocytes. Results shown are the mean ± SD from at least 3 experiments; *$p < 0.02$ relative to undifferentiated untreated control, $^{\#}p < 0.006$ relative to differentiated control, $^{\$}p < 0.003$ relative to undifferentiated untreated overexpressing LANCL1 and LANCL2 control, $^{ç}p < 0.001$ relative to differentiated overexpressing LANCL1 and LANCL2 control. P values are calculated by unpaired, two-tailed t-test.

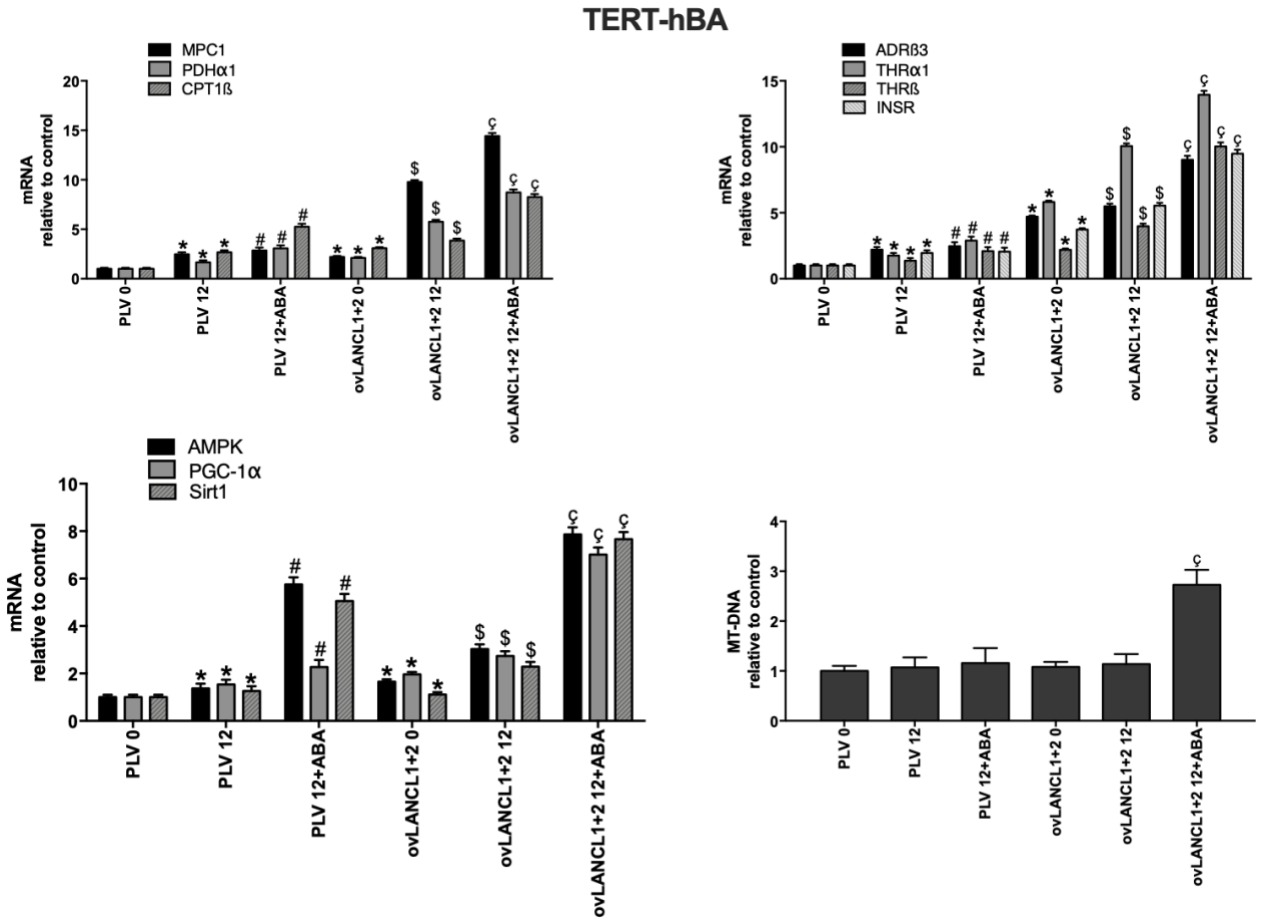

Figure 38. qPCR analysis; human TERT-hBA pre-adipocytes overexpressing LANCL1 and LANCL2 (ovLANCL1+2) differentiated to adipocytes in the absence (control) or presence of 100 nM ABA: at the indicated time points (day 0, day 12 or day 15), the mRNA levels of the indicated genes were evaluated by qPCR; upper left panel, MPC1, PDHα1 and CPT1ß mRNAs; upper right panel, ADRß3, THRα1, THRß and INSR mRNAs; lower left panel, AMPK, PGC-1α and Sirt1 mRNAs; lower right panel, the mitochondrial DNA content (MT-DNA) in TERT-hBA adipocytes. Results shown are the mean ± SD from at least 3 experiments; *$p < 0.02$ relative to undifferentiated untreated control, $^{\#}p < 0.006$ relative to differentiated control, $^{\$}p < 0.003$ relative to undifferentiated untreated overexpressing LANCL1 and LANCL2 control, $^{ç}p < 0.001$ relative to differentiated overexpressing LANCL1 and LANCL2 control. P values are calculated by unpaired, two-tailed t-test.

The expression levels of LANCL proteins in differentiated TERT-hBA and TERT-hWA adipocytes overexpressing LANCL1 and LANCL2 were significantly higher compared to control cells (4-fold for LANCL1 and 12-fold for LANCL2 in white pre-adipocytes (**Figure 39**, left panel) and of approximately 4-fold for LANCL1 and 6-fold for LANCL2 in brown pre-adipocytes (**Figure 39**, right panel)), in line with what was observed in undifferentiated adipocytes of Figure 31. Furthermore, the only overexpression of LANCL proteins induces a high gene expression, indicating a fundamental involvement. The 15-day differentiation of white adipocytes shows similar or increased expressions of the 12-day differentiation of brown adipocytes, regulating the browning process.

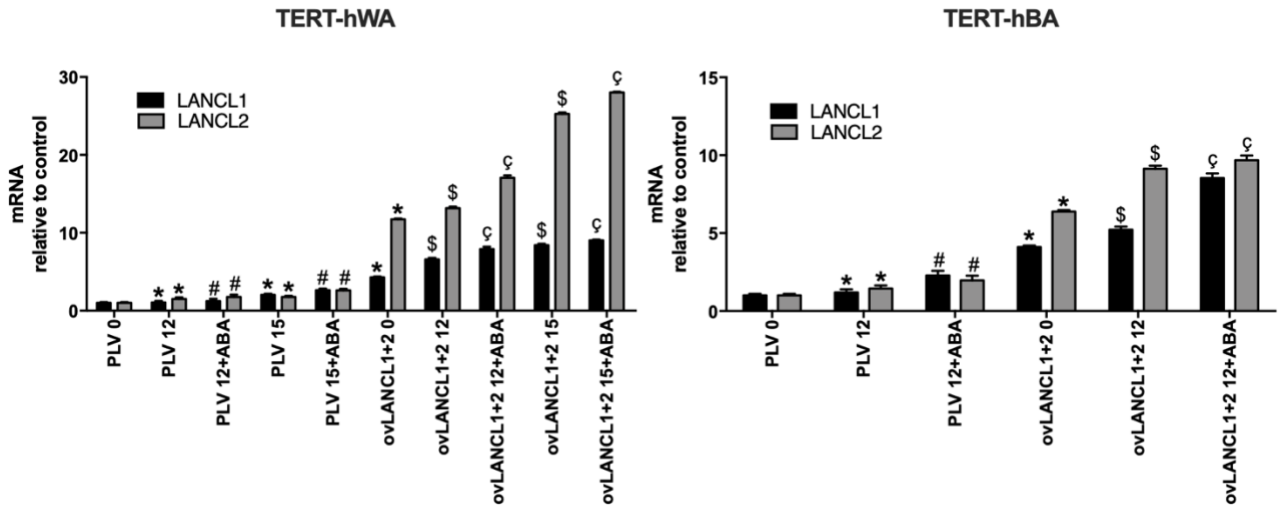

Figure 39. qPCR analysis; human TERT-hWA and TERT-hBA pre-adipocytes overexpressing LANCL1 and LANCL2 (ovLANCL1+2) differentiated to adipocytes in the absence (control) or presence of 100 nM ABA: at the indicated time points (day 0, day 12 or day 15), the expression levels of LANCL1 and LANCL2 were evaluated by qPCR. Left panel, LANCL1 and LANCL2 mRNAs in TERT-hWA adipocytes; right panel, LANCL1 and LANCL2 mRNAs in TERT-hBA adipocytes. Each panel shows the mean ± SD of at least 3 separate experiments. *$p < 0.01$ relative to undifferentiated untreated control, $^{\#}p < 0.005$ relative to differentiated control, $^{\$}p < 0.0007$ relative to undifferentiated untreated overexpressing LANCL1 and LANCL2 control, $^{ç}p < 0.001$ relative to differentiated overexpressing LANCL1 and LANCL2 control. P values are calculated by unpaired, two-tailed t-test.

3.9. Chronic ABA treatment stimulates mitochondrial DNA content in the brown adipose tissue of mice

To further investigate a possible browning effect of ABA on adipose tissue *in vivo*, CD1 LANCL2$^{+/+}$ (WT) and LANCL2$^{-/-}$ (KO) mice (5/group) were fed a standard diet without (controls), or with ABA, administered in the drinking water, at a dose of approximately 1 μg/kg BW. After 30 days, the animals were sacrificed and samples of interscapular BAT were taken to evaluate the expression of several proteins. Results obtained are shown in **Figure 40**. In LANCL2$^{-/-}$ mice, mRNA levels of LANCL1 were significantly higher relative to those in WT mice (**Figure 40**, left panel) [72], similar to those in the skeletal muscle (**Figure 27**). The mitochondrial DNA content (MT-DNA) in the BAT from ABA-treated WT mice increased (1.7-fold) compared to untreated controls, whereas KO mice had lower levels of mitochondrial DNA compared to WT animals, which further slightly increased upon treatment with ABA (**Figure 40**, right panel).

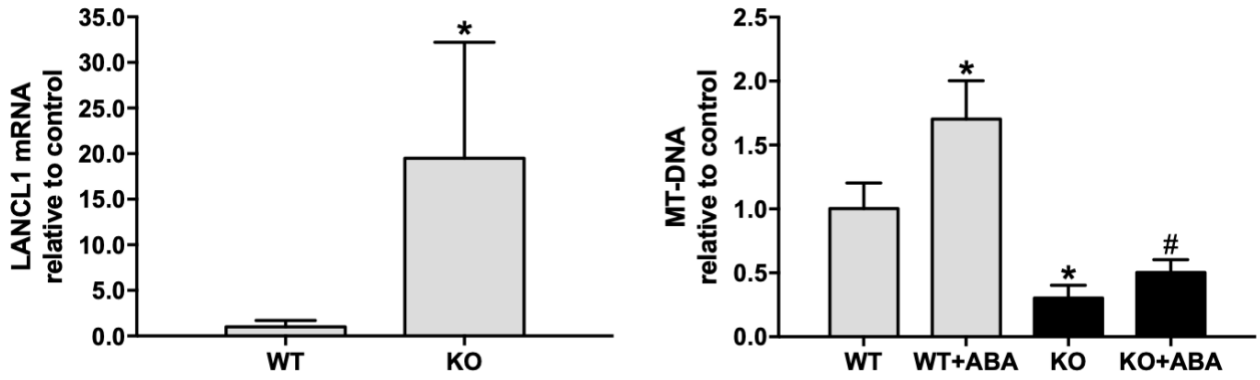

Figure 40. LANCL2$^{-/-}$ and WT mice were treated without or with ABA (1 μg/kg BW/day administered in the drinking water) for 4 weeks. At the end of treatment, mice were euthanized and samples of brown adipose tissue were taken for qPCR analysis. Left panel, LANCL1 mRNA; right panel, the mitochondrial DNA content (MT-DNA). Results shown are relative to the WT expression level and are the mean ± SD from 5 mice per group. *$p < 0.008$ relative to WT; $^{\#}p < 0.001$ relative to KO. P values are calculated by unpaired t-test.

4. DISCUSSION

Non-overlapping roles of ABA and insulin. The hypoglycemic action of insulin largely depends on its ability to stimulate glucose uptake and metabolism by adipose tissue and skeletal muscle, the latter accounting for approximately 70-80% of the total body glucose consumption [77]. Insulin alone is capable of this action; thus, the unique role of this hormone in the regulation of peripheral glucose uptake during hyperglycemia represents a bottleneck in the physiology of whole body glucose disposal and in the pharmacological approaches to improve its dysregulation. As Nature always provides multiple mechanisms for physiological functions that are essential to cell and species survival, the identification of a new hormone with the capacity to stimulate muscle glucose uptake independently of insulin fulfils a general principle of redundancy and is amenable to clinical exploitation. Abscisic acid is an isoprenoid plant stress hormone present and active also in mammals, where it stimulates tissue glucose uptake. Previously obtained data suggest that, in the absence of insulin, ABA stimulates GLUT4 expression and glucose uptake in preadipocytes, quantitatively similarly to insulin [3,27]. The effect of ABA on lipid synthesis and storage in preadipocytes is, however, different from that of insulin: ABA does not induce preadipocyte differentiation and accumulation of triglycerides, instead promoting browning features, such as increased O_2 consumption, mitochondrial content and expression of browning genes in white adipocytes *in vitro* and increased PGC-1α and UCP1 expression and glucose uptake in the brown adipose tissue of ABA-treated mice [27]. Experiments performed with two different techniques *in vitro* on L6 myoblasts and *ex vivo* on murine skeletal muscle demonstrate that ABA stimulates muscle glucose transport in the absence of insulin and that activation of AMPK is responsible for this effect, as it is abrogated by inhibition of AMPK with dorsomorphin. ABA indeed increases phosphorylation of AMPK on Thr172 in L6 cells and in mouse muscle and also stimulates AMPK transcription [26]. The activation of AMPK is in agreement with the metabolic effects exerted by ABA in skeletal muscle and in AT [27]. Indeed, AMPK directly phosphorylates and activates PGC-1α in skeletal muscle and activation of PGC-1α increases GLUT4 expression [78] and glycogen accumulation [79]. AMPK also activates PGC-1α in white visceral AT [80] and PGC-1α increases expression of thermogenic and mitochondrial genes in human and murine adipocytes [58,81]. The transcription of PGC-1α is indeed upregulated by low-dose ABA in AT, both *in vitro* and *in vivo* [27]. In addition, AMPK is known to phosphorylate and inhibit the transcriptional activity of PPAR-γ, the chief regulator of adipogenesis, thereby inhibiting preadipocyte differentiation [31] and accumulation of triglycerides [32]. AMPK-mediated suppression of PPAR-γ transcriptional activity has been linked to the anti-obesity effect of several natural products [31,82]. In line with an AMPK-dependent inhibition of adipogenesis and triglycerides accumulation in AT, chronic low-dose ABA significantly reduces BW in high-glucose

fed mice and in humans [39]. AMPK is also an upstream positive regulator of p38 MAPK [33], which was demonstrated to promote PPAR-γ phosphorylation on Ser122, thus preventing PPAR-γ mediated inhibition of GLUT4 expression [34,35]. Heterozygous PPAR-γ deficient mice have an improved insulin sensitivity and a reduced tendency to obesity [36,37] and mice chimeric for wild-type and PPAR-γ null cells exhibit little or no contribution to AT formation by null cells [38]. Natural products capable of activating AMPK, such as curcumin, genistein and ursolic acid are being proposed as treatments against obesity and the metabolic syndrome [31]. Differently from these natural compounds, ABA is also an endogenous mammalian hormone [8] and its plasma levels increase after a glucose load in healthy subjects, but not in diabetic patients [30]: this fact allows to hypothesize that low endogenous plasma ABA may concur to the metabolic derangement of the metabolic syndrome (obesity, T2D and hyperlipidemia). The role of Akt in the ABA signaling pathway is more difficult to dissect. Results obtained in our recent studies show that, in serum-starved L6 myoblasts, ABA induces an approximate 2-fold increase in both pAkt (Ser473) and total Akt, in the absence and in the presence of 5 mM glucose. Preincubation of L6 myoblasts with AZD5363, a pan-Akt competitive inhibitor [83], significantly increased pAMPK levels in ABA-treated compared with untreated cells, indicating presence of a moderating effect by Akt on ABA-induced AMPK activation [26]. Indeed, activation of Akt by phosphorylation on both Thr308 and Ser473 inhibits AMPK phosphorylation on Thr172 by LKB1 [84]. Akt lies at the crossroads between starved and fed state: in the fed state, insulin and high glucose favor the double phosphorylation of Akt on Ser473 and on Thr308 [85,86]. It is possible that, despite the 12 hours serum starvation of L6 cells, some amount of Akt phosphorylated on Thr308 was present, accounting for the observed increase in pAMPK levels in ABA-treated L6 in the presence of AZD5363. Based on previous results, a non-overlapping role for ABA and insulin in muscle glucose transport and in adipocyte metabolism can be envisaged [26]. Insulin induces phosphorylation of Akt on both Ser473 and Thr308, thus inhibiting AMPK and shifting the metabolic program from the starved to the fed state, activating not only glucose transport and metabolism, but also lipid and protein synthesis and adipogenesis. ABA instead induces phosphorylation of AMPK on Thr172, thereby activating the metabolic response to starvation and/or low glucose availability. This response includes stimulation of glucose transport in adipocytes, but not lipid synthesis, instead favoring UCP1 expression, O_2 consumption and mitochondrial biogenesis [27]. This consideration allows hypothesizing a role for ABA as the first hormonal response, capable of stimulating muscle and adipocyte glucose uptake and oxidative metabolism in the presence of low glucose availability. Persistence of hyperglycemia, indicating glucose availability in excess of normal tissue requirements, then triggers insulin release, which is however moderated by the concomitant action of ABA. Eventually, fully phosphorylated Akt downstream of the insulin signaling pathway

in turn moderates activation by ABA of AMPK and starts the metabolic response to hyperglycemia, which includes lipid synthesis and storage. A different role for Akt phosphorylated on Ser473 alone, or both on Ser473 and on Thr308 might be envisaged also based on the facts that defective Ser473 phosphorylation affects only a subset of Akt targets [87] and that different phosphatases specifically dephosphorylate these residues [88]. Phosphorylation of both Akt and AMPK at Ser473 and Thr172, respectively, with stimulation of muscle glucose uptake has been reported for other natural products [89]: thus, it is tempting to speculate that ABA may be the endogenous hormone responsible for activation of this pathway, the details of which remain to be clarified.

ABA effect on glycemia control and glucose uptake. Glucose uptake, detected in skeletal muscle by dynamic micro-PET, increases 2-fold in ABA-treated compared with untreated rats during an oral glucose load [26]. Given the high percentage of BW represented by skeletal muscle in rats, approximately 45% [90], this increase of muscle glucose uptake may account for the accelerated blood glucose clearance observed in the ABA-treated compared with the control rats. BAT glucose uptake also increased approximately 2-fold in the ABA-treated rats compared with untreated controls, in line with previous observations [27]. Brown adipose tissue glucose uptake is a measure of its metabolic activity, which allows energy dissipation through heat production; thus, an increased BAT glucose uptake in the ABA-treated rats should increase the overall body energy expenditure. Indeed, male mice fed for 4 weeks a high-glucose diet containing ABA at the same low dose used in the rat OGTT experiments (1 μg/kg BW) showed a slight reduction of BW compared with ABA-untreated controls [27]. This trend towards a weight reduction of ABA-treated mice was confirmed when a 4-month ABA supplementation to a high-glucose diet was performed [39]. To compare the physical performance in ABA-treated and -untreated mice, we adopted the running wheel test, which is often used to assess levels of general physical activity, as it allows a quantifiable measure of physical activity [91]. Open-field activity is instead mostly used to evaluate stress, anxiety or locomotor response to novelty rather than overall spontaneous activity levels [92]. The mice were allowed access to the running wheel for a relatively short time (12 hours), during the night-time only and without prior acclimation, to reduce possible confounding aspects related to wheel running, such as alteration of behavior, metabolism and energy expenditure due to protracted exercise on the wheel [26]. Interaction with the wheel may depend in part on the curiosity for a new gadget; however, the facts that the ABA-treated animals kept the wheel running for approximately twice the time of their untreated peers, covered approximately twice their total distance and reached a three-times higher maximal speed on the wheel, altogether indicate a significantly higher endurance of the ABA-treated animals, in line with the higher glycogen content detected in their muscles [91]. The increased muscle

glucose uptake *per se* could be responsible for an increased glycogen synthesis, as muscle glycogen synthase is allosterically activated by glucose 6-phosphate [93]. Genetic or pharmacological interventions that increase glycogen synthesis relative to glycogenolysis can indeed promote glucose tolerance [94,95] and the cellular physiology controlling the flux through these opposite pathways is being explored for new anti-diabetic drug targets. The fact that similar effects of chronic low-dose ABA as observed on CD1 mice fed a high-glucose diet were also observed on TRPM2 knock-out mice, which are defective in insulin secretion, indeed suggests that ABA may at least in part substitute for insulin action on glycemia control and muscle glucose uptake. To address the issue of how the results obtained on a mouse model of impaired insulin secretion may translate to diabetic humans, future studies should investigate muscle glucose uptake in subjects with prediabetes or T2D, treated or not with microgram amounts of oral ABA. Altogether, past results indicate that ABA shares with insulin the ability to stimulate muscle glucose uptake, albeit through a different signaling pathway, involving activation of AMPK. Interventions aimed at increasing AMPK activity are among the most successful current strategies to improve glucose tolerance in diabetic subjects. Physical activity and the AMPK activator metformin are currently prescribed as means to improve glucose tolerance in diabetic or prediabetic subjects, both acting through activation of AMPK. ABA is the endogenous hormone in charge of AMPK activation and imply that low-dose oral ABA may alleviate insulin deficiency, as occurs in hypoinsulinemic TRPM2 knock-out mice, or contribute to reduce the dose of insulin required to control hyperglycemia in insulin-resistant T2D and in insulin-deficient T1D [26].

ABA receptors in the skeletal muscle. The ABA receptor LANCL2 appears to be involved in the ABA-induced effects on skeletal muscle, as silencing of LANCL2 significantly reduced ABA-stimulated glucose uptake and AMPK phosphorylation and PGC-1α expression in L6 cells. The fact that the effect of ABA was not abrogated by LANCL2 silencing, despite the very high percentage of reduction of protein and mRNA expression, suggests that other ABA receptors might be partly involved in the effect of ABA on muscle. LANCL1, a LANCL2 homolog, is indeed expressed in murine skeletal muscle at levels similar to those of LANCL2. Thus, it is possible that stimulation by ABA of AMPK phosphorylation and of PGC-1α expression, which retain a significant increase over control values in LANCL2-silenced cells, may depend also on LANCL1. The kinase(s) activated by ABA and responsible for AMPK phosphorylation remain to be identified. Two kinases, LKB1 and Ca^{2+}/calmodulin dependent protein kinase-β (CamKK-β) are known to phosphorylate and activate AMPK [96]. Activation of CamKK-β downstream of LANCL2 could be expected on the basis of previous findings in inflammatory cells, showing PKA-dependent phosphorylation and activation of the ADP-ribosyl cyclase CD38, resulting in an increase of the Ca^{2+}-mobilizing second messenger

cyclic ADP-ribose [4,97]. LKB1 is also a target of PKA [98,99]. Thus, activation of PKA by LANCL2 could lead to the activation of both CamKK-β and LKB1. In the present study, we focused our attention on the role of LANCL1, as a second ABA receptor, in addition to LANCL2. LANCL1 binds ABA with a calculated K_d in the low micromolar, a value which lies in between those of the high- and low-affinity binding sites of LANCL2 for ABA (0.1 and 10 μM, respectively [20]). The lower affinity for the ABA of LANCL1 compared to LANCL2 may be responsible for the impairment of glucose tolerance observed in LANCL2$^{-/-}$ mice in both males (**Figure 26**, left panel) and females (**Figure 41**) [72].

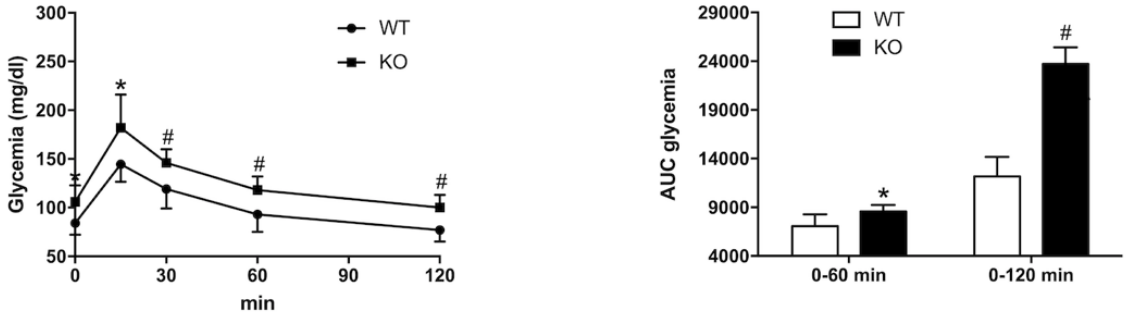

Figure 41. Female, nine week-old LANCL2$^{-/-}$ (KO) or WT mice (9/group), derived from heterozygous breeding, were subjected to an OGTT (1g glucose/kg BW). Left panel, glycemia was evaluated on blood samples taken from the tail vein, at the indicated time points immediately before (time zero) and after gavage. *$p < 0.03$ and $^{\#}p < 0.005$ relative to WT. Right panel, AUC of glycemia calculated with the trapezoidal rule, in the indicated time frames. *$p < 0.007$ and $^{\#}p < 0.00000003$ relative to WT.

LANCL2$^{-/-}$ mice showed a higher glycemia AUC after glucose load than WT siblings, despite an increased expression of LANCL1 in the SM (**Figure 27**). It may be hypothesized that glucose tolerance would have been worse in LANCL2$^{-/-}$ mice if LANCL1 were not concomitantly overexpressed in the SM. However, exogenous ABA administration resulting in an approximately 1-log higher plasma ABA concentration in ABA-treated vs. untreated mice improves glucose tolerance in LANCL2$^{-/-}$ mice (**Figure 26**, right panel). This result suggests that an increase of ABAp, obtained by administering a daily dose of 1 μg/kg BW, elicits a fully functional response by LANCL1. A 10-fold increase of ABAp can occur after consuming large amounts of ABA-rich food or vegetal extracts containing ABA [7]. Interestingly, ABA treatment further increases the expression of LANCL1 in the SM up to 3-fold over untreated WT levels (**Figure 27**). Indeed, the overexpression of LANCL1 stimulates important metabolic functions in L6 myoblasts: glucose uptake (**Figure 16**), *via* an increased expression of GLUT1 and GLUT4 (**Figure 17**), and O_2 consumption (**Figure 24**), *via* an increased expression of the uncoupling proteins sarcolipin and UCP3 (**Figure 22**). In LANCL2$^{-/-}$ mice, in which the expression of LANCL1 in the SM is significantly higher than in WT mice, the

same molecular effects are observed. In addition, mitochondrial DNA is also increased, indicating a higher mitochondrial content in the SM from LANCL2$^{-/-}$ mice, particularly after treatment with ABA (**Figure 30**). These effects appear to be mediated by the same regulators activated by LANCL2. In addition, LANCL1 overexpression in both L6 cells and the SM from LANCL2$^{-/-}$ mice elicits increased mRNA levels of Sirt1 and NAMPT (**Figure 17** and **Figure 28**). The AMPK/PGC-1α/Sirt1 axis is implicated in several pivotal functions in SM, including mitochondrial biogenesis and fusion, conservation of muscle contractility and recovery of muscle function caused by disuse or ageing [67] and protection of muscle cells from apoptosis induced by nutrient deprivation or ischemia-reperfusion injury [100,101,102]. The overexpression of NAMPT in SM improves physical endurance in mice [71] and maintains mitochondrial NAD^+ levels, membrane potential, respiration and cell survival to oxidative stress [70]. Thus, the role of LANCL1/2 and ABA in promoting the activity of the AMPK/PGC-1α/Sirt1/NAMPT axis adds new key players to this molecular pathway in SM physiology.

Functional redundancy of the LANCL proteins. Given the relevant role of ABA as an insulin-independent stimulator of cell glucose uptake via an increased expression of both GLUT4 [27,103 and **Figure 17**] and GLUT1 (**Figure 17**), receptor redundancy may be interpreted as a protective mechanism to safeguard ABA-responsiveness and glucose entry into cells, even in the face of one receptor mutation or genetic ablation. Screening the genome databases for the reported association between SNPs in LANCL1 or LANCL2 and specific clinical phenotypes does not produce many results. Interestingly, the LANCL1 gene lies within the insulin-dependent diabetes (Idd) 5.3 locus, which provides resistance to T1D in NOD mice [103]. LANCL1 is also among the candidate genes responsible for an observed complex phenotype of impaired neuronal function due to a microdeletion on the chromosomal region 2q34 [104]. However, the overlapping functions of LANCL1 and LANCL2 on glucose transport and mitochondrial respiration unveiled in this study suggest that both proteins may need to be mutated to observe a significant phenotype. LANCL3, the third member of the LANCL protein family, is, indeed, expressed at a much lower level compared to the other two LANCL proteins (**Figure 42**, lower panel) [72].

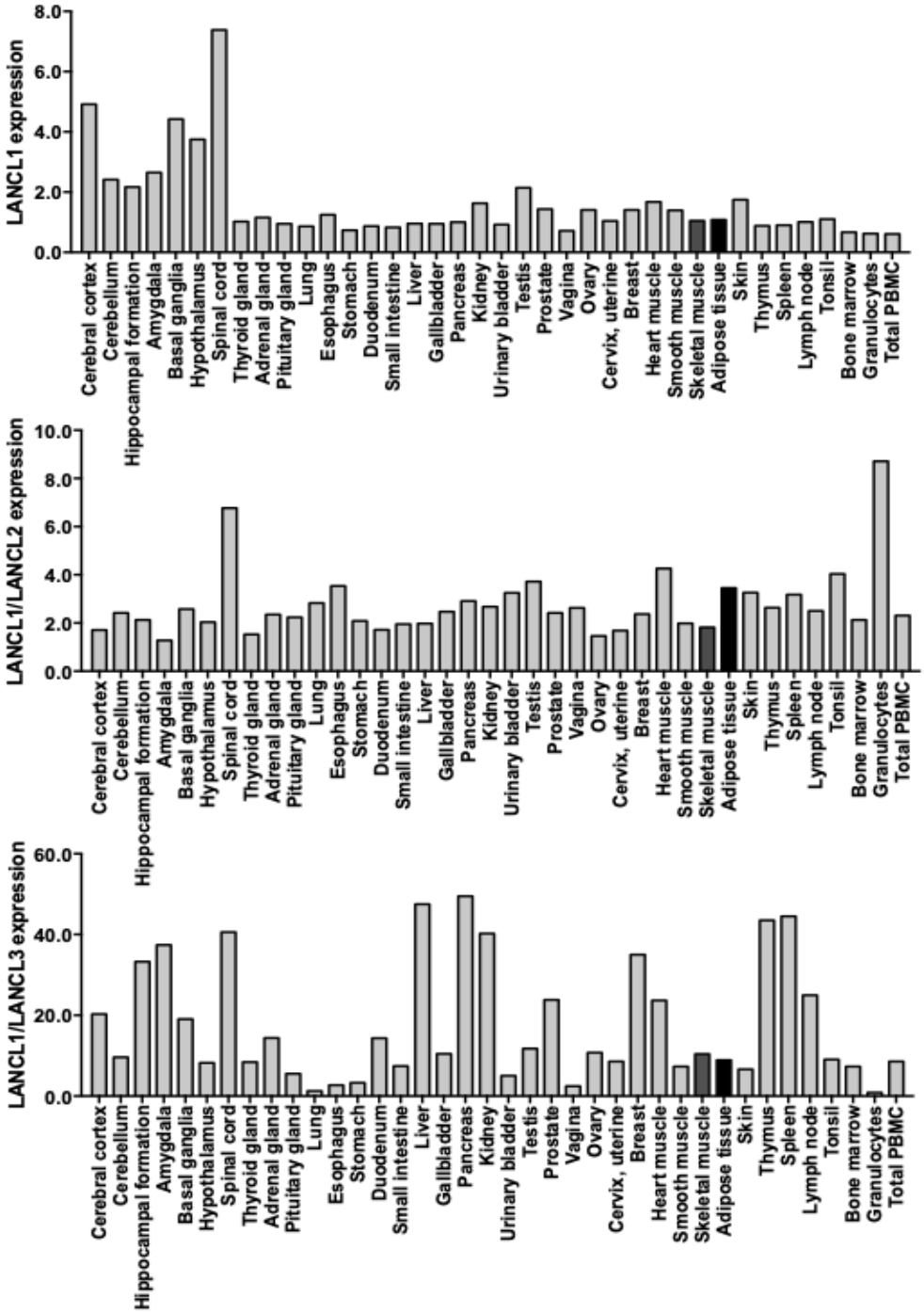

Figure 42. The data reported are from The Human Protein Atlas portal. LANCL1 expression levels in various tissues relative to the pancreas (upper panel), LANCL1/LANCL2 expression (central panel) and LANCL1/LANCL3 expression (lower panel) in different tissues. The mRNA expression levels in human tissue are based on RNA-seq data generated by the Human Protein Atlas, Genotype-Tissue Expression portal and CAGE data generated by the FANTOM5 consortium. Consensus normalized expression levels for human tissue is created by combining the data from these three transcriptomics datasets. SM is indicated by a dark gray bar while AT is indicated by a black bar; in these tissues, LANCL1 expression levels are higher than LANCL2 (2-fold and 3-fold, respectively) and LANCL3 (10-fold and 9-fold, respectively) expression levels.

Regarding receptor function redundancy, it may be relevant to observe that a transcriptional control appears to link LANCL1 and LANCL2 in both L6 cells and *in vivo* in LANCL2$^{-/-}$ mice. In L6 cells, in which the expression of LANCL2 or LANCL1 were silenced, significantly increased mRNA levels of the other LANCL protein were observed (**Figure 43**) [72].

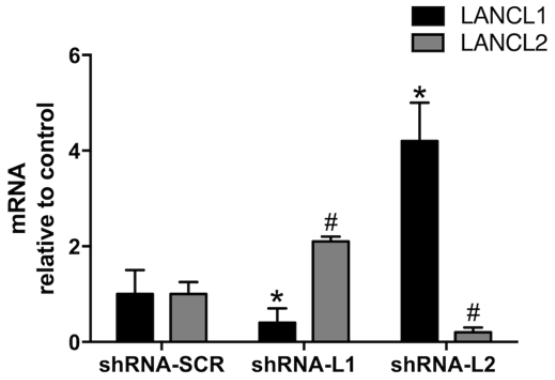

Figure 43. qPCR analysis; LANCL1 (shRNA-L1) or LANCL2 (shRNA-L2) were stably silenced in rat L6 myoblasts by viral infection; LANCL1/2 mRNA levels in LANCL1 and LANCL2-silenced cells are shown. Results are the mean ± SD values from 3 different determinations. *$p < 0.0002$ and $^{\#}p < 0.001$ by unpaired two-tailed t test compared with control cells infected with the scramble shRNAs (shRNA-SCR).

In LANCL2$^{-/-}$ mice, mRNA levels of LANCL1 were significantly higher relative to those in WT mice, in both the SM (**Figure 27**) and the BAT (**Figure 40**, left panel). It is also possible that different tissue expression levels of LANCL1 and LANCL2 could mediate a tissue-specific function of these proteins, either ABA-related or -unrelated. However, LANCL1 and LANCL2 are both similarly and highly expressed in the CNS (**Figure 42**, upper and central panels), whereas the glucose transporters present in brain also comprise GLUT1 and GLUT4 [The Human Protein Atlas portal], both targets of LANCL1/2-mediated increased expression. Heart and germinal cells follow the brain in the ranking of the tissues with the highest LANCL1/2 expression level (**Figure 42**, central panel) [72]. It could be argued that these tissues are essential to species and individual survival. Both LANCL1 and LANCL2 bind to reduced glutathione (GSH) and have an SH3-binding domain. These features have been proposed to allow these proteins to sense the cell redox state and be actors in response to its dysregulation. Indeed, it has been reported that loss of LANCL1 leads to neuronal death, oxidative stress and inflammation in the brain, whereas LANCL1 overexpression protects neurons against exogenous peroxide-induced apoptosis [105]. In addition, LANCL1 overexpression protects motor neurons from apoptosis in mice with a genetic mutation of SOD, a model of amyotrophic lateral sclerosis, possibly by activating Akt [106]. The biochemical mechanism underlying the protective effect of LANCL1, particularly regarding a possible role for LANCL1 in stimulating glucose transport/mitochondrial respiration, remains to be investigated but should be attempted in light of the

findings presented here. Another observation pointing to a protective role of LANCL1 in neuronal cells comes from an *in vitro* study on a model of neuronal cell death caused by oxygen- and glucose-deprivation. The overexpression of LANCL1 reduced cell death through a signaling pathway dependent on Akt, PGC-1α and Sirt3 activation [107]. Our observation that the overexpression of either LANCL1 or LANCL2 similarly increases cell respiration, sarcolipin and UCP3 expression in rat L6 cells and that their combined silencing dramatically reduces mitochondrial DNA and the expression of sarcolipin and UCP3 (**Figure 22** and **Figure 24**) are consistent with the general role of these proteins in stimulating cell glucose transport and mitochondrial respiration *via* an AMPK/PGC-1α-dependent mechanism (**Figures 19-22**, **Figure 24** and [26]). In addition, a significant correlation exists between the level of (over)expression of LANCL1 or LANCL2 in L6 cells and the extent of increase of cell O_2 consumption (**Figure 25**). The overexpression of PGC-1α in the SM has been shown to increase cell respiration [108]. The high expression level of LANCL1/2 in the brain may be related to this effect on mitochondria. LANCL1 has been shown to bind to the SH3 domain of the signaling protein Eps8, thereby allowing for the nerve growth factor-induced neurite outgrowth in the model neuronal cells PC12 [109]. Interestingly, this feature is also shared by LANCL2, another possible example of functional redundancy of the LANCL proteins. Recent reports indicate that LANCL2 may also be involved in the protection of neurons against oxidative stress, possibly through its capacity to bind glutathione and its ability to interact with several proteins involved in kinase-dependent signaling and gene transcription. No clear distinction between the functional effect of the overexpression of LANCL1 vs. LANCL2 emerged from our study, suggesting that either one can similarly stimulate glucose uptake and cell respiration in L6 myoblasts. Some of the functional features attributed to one of the proteins have not yet been concomitantly explored in the other one; thus, it is possible that further functional overlapping exists. One function attributed to LANCL2, in which LANCL1 shared no role, is the effect of LANCL2 overexpression or silencing on developing preadipocytes. LANCL2, but not LANCL1, activates the PPAR-γ-mediated transactivation of adipogenic genes in 3T3-L1 murine pre-adipocytes induced to differentiate with insulin and dexamethasone [41]. It should be noted that, in the absence of insulin, the overexpression of LANCL2 does not induce adipocyte differentiation and that the overexpression of LANCL2 sensitizes cells to the adipogenic effect of insulin [27], possibly via the activation of the mTORK/Akt pathway. Thus, this insulin-sensitizing feature may be a distinguishing property between LANCL2 and LANCL1. Most recently, modified gut microbiota was observed in LANCL1$^{-/-}$ mice compared to wild-type animals, an alteration the authors suggested may alleviate the oxidative damage to the brain, which they expected, but did not observe [110]. There is the possibility that LANCL2 vicariated the function of LANCL1 in these mice. Regarding the signaling pathways downstream of LANCL1 and LANCL2,

there are again several reports indicating shared features. Akt, AMPK, PGC-1α and Sirtuins 1 and 3 lie downstream of LANCL2 and LANCL1 [26,27,40,107 and this study]. Increased AMPK activity could result from an increased ratio between pAMPK and total AMPK or from an increased protein expression of AMPK with an unchanged ratio between the phosphorylated and the unphosphorylated protein. The ABA/LANCL1-2 system acts through the latter mechanism in both LANCL1/2 overexpressing L6 cells and LANCL1 overexpressing LANCL2$^{-/-}$ mouse muscle. *Ex vivo* treatment of skeletal muscle samples from WT mice for 30 or 60 min with 100 nM ABA also increased Sirt6 mRNA levels, more than levels in untreated samples. Interestingly, Sirt6 deletion in AT impairs the thermogenic function of BAT, causing a "whitening" of brown fat. Conversely, Sirt6 overexpression in primary fat cells stimulates browning [111]. In mice with a muscle-specific Sirt6 deficiency, impaired glucose homeostasis, insulin sensitivity and reduced physical performance are observed [112]. Our results and literature data warrant an in-depth exploration into the role of the ABA/LANCL1-2 system in the activation of muscle and BAT Sirt6. Interestingly, increased mRNA level of TBC1D1 was also observed in L6 cells overexpressing either LANCL1 or LANCL2, compared to control cells infected with the empty vector PLV. The RabGAPs TBC1D1 and TBC1D4 are key signaling factors in skeletal muscle glucose utilization. In mice, deficiency of both RabGAPs reduces skeletal muscle glucose transport in response to insulin and lowers GLUT4 abundance. Both RabGAPs are targets of AMPK: TBC1D1 appears to control exercise endurance by maintaining high muscle glucose uptake after contraction and TBC1D4 improves muscle insulin sensitivity after contraction [113,114]. Thus, these proteins are among those responsible for the beneficial effect of physical exercise on blood glucose control in insulin-resistant or -deficient subjects. The increased mRNA level of TBC1D1 observed in L6 cells overexpressing LANCL1 or LANCL2 warrants further studies to explore a possible correlation between the expression levels of the LANCL proteins and of TBC1D1/4. A clear correlation exists between the expression levels of LANCL1 and LANCL2 and mRNA levels, along with protein expression and plasma membrane translocation of GLUT1 and GLUT4 (**Figures 19-21**). LANCL2 has been shown to translocate to the nucleus, particularly upon ABA binding [22]. The possible nuclear translocation of LANCL1 has not been explored in this study and to our knowledge has not been described in other reports. The results summarized in this thesis allow to draw some conclusions, but also provide the starting point for future investigations, both clinical and preclinical. Data indicate an overlapping of downstream signaling proteins activated by both LANCL2 and LANCL1, both *in vitro* in L6 myoblasts overexpressing one or the other LANCL proteins (**Figure 17** and **Figure 19**) and *in vivo* in the SM of LANCL2$^{-/-}$ mice (**Figure 28**). Expression of LANCL1 in the SM from LANCL2$^{-/-}$ mice was higher compared to that in WT (**Figure 27**) and was further increased, particularly at the mRNA level by ABA treatment of the mice, as also occurred

in WT animals (**Figure 27**, right panel). ABAp was similar in WT and LANCL2$^{-/-}$ mice; thus, the increased expression of LANCL1 in ABA-untreated LANCL2$^{-/-}$ mice cannot depend on a higher ABAp. Instead, it could be hypothesized that LANCL2 controls to some extent LANCL1 transcription and that the hormone itself is part of this regulatory network, possibly by promoting the nuclear translocation of its receptor(s). The existing literature, taken together with the results reported in this study, reveals a complex picture of the pleiotropic functions of LANCL1 and LANCL2 in mammalian physiology. LANCL1 appears to be involved in cell glucose uptake and mitochondrial respiration and cell survival to low oxygen/nutrient availability and oxidative stress. It remains to be assessed whether these survival-related functions may be affected via ABA binding. As ABA is present in the serum, complete cell culture media contain nanomolar ABA. Thus, cells cultured with an animal serum-containing medium will have been in contact with ABA during culture, if not during the experimental condition. Here we show that LANCL1/2-overexpressing cells cultured with nanomolar ABA for 24 h and then resuspended in serum- and ABA-free buffers have a significantly higher oxygen consumption than ABA-untreated cells. *Ex vivo* incubation of the SM from WT mice with nanomolar ABA for 60 min resulted in a 15-fold overexpression of NAMPT (**Figure 29**). Thus, the effect of ABA on mitochondrial respiration and NAD^+ synthesis and possibly on other cellular functions as well can persist for hours after the removal of the hormone and can be fast. Interestingly, ABA is particularly abundant in the brain, with concentrations of approx. 1 log higher compared to other tissues [8]. It is possible that the distinctive and unifying feature of their ABA-binding capacity makes the LANCL proteins part of an ancestral mechanism of stress response to changing conditions of nutrient/oxygen availability, mitochondrial respiration and ROS generation. The abundance of LANCL1/2 (and ABA) in the brain may be related to their role in individual and species survival.

Role of ABA in the adipose tissue. BAT is a promising therapeutic target for combating obesity and related metabolic disorders due to its inherent capacity to dissipate energy as heat through the action of UCP1 [115]. In the last 20 years, a large number of mouse models have documented the potential of BAT to combat metabolic dysfunction. The molecular circuitry of mouse brown adipocyte differentiation and function has been studied intensely due to easily accessible primary cell cultures and the existence of a number of useful cell models. The selection of human adipocyte cell models derived from adult BAT is limited, thereby hampering studies of the molecular control of human brown adipocyte differentiation and function. A number of human white adipocyte cell models have been described, including unipotent models such as LiSa-2 [116], SGBS [117], Chub-S7 [118] and LS14 [119], but also multipotent models like hMADS [120]. The availability of primary human white adipocytes from liposuctions has made primary white adipocyte cultures an easily accessible

supplement to cell models. Conversely, primary human brown adipocytes are mainly available by surgical procedures where cancer is suspected in cervical and supraclavicular areas and the amount of material is often limited. Only two studies have reported the generation of immortalized BAT cell models obtained from adult humans [121,122]. Shinoda et al. established sub-cloned human brown-like and white pre-adipocyte cell models immortalized with simian virus 40 large T antigen from non-matched patients [121] while Xue et al. established patient-matched, sub-cloned human brown-like and white pre-adipocyte cell models immortalized with telomerase reverse transcriptase (TERT) [122]. The characterization of these derived cell clones elegantly demonstrated the heterogeneity of human BAT. Studies with immortalized clonal lines can provide very important information but are unlikely to represent the response of the intact tissue. Although speculative, cell cultures that have not undergone subcloning might elicit a response to a stimulus that is more closely reflecting the response of the intact tissue to the same stimulus. Since the discovery of active BAT in humans, the therapeutic interest concerning browning of WAT to treat obesity and reduce insulin resistance has increased. In recent studies, inducible brown-like fat cells in WAT, namely, “beige” or “brite” adipocytes have been discovered. Despite having different origins, beige adipocytes and brown adipocytes possess similar morphological and biochemical characteristics, such as the presence of multilocular lipid droplets, enriched mitochondria and UCP1 expression. Like brown adipocytes, beige adipocytes can dissipate stored energy upon exposure to chronic cold or adrenergic signaling through UCP1-mediated non-shivering thermogenesis. Given the importance of increased energy expenditure in anti-obesity strategy, many studies have been carried out to find endogenous proteins or drugs that induce beige adipocyte in order to establish new therapeutic interventions for obesity [51,123,124,125,126]. Based on previous experiments, the discovery that LANCL2 expression levels affect the sensitivity of adipocytes to insulin-stimulated glucose uptake and the recent demonstration of its non-canonical properties as a G protein-coupled receptor also capable of nuclear translocation [22] identify LANCL2 as a new target for investigations on the genetic background of adipocyte insulin resistance and for therapeutic interventions aimed at increasing adipocyte glucose uptake without increasing triglyceride deposition. *In vivo*, a single dose of oral ABA (1 μg/kg BW) increased BAT glucose uptake 2-fold in treated rats compared with untreated controls. One-month-long ABA treatment at the same daily dose significantly upregulated expression of browning genes (UCP1, PGC-1α, TMEM26, PRDM16, CIDE-A, TBX and FGF21) and of mitochondrial DNA content in the WAT and in WAT-derived preadipocytes differentiated *in vitro* from treated mice compared with untreated controls and increased UCP1 expression in the BAT. This finding indicates that exposure of adipose tissue to ABA *in vivo* modified the expression pattern of those genes when primary preadipocytes were induced to differentiate. This effect of ABA may be of consequence *in vivo*, as it

may allow browning of WAT, by acting on its preadipocytes' genetic background [27]. *In vitro*, ABA *per se* did not induce murine or human preadipocyte differentiation to white/brown adipocytes but increased transcription and plasma membrane translocation of GLUT4 in 3T3-L1 cells differentiated to white adipocytes [3,27]. The hormone induces browning of 3T3-L1 cells differentiated to WAT (increased expression of BAT genes, O_2 consumption, mitochondrial content and CO_2 production with no significant increase of triglyceride synthesis). ABA stimulated expression of GLUT4, FAS, AP2 and LPL in human ATMSC [27]. Silencing of LANCL2 abrogated both the ABA- and insulin-induced increase of GLUT4 expression and of glucose uptake in differentiated 3T3-L1 murine adipocytes; conversely, overexpression of LANCL2 enhanced basal, ABA- and insulin-stimulated glucose uptake. These data showed the role of the ABA/LANCL2 system in the regulation of glucose uptake and metabolism in adipocytes. But which is the role of LANCL1 in the BAT? Our current study has demonstrated that LANCL1 is overexpressed in the BAT of LANCL2$^{-/-}$ mice (20-fold) ([72] and **Figure 40**). In muscle, LANCL1 protein regulates energy expenditure *via* the AMPK/PGC-1α/Sirt1 axis by stimulating glucose uptake, O_2 consumption, mitochondrial content and expression of muscle uncoupling proteins sarcolipin and UCP3. In light of these data, our group decided to overexpress the LANCL receptors in TERT-hBA and TERT-hWA human pre-adipocytes and to carry out adipocyte differentiation, subjecting the cells to ABA or not (**Figure 31**). TERT-immortalized polyclonal brown (TERT-hBA) and white (TERT-hWA) pre-adipocyte cell models, generated from the cervical region of the same patient, exhibited high proliferative and adipogenic capacities up to at least passage 20. TERT-hBA adipocytes maintained classical features of thermogenic adipocytes, being UCP1-positive as well as displaying higher levels of mitochondrial markers and higher maximal respiratory capacity compared with TERT-hWA adipocytes. TERT-hBA adipocytes were highly receptive and responsive to β-adrenergic stimuli, as demonstrated by activation of the PKA-mitogen-activated protein kinase (MAPK) kinase 3/6 (MKK3/6)-p38 MAPK signaling module and increased thermogenic gene expression and oxygen consumption. Mature TERT-hWA adipocytes underwent browning in response to treatment with rosiglitazone [64]. The field of BAT research received renewed focus in 2009 with the finding that adult humans possess active BAT. Since then, mouse models have revealed a wealth of information on the molecular control of formation, function and therapeutic potential of BAT [50]. TERT-hBA and TERT-hWA pre-adipocytes robustly differentiated into mature adipocytes (**Figure 34**) that recapitulated key features of thermogenic and white adipocytes, respectively. The specific isolation of human classical brown versus brown-like adipocytes from biopsy material can be challenging due to the anatomical localization (perivascular) and reduced mass of BAT in humans. The biopsy material to generate TERT-hBA cells was obtained from the deep neck adipose tissue around the thyroid gland, an area that has been suggested to exhibit

a heterogeneous population of classical brown and brown-like adipocytes [127,128]. We attempted to determine if ABA and its LANCL1 and LANCL2 receptors are involved in adipocyte differentiation, involving the pathway downstream of AMPK. In pre-adipocytes overexpressing LANCL1 and LANCL2, ABA increases AMPK phosphorylation and AMPK and PGC-1α protein levels (**Figure 32** and **Figure 33**) and, in differentiated cells, ABA displayed markedly higher expression of thermogenic markers (UCP1, PGC-1α, CIDE-A and PPAR-γ), of oxidative metabolism-related genes (CPT1ß, MPC1 and PDHα1), of glucose transporter GLUT4 and of mitochondrial DNA content (MT-DNA), in mature adipocytes of both white and brown lines (**Figure 35**). However, it is important to note that the adipocyte type identity marker genes are relative rather than absolute and they are unlikely to provide unequivocal evidence for a brown or brown-like adipocyte origin. Our preliminary results indicate that ABA indeed stimulates browning of white adipocytes by increasing the expression levels of several key proteins involved in the browning process including UCP1. UCP1 is the key marker of brown adipose tissue and its expression is regulated by several transcriptional factors. Among them, PPAR-γ [53,55,129] is critical to initiate both white and brown adipogenesis, whereas PPAR-γ coactivator-1α (PGC-1α) is essential to brown fat determination, by stimulating expression of brown-specific genes [57,130,131,132]. The increased expression of the brown cell marker CIDE-A [73] in the ABA- treated adipocytes suggests that ABA may be able to convert white into beige/brown adipocytes. Several recent studies suggest that browning of WAT and expansion or activation of BAT could counteract obesity and related metabolic disorders [57,133]. In fact, BAT also regulates glucose homeostasis and improves insulin sensitivity and brown adipogenesis is suppressed in human subjects with insulin resistance. To support a distinction based on gene expression, metabolic differences could be investigated in the near future. It has been reported that the mouse brown-like adipocyte mitochondrion has a lower capacity to utilize glycerol-3-phosphate relative to the brown adipocyte mitochondrion [134] and it was recently elucidated that mouse brown-like adipocytes, but not brown adipocytes, use creatine to dissipate energy when ADP is limiting [135]. Moreover, TERT-hWA adipocytes underwent efficient rosiglitazone-induced browning, demonstrating the capability to activate a brown-like adipocyte gene program in these cells. A new observation refers to the synergistic effect of ABA and rosiglitazone, which together seem to strengthen the single effects performed. After brown and white differentiation, LANCL1 and LANCL2 overexpressing adipocytes were treated or not with 100 nM ABA and stained with Oil Red O staining. A slight increase of accumulation of lipid droplets is revealed after exposure with ABA and, basally, in cells overexpressing ABA receptors (**Figure 36**). Differentiation after LANCL1+2-overexpression increased the transcription of genes related to uncoupling proteins (UCP1 and UCP3), to oxidative metabolism (MPC1, PDHα1 and CPT1ß), to

AMPK/PGC-1α/Sirt1 axis, to receptors for browning hormones (ADRß3, THRα1, THRß and INSR), to mitochondrial DNA content (MT-DNA) and to LANCL proteins (LANCL1 and LANCL2) (**Figure 37**, **Figure 38** and **Figure 39**). ABA further increases the levels of all mRNAs explored, indicating an additive function to rosiglitazone-induced browning. Furthermore, overexpression of LANCL proteins, ABA treatment and adipocyte differentiation induce a high gene expression, indicating a fundamental involvement in browning. To evaluate whether TERT-hBA and TERT-hWA adipocytes overexpressing LANCL1 and LANCL2 treated with 100 nM ABA possess features of thermogenicity, preliminary tests were performed to assess mitochondrial function of the cell models using the Seahorse XFp Analyzer with sequential addition of oligomycin, FCCP and rotenone/antimycin A. Substantially larger maximal respiration and spare respiratory capacity were observed in both adipocytes overexpressing LANCL proteins and ABA-treated relative to control cells infected with the empty vector and untreated, reflecting a higher mitochondrial capacity of these cells (data not shown). Regarding the thermogenic effect, it also would be interesting to assess whether ABA-treated mice preserve body temperature better than untreated ones and whether LANCL2$^{-/-}$ mice fail to maintain body temperature in a cold challenge test. This issue is open to investigation. Furthermore, mitochondrial DNA content (MT-DNA) in the BAT from ABA-treated WT mice increased (1.7-fold) compared to untreated controls, whereas KO mice had lower levels of mitochondrial DNA compared to WT animals, which further slightly increased upon treatment with ABA (**Figure 40**). At this point, the effects of ABA also would be evaluating in the WAT of mice. Indeed, the possible browning of inguinal white fat could be tested by measuring the expression of marker genes of brown fat. ABA does not *per se* induce adipocyte differentiation but has a synergistic effect with the differentiation cocktail, further increasing protein and gene expression.

ABA as a promising aid to combat prediabetes and the metabolic syndrome. The significant beneficial effect of micrograms of oral ABA observed in volunteers with metabolic and morphometric parameters borderline with the metabolic syndrome allows to forecast similar positive results in trials of the ABA-containing nutraceutical on a higher number of prediabetic subjects and of subjects with the metabolic syndrome. The primary outcomes of this study would be the improvement of glucose and lipid tolerance and the reduction of body weight. In addition, studies on murine model(s) of insulin-dependent diabetes could provide preclinical evidence supporting the use of oral low-dose ABA to improve glycemia control in combination with insulin. This result in turn would warrant clinical studies aimed at confirming whether ABA-containing nutraceuticals could represent an adjunctive therapy in insulin-dependent diabetic patients (both T1D and T2D), improving the daily glycemia profile, reducing blood lipids and contributing to the control of body

weight by reducing the amount of insulin required for glycemic control. The physiology and possible dysfunction of LANCL2 and of other ABA receptors still to be identified is another important area of research. Intake of the ABA-containing nutraceutical would provide the amount of ABA sufficient to increase ABAp 5- to 10-fold over endogenous levels, overtaking ABA resistance. Another issue requiring further study is the identity of the ABA-producing cells in mammals. Results obtained on T1D patients seem to indicate that β-pancreatic cells are the main ABA producers, since ABAp is reduced by approximately 90% compared to values measured in healthy controls. In addition, rat insulinoma cells and human pancreatic islets release ABA after stimulation with GLP-1 [3]. In mice, a very high ABA concentration has been measured in the BAT, but not in the WAT, suggesting that BAT could be another source of endogenous ABA in mammals. The identification of the main ABA-releasing cells in humans is relevant to understand which physiological stimuli induce an ABA response in humans. In particular, if β-pancreatic cells were indeed the main ABA producers, the demise of these cells in T1D would compromise secretion of both hormones regulating glycemia, insulin and ABA, of which only one is currently replaced by therapy. Finally, a field of exploration on mammalian ABA physiology which lies at the crossroad between metabolism and inflammation is the role of ABA in the central nervous system. The fact that brain has the highest ABA content among the various tissues, as first reported by Le Page-Degivry et al. [8], raises the possibility that ABA is produced and acts locally in the brain. ABA administration improves neuroinflammation and cognitive impairment and anxiety in rodents [136,137]. Interestingly, phaseic acid, the principal ABA metabolite in plants, is apparently endogenously produced in the brain and protects from ischemic injury by acting as a non-competitive inhibitor of glutamate receptors [138]. It would be informative to compare glucose tolerance and insulin sensitivity on the LANCL2 knock out and on the double (LANCL1+2) knock out mice [15]. Further studies are definitely needed to deepen our understanding of the physiology of mammalian ABA receptors, their tissue distribution and affinity for the hormone.

The potential benefit of oral ABA supplementation. In conclusion, these results warrant clinical studies, aimed at evaluating the potential benefit of oral ABA supplementation to ameliorate glycemic control in insulin-deficient, as well as in insulin-resistant, patients. In insulin-deficient patients, ABA supplementation should improve and prolong the action of exogenous insulin, perhaps allowing to reduce the daily dose of insulin (and the risk of hypoglycemia), while at the same time ameliorating glycemic control. In insulin-resistant patients, ABA supplementation could contribute to the reduction of postprandial hyperglycemia, in adjunct to oral hypoglycemic drugs, by synergizing with the action of endogenous insulin, *via* a different signaling pathway, eliciting an increased muscle and adipocyte glucose uptake, without stimulating triglyceride accumulation in the adipose tissue.

Finally, pre-treatment with ABA prior to development of overt diabetes is achievable in prediabetic subjects, and results from preliminary clinical studies [39,139] encourage to pursue an ABA-based nutraceutical approach to reverse the prediabetic condition.

5. BIBLIOGRAPHY

[1] Zocchi E. et al. The temperature-signaling cascade in sponges involves a heat-gated cation channel, abscisic acid and cyclic ADP-ribose. Proc Natl Acad Sci USA 98, 14859-14864 (2001).

[2] Puce S. et al. Abscisic acid signaling through cyclic ADP-ribose in hydroid regeneration. J Biol Chem 279, 39783-39788 (2004).

[3] Bruzzone S. et al. The plant hormone abscisic acid increases in human plasma after hyperglycemia and stimulates glucose consumption by adipocytes and myoblasts. FASEB J 26, 1251-1260 (2012).

[4] Bruzzone S. et al. Abscisic acid is an endogenous cytokine in human granulocytes with cyclic ADP-ribose as second messenger. Proc Natl Acad Sci USA 104, 5759-5764 (2007).

[5] Magnone M. et al. Autocrine abscisic acid plays a key role in quartz-induced macrophage activation. FASEB J 26, 1261-1271 (2012).

[6] Scarfì S. et al. The plant hormone abscisic acid stimulates the proliferation of human hemopoietic progenitors through the second messenger cyclic ADP-ribose. Stem Cells 27, 2469-2477 (2009).

[7] Magnone M. et al. Microgram amounts of abscisic acid in fruit extracts improve glucose tolerance and reduce insulinemia in rats and in humans. FASEB J 29, 4783-4793 (2015).

[8] Le Page-Degivry M.T. et al. Presence of abscisic acid, a phytohormone, in the mammalian brain. Proc Natl Acad Sci USA 83, 1155-1158 (1986).

[9] Togashi K. et al. TRPM2 activation by cyclic ADP-ribose at body temperature is involved in insulin secretion. EMBO J 25, 1804-1815 (2006).

[10] Leckie C.P. et al. Abscisic acid-induced stomatal closure mediated by cyclic ADP-ribose. Proc Natl Acad Sci USA 95, 15837-15842 (1998).

[11] Zocchi E. et al. ABA- and cADPR-mediated effects on respiration and filtration downstream of the temperature-signaling cascade in sponges. J Cell Sci 116, 629-636 (2003).

[12] Liu X. et al. G protein-coupled receptor is a plasma membrane receptor for the plant hormone abscisic acid. Science 315, 1712-1716 (2007).

[13] Johnston C.A. et al. A G protein coupled receptor is a plasma membrane receptor for the plant hormone abscisic acid. Science 318, 914 (2007).

[14] Klingler J.P. et al. ABA receptors: The START of a new paradigm in phytohormone signalling. J Exp Bot 61, 3199-3210 (2010).

[15] He C. et al. LanCL proteins are not Involved in Lanthionine Synthesis in Mammals. Sci Rep 7, 40980 (2017).

[16] Landlinger C. et al. Myristoylation of human LanC-like protein 2 (LANCL2) is essential for the interaction with the plasma membrane and the increase in cellular sensitivity to adriamycin. Biochim Biophys Acta 1758, 1759-1767 (2006).

[17] Li B. et al. Structure and mechanism of the lantibiotic cyclase involved in nisin biosynthesis. Science 311, 1464-1467 (2006).

[18] Eley G.D. et al. A chromosomal region 7p11.2 transcript map: its development and application to the study of EGFR amplicons in glioblastoma. Neuro-Oncology 4, 86-94 (2002).

[19] Sturla L. et al. Binding of abscisic acid to human LANCL2. Biochem Biophys Res Commun 415, 390-395 (2011).

[20] Cichero E. et al. Identification of a high affinity binding site for abscisic acid on human lanthionine synthetase component C-like protein 2. Int J Biochem Cell B 97, 52-61 (2018).

[21] Sturla L. et al. LANCL2 is necessary for abscisic acid binding and signaling in human granulocytes and in rat insulinoma cells. J Biol Chem 284, 28045-28057 (2009).

[22] Fresia C. et al. G-protein coupling and nuclear translocation of the human abscisic acid receptor LANCL2. Sci Rep 6, 26658 (2016).

[23] Vigliarolo T. et al. Abscisic acid influx into human nucleated cells occurs through the anion exchanger AE2. Int J Biochem Cell B 75, 99-103 (2016).

[24] Boursiac Y. et al. ABA transport and transporters. Trends Plant Sci 18, 325-333 (2013).

[25] Bassaganya-Riera J. et al. Abscisic acid regulates inflammation via ligand-binding domain-independent activation of peroxisome proliferator-activated receptor. J Biol Chem 286, 2504-2516 (2011).

[26] Magnone M. et al. Insulin-independent stimulation of skeletal muscle glucose uptake by low-dose abscisic acid via AMPK activation. Sci Rep 10, 1454 (2020).

[27] Sturla L. et al. Abscisic acid enhances glucose disposal and induces brown fat activity in adipocytes *in vitro* and *in vivo*. Biochim Biophys Acta 1862, 131-144 (2017).

[28] Leber A. et al. Modeling the Role of Lanthionine Synthetase C-Like 2 (LANCL2) in the Modulation of Immune Responses to Helicobacter pylori Infection. PLoS One 11, e0167440 (2016).

[29] Bruzzone S. et al. Abscisic acid stimulates glucagon-like peptide-1 secretion from L-cells and its oral administration increases plasma glucagon-like peptide-1 levels in rats. PLoS One 10, e0140588 (2015).

[30] Ameri P. et al. Impaired increase of plasma abscisic acid in response to oral glucose load in type 2 diabetes and in gestational diabetes. PLoS One 10, e0115992 (2015).

[31] Feng S. et al. Potential of natural products in the inhibition of adipogenensis through regulation of PPARγ expression and/or its transcriptional activity. Molecules 21, 1278 (2016).

[32] Seo J.B. et al. Anti-obesity effects of Lysimachia foenum-graecum characterized by decreased adipogenesis and regulated lipid metabolism. Exp Mol Med 43, 205-215 (2011).

[33] Xi X. et al. Stimulation of glucose transport by AMP-activated protein kinase via activation of p38 mitogen-activated protein kinase. J Biol Chem 276, 4129-41034 (2001).

[34] Armoni M. et al. Peroxisome proliferator-activated receptor-γ represses GLUT4 promoter activity in primary adipocytes, and rosiglitazone alleviates this effect. J Biol Chem 278, 30614-30623 (2003).

[35] Leonardini A. et al. Cross-Talk between PPARgamma and Insulin Signaling and Modulation of Insulin Sensitivity. PPAR Res, 818945 (2009).

[36] Kubota N. et al. PPAR gamma mediates high-fat diet-induced adipocyte hypertrophy and insulin resistance. Mol Cell 4, 597-609 (1999).

[37] Miles P.D. et al. Improved insulin-sensitivity in mice heterozygous for PPAR-gamma deficiency. J Clin Invest 105, 287-292 (2000).

[38] Rosen E.D. et al. PPARγ is required for the differentiation of adipose tissue *in vivo* and *in vitro*. Mol Cell 4, 611-617 (1999).

[39] Magnone M. et al. Chronic intake of micrograms of abscisic acid improves glycemia and lipidemia in a human study and in high-glucose fed mice. Nutrients 10, 1495 (2018).

[40] Zeng M. et al. Lanthionine synthetase C-like protein 2 (LanCL2) is a novel regulator of Akt. Mol Biol Cell 25, 3954-3961 (2014).

[41] Dutta D. et al. Lanthionine synthetase C-like protein 2 (LanCL2) is important for adipogenic differentiation. J Lipid Res 59,1433-1445 (2018).

[42] Cannon B. et al. Brown adipose tissue: function and physiological significance. Physiol Rev 84, 277-359 (2004).

[43] Cinti S. Adipocyte differentiation and transdifferentiation: plasticity of the adipose organ. J Endocrinol Invest 25, 823-835 (2002).

[44] Grundy S.M. Obesity, metabolic syndrome, and cardiovascular disease. J Clin Endocr Metab 89, 2595-2600 (2004).

[45] Wallberg-Henriksson H. et al. GLUT4: a key player regulating glucose homeostasis? Insights from transgenic and knockout mice. Mol Membr Biol 18, 205-211 (2001).

[46] Yadav A. et al. Role of leptin and adiponectin in insulin resistance. Clin Chim Acta 18, 417 (2013).

[47] Gustafson B. et al. Insulin resistance and impaired adipogenesis. Trends Endocrin Met 26, 193-200 (2015).

[48] Moreno-Indias I. et al. Impaired adipose tissue expandability and lipogenic capacities as ones of the main causes of metabolic disorders. J Diabetes Res 2015, 970375 (2015).

[49] Moseti D. et al. Molecular regulation of adipogenesis and potential anti-adipogenic bioactive molecules. Int J Mol Sci 19, 17 (2016).

[50] Harms M. et al. Brown and beige fat: development, function and therapeutic potential. Nat Med 19, 1252-1263 (2013).

[51] Bartelt A. et al. Adipose tissue browning and metabolic health. Nat Rev Endocrinol 10, 24-36 (2014).

[52] Farmer S.R. et al. Transcriptional control of adipocyte formation. Cell Metab 4, 263-273 (2006).

[53] Tontonoz P. et al. Stimulation of adipogenesis in fibroblasts by PPARγ 2, a lipid-activated transcription factor. Cell 79, 1147-1156 (1994).

[54] Brun R.P. et al. PPARγ and the molecular control of adipogenesis. J Endocrinol 155, 217-218 (1997).

[55] Nedergaard J. et al. PPARγ in the control of brown adipocyte differentiation. Biochim Biophys Acta 1740, 293-304 (2005).

[56] Tontonoz P. et al. Adipocyte-specific transcription factor ARF6 is a heterodimeric complex of two nuclear hormone receptors, PPARγ and RXRα. Nucleic Acids Res 22, 5628-5634 (1994).

[57] Lee Y.H. et al. Recent advance in brown adipose physiology and its therapeutic potential. Exp Mol Med 46, e78 (2014).

[58] Tiraby C. et al. Acquirement of brown fat cell features by human white adipocytes. J Biol Chem 278, 33370-33376 (2003).

[59] Magnone M. et al. Abscisic acid: a conserved hormone in plants and humans and a promising aid to combat prediabetes and the metabolic syndrome. Nutrients 12, 1724 (2020).

[60] Kubista M. et al. Experimental correction for the inner-filter effect in fluorescence spectra. Analyst 119, 417-419 (1994).

[61] Crouse H.F. et al. Quenching of tryptophan fluorescence in various proteins by a series of small nickel complexes. Dalton T 41, 2720-2731 (2012).

[62] Livak J. et al. Analysis of relative gene expression data using real-time quantitative PCR and the $2^{-\triangle\triangle Ct}$ method. Methods 25, 402-408 (2001).

[63] Vigliarolo T. et al. Abscisic Acid Transport in Human Erythrocytes. J Biol Chem 290, 13042-13052 (2015).

[64] Markussen L.K. et al. Characterization of immortalized human brown and white pre-adipocyte cell models from a single donor. PLoS One 12, e0185624 (2017).

[65] Datta D. et al. Fluorescence and circular dichroism studies on the accessibility of tryptophan residues and unfolding of a jacalin-related α-d-galactose-specific lectin from mulberry (Morus indica). J Photoch Photobio B 170, 108-117 (2017).

[66] Lee J.O. et al. Metformin induces Rab4 through AMPK and modulates GLUT4 translocation in skeletal muscle cells. J Cell Physiol 226, 974-981 (2011).

[67] Petrocelli J.J. et al. PGC-1α-Targeted therapeutic approaches to enhance muscle recovery in aging. Int J Env Res Pub He 17, 8650 (2020).

[68] Vidal-Puig A. et al. UCP3: an uncoupling protein homologue expressed preferentially and abundantly in skeletal muscle and brown adipose tissue. Biochem Bioph Res Co 235, 79-82 (1997).

[69] Halling J.F. et al. PGC-1α-mediated regulation of mitochondrial function and physiological implications. Appl Physiol Nutr Me 45, 927-936 (2020).

[70] Yu A. et al. NAMPT maintains mitochondria content via NRF2-PPARalpha/AMPKalpha pathway to promote cell survival under oxidative stress. Cell Signal 66, 109496 (2020).

[71] Costford S.R. et al. Skeletal muscle overexpression of nicotinamide phosphoribosyl transferase in mice coupled with voluntary exercise augments exercise endurance. Mol Metab 7, 1-11 (2018).

[72] Spinelli S. et al. LANCL1 binds abscisic acid and stimulates glucose transport and mitochondrial respiration in muscle cells via the AMPK/PGC-1α/Sirt1 pathway. Mol Metab 53, 101263 (2021).

[73] Barneda D. et al. Dynamic changes in lipid droplet-associated proteins in the "browning" of white adipose tissues. Biochim Biophys Acta 1831, 924-933 (2013).

[74] Zou S. et al. Adipose tissues of MPC1$^{\pm}$ mice display altered lipid metabolism-related enzyme expression levels. Peer J 6, e5799 (2018).

[75] Wei T. et al. Sirtuin 3-mediated pyruvate dehydrogenase activity determines brown adipocytes phenotype under high-salt conditions. Cell Death Dis 10, 614 (2019).

[76] Oliveira M. et al. Short-term effects of triiodothyronine on thyroid hormone receptor alpha by PI3K pathway in adipocytes, 3T3-L1. Arq Bras Endocrinol Metabol 58, 833-837 (2014).

[77] Kowalski G.M. et al. The regulation of glucose metabolism: implications and considerations for the assessment of glucose homeostasis in rodents. Am J Physiol Endocrinol Metab 307, e859-871 (2014).

[78] Jager S. et al. AMP-activated protein kinase (AMPK) action in skeletal muscle via direct phosphorylation of PGC-1α. Proc Natl Acad Sci USA 104, 12017-12022 (2007).

[79] Leick L. et al. PGC1-α is required for AICAR-induced expression of GLUT4 and mitochondrial proteins in mouse skeletal muscle. Am J Physiol Endocrinol Metab 299, e456-465 (2010).

[80] Wan Z. et al. Evidence for the role of AMPK in regulating PGC-1 alpha expression and mitochondrial proteins in mouse epididymal adipose tissue. Obesity 22, 730-738 (2014).

[81] Kleiner S. et al. Development of insulin resistance in mice lacking PGC-1 alpha in adipose tissue. Proc Natl Acad Sci USA 109, 9635-9640 (2012).

[82] Lee M. et al. Effects of Isorhamnetin on adipocyte mitochondrial biogenesis and AMPK activation. Molecules 23, 1853 (2018).

[83] Davies B.R. et al. Preclinical pharmacology of AZD5363, an inhibitor of AKT: Pharmacodynamics, antitumor activity, and correlation of monotherapy activity with genetic background. Mol Cancer Ther 11, 73-87 (2012).

[84] Liu L. et al. Akt blocks the tumor suppressor activity of LKB1 by promoting phosphorylation-dependent nuclear retention through 14-3-3 proteins. Am J Transl Res 4, 175-186 (2012).

[85] Salmine A. et al. Age-related changes in AMPK activation: role for AMPK phosphatases and inhibitory phosphorylation by upstream signaling pathways. Ageing Res Rev 28, 15-26 (2016).

[86] Valentine R.J. et al. Insulin inhibits AMPK activity and phosphorylates AMPK Ser485/491 through Akt in hepatocytes, myotubes and incubated rat skeletal muscle. Arch Biochem Biophys 562, 62-69 (2014).

[87] Jacinto E. et al. SIN1/MIP1 maintains rictor-mTOR complex integrity and regulates Akt phosphorylation and substrate specificity. Cell 127, 125-137 (2006).

[88] Gao T. et al. PHLPP: a phosphatase that directly dephosphorylates Akt, promotes apoptosis, and suppresses tumor growth. Mol Cell 18, 13-24 (2005).

[89] Lin C.H. et al. (-)-Epicatechin-3-O-β-D-allopyranoside from Davallia formosana prevents diabetes and dyslipidemia in streptozotocin-induced diabetic mice. PLoS One 12, e0173984 (2017).

[90] Caster W.O. et al. Tissue weights of the rat. I. Normal values determined by dissection and chemical methods. Proc Soc Exp Biol Med 91, 122-126 (1956).

[91] Novak C.M. et al. The use of a running wheel to measure activity in rodents: Relationship to energy balance, general activity, and reward. Neurosci Biobehav Rev 36, 1001-1014 (2012).

[92] Stead J.D. et al. Selective breeding for divergence in novelty-seeking traits: heritability and enrichment in spontaneous anxiety-related behaviors. Behav Genet 36, 697-712 (2006).

[93] Villar-Palasi C. et al. Substrate specific activation by glucose 6-phosphate of the dephosphorylation of muscle glycogen synthase. Biochim Biophys Acta 1095, 261-267 (1991).

[94] Kelsall I.R. et al. Disruption of the allosteric phosphorylase a regulation of the hepatic glycogen-targeted protein phosphatase 1 improves glucose tolerance *in vivo*. Cell Signal 21, 1123-1134 (2009).

[95] Poucher S.M. et al. An assessment of the *in vivo* efficacy of the glycogen phosphorylase inhibitor GPi688 in rat models of hyperglycaemia. Br J Pharmacol 152, 1239-1247 (2007).

[96] Kim J. et al. AMPK activators: mechanisms of action and physiological activities. Exp Mol Med 48, e224 (2016).

[97] Bodrato N. et al. Abscisic acid activates the murine microglial cell line N9 through the second messenger cyclic ADP-ribose. J Biol Chem 284, 14777-14787 (2009).

[98] Medina E.A. et al. PKA/AMPK signaling in relation to adiponectin's antiproliferative effect on multiple myeloma cells. Leukemia 28, 2080-2089 (2014).

[99] Collins S.P. et al. LKB1, a novel serine/threonine protein kinase and potential tumor suppressor, is phosphorylated by cAMP-dependent protein kinase (PKA) and prenylated *in vivo*. Biochem J 345, 673-680 (2000).

[100] Yu Y. et al. Berberine improves cognitive deficiency and muscular dysfunction via activation of the AMPK/SIRT1/PGC-1α pathway in skeletal muscle from naturally aging rats. J Nutr Health Aging 22, 710-717 (2018).

[101] Ma L. et al. Long-term caloric restriction activates the myocardial SIRT1/AMPK/PGC-1α pathway in C57BL/6J male mice. Food Nutr Res 29, 64 (2020).

[102] Tang J. et al. Quercetin improves ischemia/reperfusion-induced cardiomyocyte apoptosis *in vitro* and *in vivo* study via SIRT1/PGC-1α signaling. J Cell Biochem 120, 9747-9757 (2019).

[103] Hunter K. et al. Interactions between Idd5.1/Ctla4 and other type 1 diabetes genes. J Immunol 179, 8341-8349 (2007).

[104] Westphal D.S. et al. MAP2–a candidate gene for epilepsy, developmental delay and behavioral abnormalities in a patient with microdeletion 2q34. Front Genet 45, 927-936 (2018).

[105] Huang C. et al. Developmental and activity-dependent expression of LanCL1 confers antioxidant activity required for neuronal survival. Dev Cell 30, 479-487 (2014).

[106] Tan H. et al. LanCL1 promotes motor neuron survival and extends the lifespan of amyotrophic lateral sclerosis mice. Cell Death Differ 27, 1369-1382 (2020).

[107] Xie, Z. et al. LanCL1 attenuates ischemia-induced oxidative stress by Sirt3-mediated preservation of mitochondrial function. Brain Res Bull 142, 216-223 (2018).

[108] Zhang L. et al. Skeletal muscle-specific overexpression of PGC-1α induces fiber-type conversion through enhanced mitochondrial respiration and fatty acid oxidation in mice and pigs. Int J Biol Sci 13, 1152-1162 (2017).

[109] Zhang W. et al. Structure of human lanthionine synthetase C-like protein 1 and its interaction with Eps8 and glutathione. Gene Dev 23, 1387-1392 (2018).

[110] Zhang F. et al. The endogenous alterations of the gut microbiota and feces metabolites alleviate oxidative damage in the brain of LanCL1 knockout mice. Front Microbiol 11, 557342 (2020).

[111] Yao L. et al. Cold-inducible SIRT6 regulates thermogenesis of Brown and beige fat. Cell Reports 20, 641-654 (2017).

[112] Cui X. et al. SIRT6 regulates metabolic homeostasis in skeletal muscle through activation of AMPK. Am J Physiol-Endoc M 313, 493-505 (2017).

[113] Kjøbsted R. et al. AMPK and TBC1D1 regulate muscle glucose uptake after, but not during, exercise and contraction. Diabetes 68, 1427-1440 (2019).

[114] Espelage L. et al. RabGAPs in skeletal muscle function and exercise. J Mol Endocrinol 64, 1-19 (2020).

[115] Rosen E.D. et al. What we talk about when we talk about fat. Cell 156, 20-44 (2014).

[116] Wabitsch M. et al. LiSa-2, a novel human liposarcoma cell line with a high capacity for terminal adipose differentiation. Int J Cancer 88, 889-894 (2000).

[117] Wabitsch M. et al. Characterization of a human preadipocyte cell strain with high capacity for adipose differentiation. Int J Obesity 25, 8-15 (2001).

[118] Darimont C. et al. Reconstitution of telomerase activity combined with HPV-E7 expression allow human preadipocytes to preserve their differentiation capacity after immortalization. Cell Death Differ 10, 1025-1031 (2003).

[119] Hugo E.R. et al. LS14: a novel human adipocyte cell line that produces prolactin. Endocrinology 147, 306-313 (2006).

[120] Rodriguez A.M. et al. Transplantation of a multipotent cell population from human adipose tissue induces dystrophin expression in the immunocompetent mdx mouse. J Exp Med 201, 1397-1405 (2005).

[121] Shinoda K. et al. Genetic and functional characterization of clonally derived adult human brown adipocytes. Nat Med 21, 389-394 (2015).

[122] Xue R. et al. Clonal analyses and gene profiling identify genetic biomarkers of the thermogenic potential of human brown and white preadipocytes. Nat Med 21, 760-768 (2015).

[123] Boon M.R. et al. Brown Adipose Tissue: A Human Perspective. Handb Exp Pharmacol 233, 301-319 (2016).

[124] Sakellariou P. et al. Chronic l-menthol-induced browning of white adipose tissue hypothesis: A putative therapeutic regime for combating obesity and improving metabolic health. Med Hypotheses 93, 21-26 (2016).

[125] Wu C. et al. Adipose tissue and age-dependent insulin resistance: New insights into WAT browning. Int J Mol Med 47, 71 (2021).

[126] Cousin B. et al. Occurrence of brown adipocytes in rat white adipose tissue: molecular and morphological characterization. J Cell Sci 103, 931-942 (1992).

[127] Jespersen N.Z. et al. A classical brown adipose tissue mRNA signature partly overlaps with brite in the supraclavicular region of adult humans. Cell Metab 17, 798-805 (2013).

[128] Cypess A.M. et al. Anatomical localization, gene expression profiling and functional characterization of adult human neck brown fat. Nat Med 19, 635-639 (2013).

[129] Tai T.A. et al. Activation of the nuclear receptor peroxisome proliferator-activated receptor gamma promotes brown adipocyte differentiation. J Biol Chem 271, 29909-29914 (1996).

[130] Barbera M.J. et al. Peroxisome proliferator-activated receptor alpha activates transcription of the brown fat uncoupling protein-1 gene. A link between regulation of the thermogenic and lipid oxidation pathways in the brown fat cell. J Biol Chem 276, 1486-1493 (2001).

[131] Uldry M. et al. Complementary action of the PGC-1 coactivators in mitochondrial biogenesis and brown fat differentiation. Cell Metab 3, 333-341 (2006).

[132] Seale P. et al. Transcriptional control of brown fat determination by PRDM16. Cell Metab 6, 38-54 (2007).

[133] Seale P. Transcriptional regulatory circuits controlling brown fat development and activation. Diabetes 64, 2369-2375 (2015).

[134] Shabalina I.G. et al. UCP1 in brite/beige adipose tissue mitochondria is functionally thermogenic. Cell Reports 5, 1196-1203 (2013).

[135] Kazak L. et al. A creatine-driven substrate cycle enhances energy expenditure and thermogenesis in beige fat. Cell 163, 643-655 (2015).

[136] Khorasani A. et al. Phytohormone abscisic acid ameliorates cognitive impairments in streptozotocin-induced rat model of Alzheimer's disease through PPARβ/δ and PKA signaling. Int J Neurosci 129, 1053-1065 (2019).

[137] Naderi R. et al. Extracellular calcium influx through L-type calcium channels, intracellular calcium currents and extracellular signal-regulated kinase signaling are involved in the abscisic acid-induced precognitive and anti-anxiety effects. Biomed Pharmacother 109, 582-588 (2019).

[138] Hou S.T. et al. Phaseic acid, an endogenous and reversible inhibitor of glutamate receptors in mouse brain. J Biol Chem 291, 27007-27022 (2016).

[139] Derosa G. et al. Abscisic Acid Treatment in Patients with Prediabetes. Nutrients 12, 2931 (2020).